



Group 3 Launch and Transfer to Orbit System

Final Design Report

Joseph Ammons, Jacob Dewey, Seth Hawkins,

Trey Philpott, Wesley Upchurch

AERO-4720-002 – Launch Vehicle Design

Department of Aerospace Engineering, Auburn University

April 26, 2022

Table of Contents

List of Figures	vi
List of Tables	viii
1. Conceptual Overview and Design Philosophy	1
1.1. Vehicle Design Methodology.....	1
1.2. Changes Made Since Concept Design Review	1
1.3. Requirements Compliance Matrix	5
1.4. Concept of Operations.....	6
1.5. Budget	7
1.6. Human-Rating Requirements	10
1.6.1. Process Overview	10
1.6.2. Overall Mission Safety Requirements	11
1.6.3. Fault Tolerance	11
1.6.4. Vehicle Monitoring and Control Requirements	12
1.6.5. Mission Abort Requirements.....	12
1.7. Timeline	12
2. G3LATTO System Specifications Overview Sheet	13
3. Launch-to-Orbit Overview.....	14
3.1. Flight Simulation.....	14
3.2. Gravity Turn.....	16
3.3. Delta-V Calculations.....	17
4. G3LATTO System Staging.....	19
4.1. 0 th + 1 st Stage.....	19
4.1.1. CAD Overview	19
4.1.2. Mass and Volume Requirements/Build Specifications	20
4.2. 2 nd Stage	21
4.2.1. CAD Overview	21
4.2.2. Mass and Volume Requirements/Build Specifications	21
5. Vehicle Propulsion.....	22
5.1. 0 th + 1 st Stage.....	22
5.1.1. 0 th + 1 st Stage Propulsion Trade Study	22
5.1.2. LOX/LCH ₄ and APCP Properties.....	23

5.1.3. BE-4 Characteristics	23
5.1.4. Ariane SRB Characteristics	23
5.1.5. 0 th + 1 st Stage Thrust Vector Arc Fan.....	24
5.2. 2 nd Stage	24
5.2.1. 2 nd Stage Propulsion Trade Study.....	24
5.2.2. LOX/RP-1 Properties	25
5.2.3. Merlin 1D Vacuum Characteristics	25
6. Cargo Module Design	26
6.1. Overview	26
6.2. Docking Equipment.....	27
6.3. Docking Methodology.....	28
7. Auxiliary Propulsion Systems.....	29
8. Liquid Propellant Tank Pressurization.....	31
9. Structural Design	33
9.1. Vehicle Stability	33
9.2. Structural Methodology.....	33
9.3. Materials.....	34
9.3.1. Material Trade Study Overview	34
9.3.2. Propellant Tanks	36
9.3.3. Skin and Structural Components	37
9.3.4. Engine Mounts.....	38
9.4. Structural Manual Calculations.....	39
9.5. Finite Element Analysis	41
9.6. Structural Design CAD Overview.....	48
10. Aerodynamic Analysis.....	53
10.1. Drag.....	53
10.2. Ascent Heating	54
10.3. Center of Pressure	54
10.4. Flight Dynamics Analysis	56
11. Electrical Systems	57
11.1. Power Supply	57
11.2. Voltage System	58

11.3. Stage Separation and Fault Tolerance.....	59
12. Avionics and Guidance, Navigation, and Control	61
12.1. Overview and Avionics Systems Diagram.....	61
12.2. GN&C Sensors.....	61
12.2.1. Overview	61
12.2.2. Inertial Measurement Units	61
12.2.3. Star Tracker Systems	62
12.3. Navigation.....	63
12.4. Control.....	63
12.5. Redundancy.....	64
13. Communications	65
13.1. Objectives.....	65
13.2. Requirements.....	65
13.3. Uplink/Downlink.....	67
14. Vehicle Health Monitoring	69
14.1. Overview	69
14.2. Structural Monitoring.....	69
14.3. Engine and Tank Monitoring	70
14.4. Data Management System.....	71
15. Flight Termination System	72
15.1. System Requirements and Overview	72
15.2. Components, Locations, and Potential Outcomes.....	73
15.3. Failure Mode and Effect Analysis.....	73
16. Flight Test Plan	77
17. Final Vehicle System Overview	78
18. CAD Modeling of Vehicle Segments	79
Appendix A. – References	83
Conceptual Overview and Design Philosophy.....	83
Launch-to-Orbit Overview	83
Propulsion.....	83
Cargo Module Design	84
Auxiliary Propulsion	84

Tank Pressurization.....	84
Structural Design.....	84
Electrical Systems	85
Avionics and GN&C	85
Communications.....	85
Vehicle Health Monitoring.....	86
Flight Termination System.....	86
Appendix B. – List of Abbreviations.....	87
Appendix C. – Propulsion Trade Study.....	89
Main Engines.....	89
Solid Rocket Boosters	90
2 nd Stage Engines	91
Appendix D. – MATLAB Scripts.....	93
Ascent Trajectory	93
Standard Atmosphere Model.....	99
Stage Mass Calculations.....	101
Propellant Mass Sizing.....	103
Engine Gimbal Radius Calculations	107
Estimated Burn Times.....	108
Structural Calculations	110

List of Figures

Figure 1: Comparison between the CDR design (left) and the final design (right). All dimensions are in meters. Note that the original design had a thrust-to-weight ratio of 1.95, which was not included on the original fly sheet being used for this comparison.	2
Figure 2: Comparison of the internal structure of the CDR design (left) and the final design (right)	3
Figure 3: Internal CAD view of the basic plumbing layout for the first (left) and second (right) stages.....	4
Figure 4: External view of the capsule with the nosecone closed (left) and open (right).....	4
Figure 5: Graphical CONOPS for the G3LATTO System	6
Figure 6: Projected yearly team budget with respect to NASA yearly budget.....	7
Figure 7: NASA Human-Rating Certification Process Flow Chart [5]	11
Figure 8: Projected System Development Timeline	12
Figure 9: Specifications Overview Sheet for the G3LATTO System	13
Figure 10: Vehicle Altitude as a Function of Time	14
Figure 11: Velocity as a Function of Time	15
Figure 12: Acceleration as a function of Time	15
Figure 13: Vehicle Flight Path Angle (FPA) vs Altitude in kilometers	16
Figure 14: Drag as a Function of Time	18
Figure 15: CAD Overview of the 0 th + 1 st stage of the G3LATTO System	19
Figure 16: CAD Overview of the 2 nd stage of the G3LATTO System.....	21
Figure 17: Thrust Vector arc fan diagram for BE-4 main engines and Ariane SRB's with gimble range in meters.....	24
Figure 18: G3LO cargo module exterior diagram. All dimensions are in meters.	26
Figure 19: NASA International Docking Adaptor [12]	27
Figure 20: The G3LO cargo module's nosecone pivots to provide access to its IDA.....	27
Figure 21: Auxiliary propulsion system vector control diagram	30
Figure 22: Cryogenic tank self-pressurization system diagram.....	31
Figure 23: Helium tank for RP-1 tank pressurization system.....	32
Figure 24: G3LATTO System Displacement Plot.....	41
Figure 25: G3LLATO System von Mises Stress Plot.....	42
Figure 26: Structural components undergoing largest loading conditions	42
Figure 27: 0 th + 1 st stage LOX (left) and LCH ₄ (right) tank displacements	43
Figure 28: 0 th + 1 st stage LOX (left) and LCH ₄ (right) tank von Mises stresses.....	44
Figure 29: 2 nd stage LOX (left) and RP-1 (right) tank displacements	44
Figure 30: 2nd stage LOX (left) and RP-1 (right) tank von Mises stresses.....	45
Figure 31: 0 th + 1 st stage LOX mount von Mises stresses (left) and displacements (right).....	45
Figure 32: 0 th + 1 st stage LCH ₄ mount von Mises stresses (left) and displacements (right).....	46
Figure 33: 2 nd stage LOX mount von Mises stresses (left) and displacements (right)	46
Figure 34: 2 nd stage RP-1 mount von Mises stresses (left) and displacements (right)	46
Figure 35: 2 nd stage auxiliary tank mount von Mises stresses (left) and displacements (right) ...	47

Figure 36: G3LATTO System 0 th +1 st stage Oxidizer Tank (Left) and Oxidizer Tank Mount (Right)	48
Figure 37: G3LATTO System 0 th +1 st stage Fuel Tank (Left) and Fuel Tank Mount (Right)	49
Figure 38: G3LATTO System 2 nd stage Oxidizer Tank (Left) and Oxidizer Tank Mount (Right)	50
Figure 39: G3LATTO System 2 nd stage Fuel Tank (Left) and Fuel Tank Mount (Right)	50
Figure 40: G3LATTO System NTO/MMH (left) and helium (right) tanks for auxiliary propulsion and tank pressurization	51
Figure 41: G3LATTO System NTO/MMH and helium tank mount.....	51
Figure 42: Assembled internal structure for all stages of the G3LATTO vehicle.....	52
Figure 43: Pressure distribution over the vehicle and in the flowfield	53
Figure 44: 2D CFD of the aerodynamic heating on the launch vehicle and flowfield	54
Figure 45: Density distribution over the vehicle and in the flowfield	56
Figure 46: Velocity field around the vehicle	56
Figure 47: Manufacturer specifications for the 8S2P 52Ah Spacecraft Lithium Ion-Polymer Battery.....	57
Figure 48: Electric power distribution diagram.....	58
Figure 49: Ariane 5 electrical system command diagram [23].....	58
Figure 50: Ariane 5 launch pad umbilical linkage interface diagram [23].	59
Figure 51: Ariane 5 pyrotechnical command diagram [23].....	60
Figure 52: Avionics and GN&C Systems Diagram [24]	61
Figure 53: Gyroscope used in IMU sensor	62
Figure 54: Star tracker camera view	62
Figure 55: Kalman Filter system diagram	63
Figure 56: Avionics and GN&C Control System Block Diagram.....	64
Figure 57: Security standards for communications data systems [30]	65
Figure 58: Communications system diagram for the G3LATTO System [31]	66
Figure 59: Space Network ground satellite locations [32].....	67
Figure 60: TRDS forwards and return bands and data rates [33]	68
Figure 61: First, second, and third generation TDRS architecture [33].....	68
Figure 62: Example FOSS structural sensor system layout [34]	69
Figure 63: Cryogenic liquid level sensor operation example [34].....	70
Figure 64: Locations of the charges for unzipping the propellant tanks (red) and blowing the SRB bulkheads (blue).	73
Figure 65: Full-Stack launch configuration of G3LATTO system, all dimensions are in meters	79
Figure 66: 1 st stage of G3LATTO system – Post SRB separation, all dimensions are in meters.	80
Figure 67: 2 nd stage of G3LATTO system – Post 1 st stage separation, all dimensions are in meters	81
Figure 68: Full-Stack internal structural design, all dimensions are in meters.....	82

List of Tables

Table 1: Requirements Compliance Matrix for G3LATTO system	5
Table 2: Yearly program budget.....	8
Table 3: Variables for use in AMCM	9
Table 4: Recurring program costs.....	10
Table 5: G3LATTO System delta-V by stage	17
Table 6: Total delta-V losses	17
Table 7: Mass and volume specifications for the 0 th +1 st stage of the G3LATTO System	20
Table 8: Mass and volume specifications for the 2 nd stage of the G3LATTO System.....	21
Table 9: Results of 0 th + 1 st Stage Core Propulsion Weighted Values Trade Study.....	22
Table 10: Results of 0 th + 1 st Stage External SRB Propulsion Weighted Values Trade Study	22
Table 11: LOX/LCH ₄ Propellant Properties	23
Table 12: AP/HTPB + Aluminum Propellant Properties	23
Table 13: Results of 2 nd Stage Propulsion Weighted Values Trade Study	25
Table 14: LOX/RP-1 Propellant Properties	25
Table 15: Results of Auxiliary Propulsion Systems Weighted Values Trade Study	29
Table 16: Notable specifications for the R-4D thrusters to be used in the G3LATTO System ...	29
Table 17: Properties of materials considered for G3LATTO Structural Design	34
Table 18: Normalization values for materials considered for G3LATTO Structural Design.....	35
Table 19: Unweighted values for materials considered for G3LATTO Structural Design	35
Table 20: Weighting factors for materials considered for propellant tank design.....	36
Table 21: Result of weighted values study for materials considered for propellant tank design .	36
Table 22: Weighting factors for materials considered for skin and structural component design	37
Table 23: Result of weighted values study for materials considered for skin and structural component design	37
Table 24: Weighting factors for materials considered for engine mount design.....	38
Table 25: Result of weighted values study for materials considered for engine mount design....	38
Table 26: Results of Manual Calculations for G3LATTO System Propellant Tank Structures...	40
Table 27: Stringer buckling and launch loading	40
Table 28: Component factors of safety, maximum displacement, and maximum stress.....	47
Table 29: FMEA for BE-4 Liquid Core Main Engine	74
Table 30: FMEA for Ariane SRB's.....	75
Table 31: FMEA for 2 nd Stage Assembly	76
Table 32: Launch system prototype descriptions and objectives.....	77
Table 33: List of Abbreviations and Acronyms.....	87
Table 34: Main engine actual values	89
Table 35: Main engine normalization values.....	89
Table 36: Main engine normalized values	89
Table 37: Main engine weighting factors	89
Table 38: Final weighted values result for the main engines.....	90
Table 39: SRB actual values	90
Table 40: SRB normalization values	90

Table 41: SRB normalized values.....	90
Table 42: SRB weighting factors	91
Table 43: Final weighted values result for the solid rocket boosters.....	91
Table 44: Actual values for the 2 nd stage engines.....	91
Table 45: Normalization values for the 2 nd stage engines	91
Table 46: Normalized values for the 2 nd stage engines.....	92
Table 47: Weighting factors for the 2 nd stage engines.....	92
Table 48: Final weighted values result for the 2 nd stage engines.....	92

1. Conceptual Overview and Design Philosophy

1.1. Vehicle Design Methodology

The Group 3 Launch Alliance (G3LA) is tasked with designing a launch system capable of transporting a 75 metric ton payload to an 800 km equatorial orbit. This launch will take place in Cape Canaveral, Florida. This design process will be conducted in such a way that the design, analysis, and test flight stages will be completed by 4th Quarter, FY 2036. In addition to this fundamental requirement, the vehicle is required to be human rated. The command capsule must also be able to dock with the NASA International Docking Adapter.

The Group 3 Launch and Transfer to Orbit System (G3LATTO System) is the G3LA's answer to this challenge, with seamless incorporation of existing technology and infrastructure serving as a primary driving principle, pulling technologies together from Blue Origin, SpaceX, and the Ariane program. While the primary cargo configuration of the launch system does not call for human factor considerations, secondary configurations require the ability to maintain the safety of a human crew through meeting relevant human rating requirements. As such, the safety of a human crew will be considered with the utmost importance. The vehicle will be human-rated, meeting requirements set in NPR 8705.2C and the Commercial Crew Transportation System Certification Requirements (12/9/2010).

1.2. Changes Made Since Concept Design Review

Several changes were made to the design of the G3LATTO launch system as a result of internal analysis and external feedback received on the Concept Design Review (CDR). These changes were made with the goal of making our launch vehicle more realistically viable by revisiting and rectifying incorrect initial design assumptions and then applying these changes to our vehicle.

The first and most impactful change made to the design of the G3LATTO vehicle was that the amount of delta-v expected to be achieved by the launch configuration (full stack plus boosters) was reduced from seven kilometers per second to four kilometers per second. This change was made because the original delta-v allocation was determined to be infeasible and would have resulted in an average acceleration of over five g's during the initial stage of the flight. Making this change required us to redistribute three kilometers per second of delta-v among the other stages, which drastically changed the overall size of the launch vehicle. The figure below visualizes the differences in size between the original CDR design and the final design.

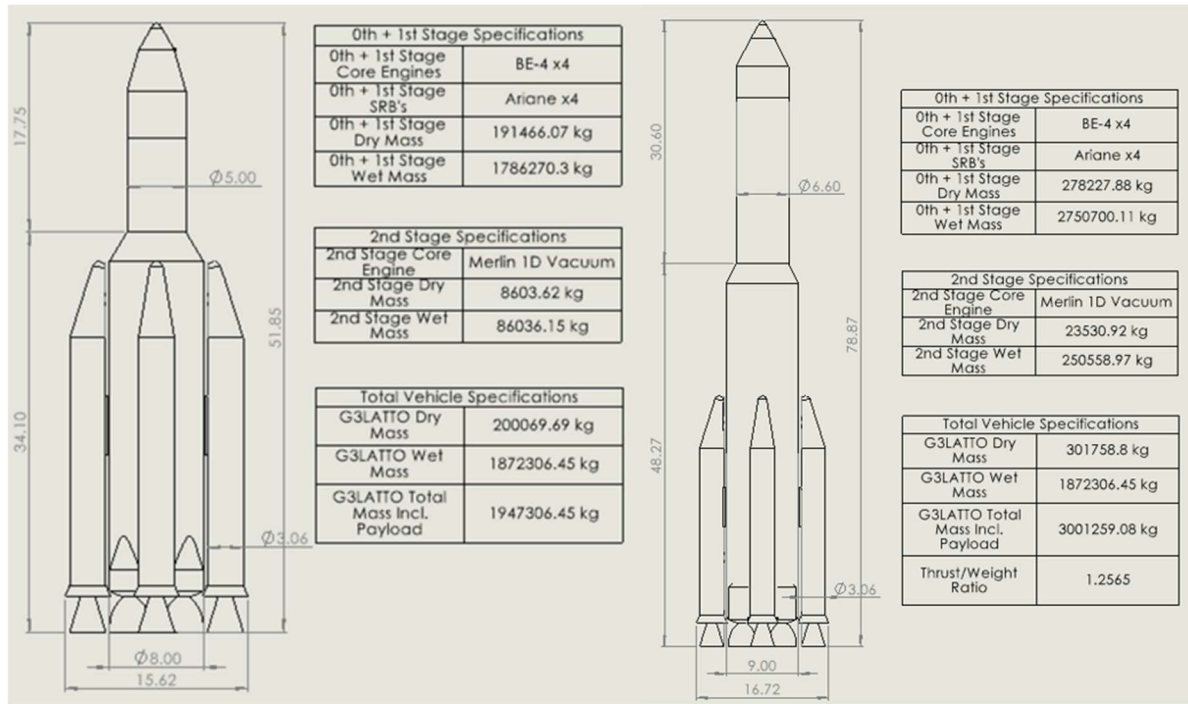


Figure 1: Comparison between the CDR design (left) and the final design (right). All dimensions are in meters. Note that the original design had a thrust-to-weight ratio of 1.95, which was not included on the original fly sheet being used for this comparison.

This design change resulted in the G3LATTO system becoming significantly taller while also slightly wider across all stages as well. This led to the vehicle's overall mass increasing considerably as well due to the additional propellant, tank mass, and structural mass. However even with all of the additional mass, the final design of the G3LATTO system still reaches a thrust-to-weight ratio (TWR) of 1.26 in its launch configuration. This is thanks to the design team's foresight when generating the initial design, which left us with enough headroom in the amount of thrust to be able to make these changes without having to redesign the entire propulsion system.

The next major design change from the CDR is that the internal structure was simplified from six stringers and tank supports to four. This change was made because initial analysis of the original six stringer structure revealed that it was overbuilt and as a result was contributing unneeded additional mass. Reducing the number of stringers from six to four allowed us to use Finite Element Analysis (FEA) to better optimize the structure's mass and also freed up more internal space for plumbing, electrical, and other systems that needed to be contained between the tanks and outer skin of the vehicle. The following figure visualizes the differences between the CDR design and the final design.

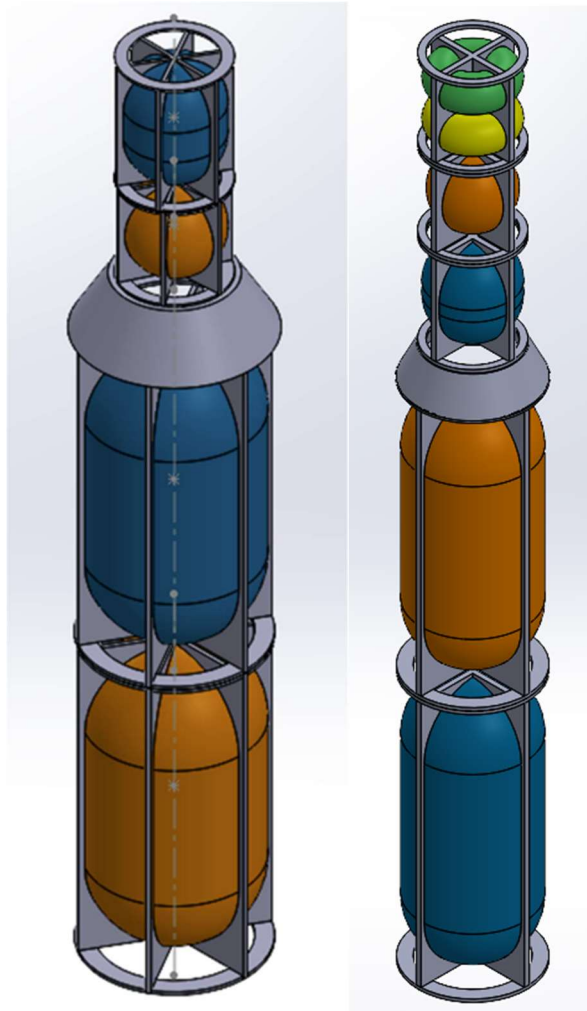


Figure 2: Comparison of the internal structure of the CDR design (left) and the final design (right)

Another change in the G3LATTO's final design is the inclusion of a helium tank and an RCS tank to the second stage. These tanks can be seen above in Figure 2 with the helium tank in yellow and the NTO/MMH divided propellant tank in green. These tanks were discussed in the CDR documentation for the original design but were not implemented into the model at the time. That oversight has been rectified in this final design with their inclusion and integration into the second stage.

Next, basic plumbing was added to the design for the propulsion system. This addition can be seen in Figure 3 below.

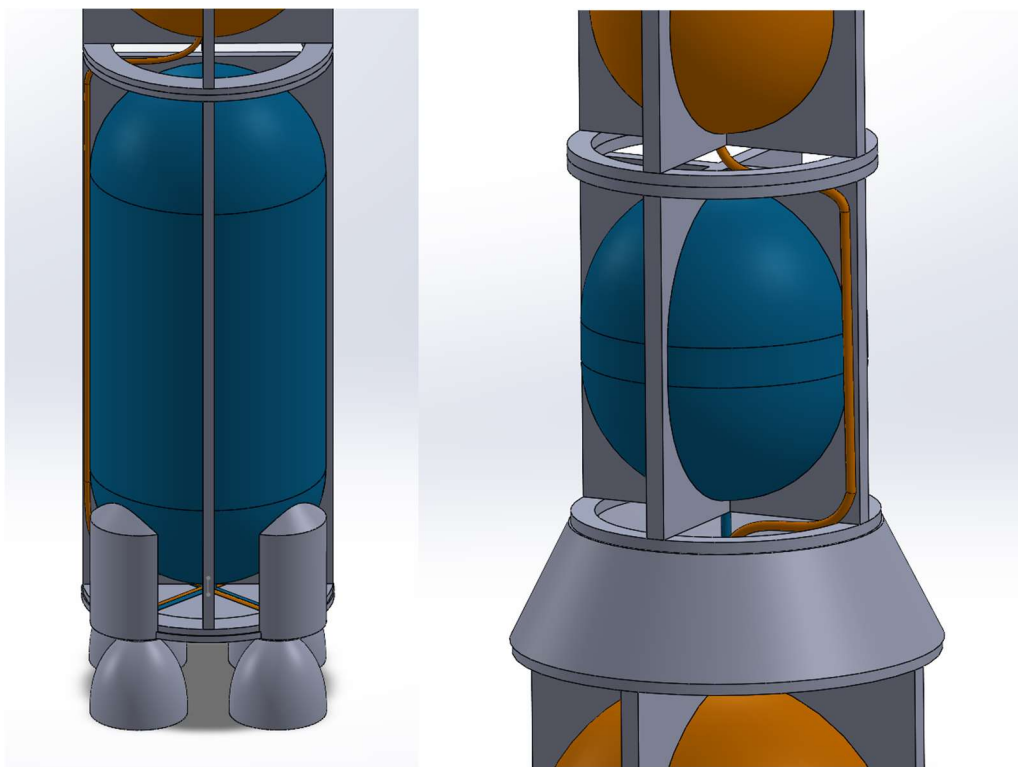


Figure 3: Internal CAD view of the basic plumbing layout for the first (left) and second (right) stages

Finally, a hinge system was added to the capsule that allows the nosecone to open to facilitate access to an International Docking Adaptor (IDA) for docking with other spacecraft. This can be seen below in Figure 4.

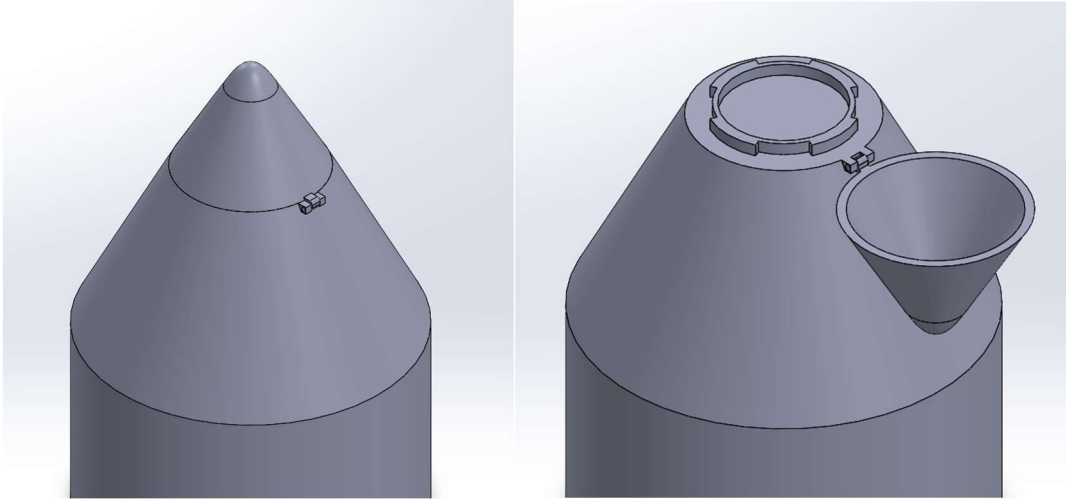


Figure 4: External view of the capsule with the nosecone closed (left) and open (right)

1.3. Requirements Compliance Matrix

Table 1: Requirements Compliance Matrix for G3LATTO system

Requirement	Compliance Approach
<p>The launch vehicle shall be capable of placing a 75 metric ton un-crewed payload into low Earth orbit (LEO) at an equatorial orbit of a minimum of 800km altitude</p>	<p>The G3LATTO vehicle has two core stages with four external solid rocket boosters providing the initial thrust required to get off the ground. The 0th+1st stage is powered by four Blue Origin BE-4 engines in addition to four Ariane 5 EAP P241 SRBs. The 2nd stage employs a Space-X Merlin Vacuum engine to propel the payload from the edge of Earth's atmosphere to the targeted 800km orbit.</p>
<p>The vehicle cargo module shall be capable of docking with the NASA International Docking Adapter</p>	<p>The Group 3 Low-Earth Orbiter (G3LO) capsule is equipped with an International Docking Adaptor underneath its nose cone. The nose cone remains closed for the duration of the launch but is equipped with a hydraulic actuator to rotate it out of the way and allow unrestricted access to the underlying docking port.</p>
<p>The vehicle design process shall complete the design, analysis, and test flight stage no later than 4th Quarter, FY 2036 and your design shall have a complete Gantt chart of the anticipated design, testing, and flight schedule</p>	<p>The G3LATTO rocket's first operational test flight is scheduled for FY 2036, allowing for the launch vehicle to commence commercial launch operations thereafter. The Gantt chart included in this report outlines the anticipated development timelines for the rocket and its systems.</p>
<p>The vehicle shall be designed such that current infrastructure can be utilized with minimal or no modifications. No stand-alone or new large-scale facilities can be built as a result of the design</p>	<p>The G3LATTO system's development and operation will not require any new large-scale infrastructure. The development and production of the launch vehicle and its systems will utilize the existing NASA and NASA-partner facilities detailed in Section 16 of this document.</p>
<p>Either vehicle shall be designed to meet human-rating requirements in NPR 8705.2C and design constraints set forth in the Commercial Crew Transportation System Certification Requirements dated 12/9/2010.</p>	<p>The G3LATTO vehicle will be designed and produced in compliance with the NASA Commercial Crew Transportation System Certification Requirements. The design process of the G3LATTO rocket will be structured such that the vehicle will comply with NASA-STD-4003, NASA-STD-6001, NAS410, NASA-STD-5001, NASA-STD-7001, NASA-STD-7002, NASA-STD-7003, ASTM, ANSI, DOT, FAA, and IEEE requirements in addition to the systems engineering and human rating requirements found in NPR 8705.2C.</p>

1.4. Concept of Operations

The gravity turn is the primary factor that determines the flight path of the vehicle after launch. The G3LATTO rocket will begin this maneuver at T+40 seconds by executing a 2° deflection from vertical via thrust gimbling from the first stage's BE-4 engines. From this point, the vehicle will follow the natural path that the gravity turn initiated in order to minimize atmospheric drag during the rest of the ascent. 140 seconds after ignition, the four Ariane-5 solid rocket boosters will separate and be pushed clear of the launch vehicle while the main engines continue to burn. At T+473 seconds, main engine cutoff (MECO) will occur as the first stage tanks run out of propellant. Immediately following this, stage separation will occur quickly followed by the ignition of the 2nd stage's Merlin Vacuum engine. The G3LO second stage will then complete the initial orbital insertion to an altitude of 136km, which it will reach at T+1,821 seconds. Once this has been completed, the G3LO will then perform a brief final burn up to the target altitude of 800km. Once the orbital altitude of 800km has been achieved, secondary engine cutoff (SECO) will occur and payload deployment can begin. This brings the total mission duration to 1,900 seconds, or about 32 minutes.

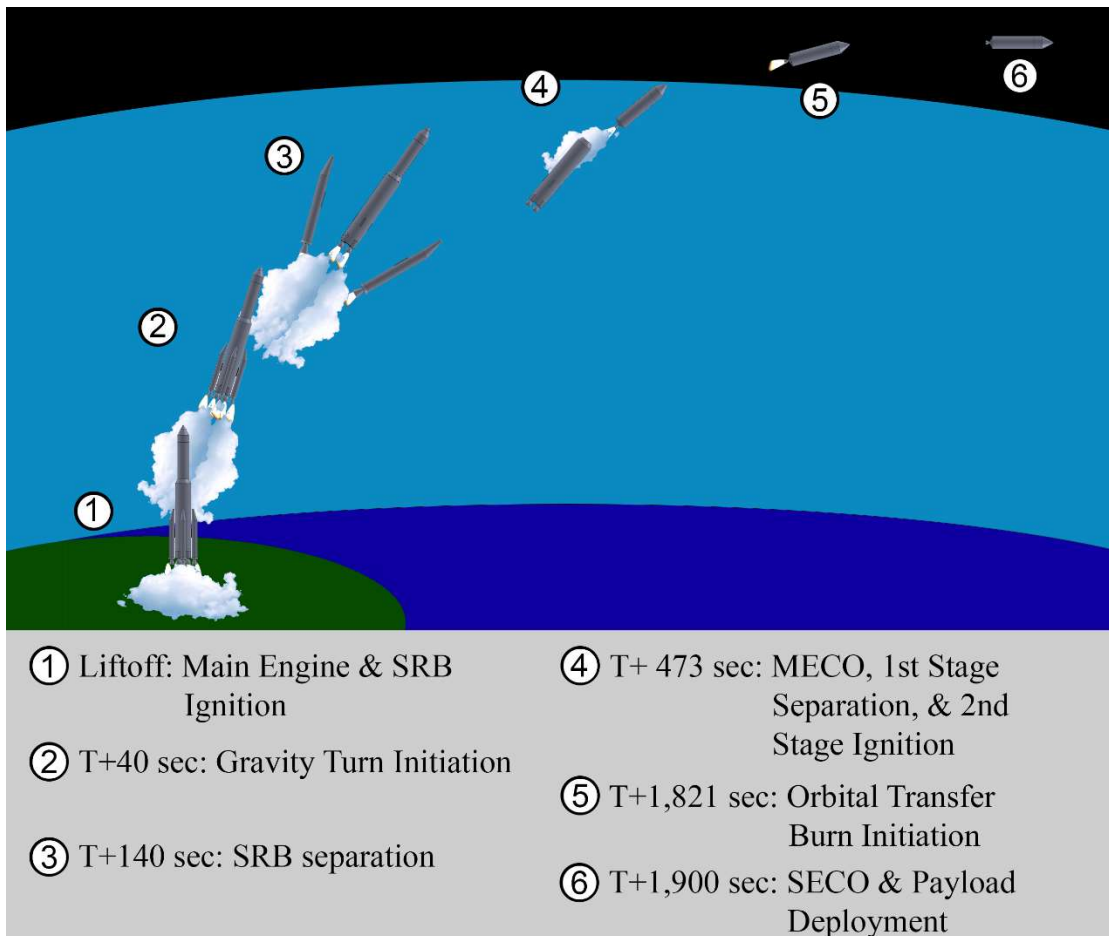


Figure 5: Graphical CONOPS for the G3LATTO System

1.5. Budget

This project allows for 20% of the NASA FY2020 budget, which will be used each year of the program. The program will take place starting in 2022 with completion by 2037, utilizing the NASA budget for FY20 of \$22.6 Billion [1]. Additionally, to account for inflation, the budget will be adjusted using data from the Bureau of Labor Statistics which states a yearly inflation rate of 7.9% [2]. To better account for fluctuations in inflation rates, the large initial inflation rate will decrease to 4% then 3% over five-year intervals in order to more accurately predict inflation rates through the use of historical trends. To account for the yearly inflation rate, the following relation is used:

$$C_{y+1} = C_y + IR * C_y \quad (\text{Eq. 1})$$

Where C_y is the cost at a particular year, IR is the yearly inflation rate, and C_{y+1} is the cost of the next year. This results in a yearly program budget of \$4.52 billion. This is the baseline budget without any attributions to inflation. To obtain a breakdown of the budget by year with the additions of the inflation rates, the NASA FY20 budget as well as program budget are calculated using the formula and rates mentioned prior.

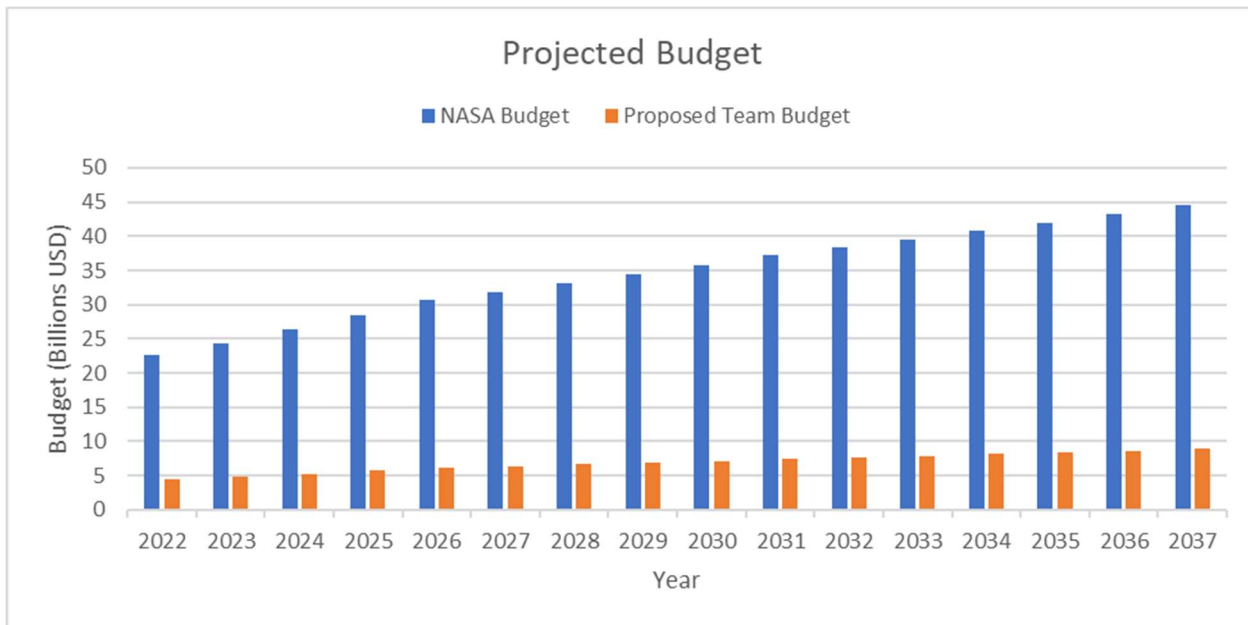


Figure 6: Projected yearly team budget with respect to NASA yearly budget

In the following table, the program budget by year has two categories, the fixed and actual budgets. The fixed budget is the \$22.6 Billion found for the NASA budget, as well as the 20% team budget. This value is constant over the years as there is no attribute to yearly inflation. The actual budget then incorporates yearly inflation rates. The first five years, from 2023 to 2027

have an inflation rate of 7.9%, the second five years, from 2028 to 2032, have an inflation rate of 4%, and the final five years, from 2033 to 2037, have an inflation rate of 3% as stated previously.

Table 2: Yearly program budget

Year	Fixed Team Budget (Billions of Dollars)	Actual Team Budget (Billions of Dollars)
2022	4.52	4.52
2023	4.52	4.87708
2024	4.52	5.26236932
2025	4.52	5.678096496
2026	4.52	6.126666119
2027	4.52	6.371732764
2028	4.52	6.626602075
2029	4.52	6.891666158
2030	4.52	7.167332804
2031	4.52	7.454026116
2032	4.52	7.6776469
2033	4.52	7.907976307
2034	4.52	8.145215596
2035	4.52	8.389572064
2036	4.52	8.641259226
2037	4.52	8.900497003
Totals	72.32	110.6377389

From this analysis, the total program budget was found to be \$110.63 Billion when accounting for inflation. This budget is then compared to the Advanced Mission Cost Model (AMCM), which is a proposed budget based on mass. The AMCM is found from the following relation:

$$C = \alpha Q^\beta M^\Xi \delta^S \epsilon^{\left(\frac{1}{I\!O\!C - 1900}\right)} B^\phi \gamma^D \quad (Eq. 2)$$

The values and definitions for the variables can be seen in the table below.

Table 3: Variables for use in AMCM

Variable	Value	Definition
α	9.077e-4	Constant
Q	2	Quantity
β	0.59418	Constant
M	75,000 kg	Mass
Ξ	0.65395	Constant
δ	76.9994	Constant
S	1.93	Specification (Launch Vehicle)
ϵ	1.6805e-52	Constant
IOC	2037	Initial Operational Capability
B	1	Block
ϕ	-0.3553	Constant
γ	1.5549	Constant
D	1	Difficulty

From this, the budget can be calculated using the Advanced Mission Cost Model. The analysis results in a mission cost of \$65.72 Billion. In the analysis, there were a few variable assumptions needed, namely quantity, specification, block, and difficulty. The quantity was set to 2 as there will be a launch vehicle produced for flight termination testing and for a full test launch. The block is assumed to be 1 due to the vehicle being a new design. This vehicle does utilize many existing components so a block value of 1.5 or 2 could be valid, but knowing that a lower block value increases the program cost seemed viable for an assumption of higher projected cost. Finally, the difficulty was assumed to be 1. An average difficulty is rated at 0.0, but due to the additional assumption of the block of the vehicle, as well as the increased cost due to this assumption, the difficulty is rated as difficult, or two steps above average difficulty. The obtained value is a result from 1999 to 2020, thus an average inflation rate needs to be incorporated for a more accurate result. From [3], an average inflation rate of 2% is used to find the total cost of the launch vehicle. The total cost after inflation adjustment is \$86.716 Billion which is within the proposed budget. This buffer between projected cost and budgetary restrictions will aid in the event of unexpected costs or improper rate/variable assumptions.

The analysis of recurring and nonrecurring costs will be derived from cost models developed by NASA for launch vehicle and Earth departure stages. The total operational cost will be broken down into four categories to operate the program, namely program costs, vehicle costs, launch costs, and flight operations [4]. This model was developed with the assumptions to produce

manned systems to low-earth orbit whether designated as either crew or cargo. Due to the development of the model from previous programs, this model is used and modified for unmanned systems to better predict future costs. Below is a chart for the different recurring costs for each category.

Table 4: Recurring program costs

Program Costs	Vehicle Costs	Launch Operations	Flight Operations
-Program Management and Logistics	-Expendable Hardware -Vehicle Development and Testing	- Propellants -Facilities Operations and Management -Recovery Operations	-Flight Planning and Software -Mission Control Operations -Communications Network Support
-Systems Engineering			

1.6. Human-Rating Requirements

1.6.1. Process Overview

As noted in the requirements compliance matrix found in Section 1.3, it is mandatory that the G3LATTO System be entirely human-rated. To accomplish this, the design of this vehicle will comply with standards laid out in both NASA Procedural Requirements 8705.2C (NPR) [5] and the Commercial Crew Transportation System Certification Requirements (CCTSCR, 12/9/2010) [6] documentation. These documents provide a baseline for the goals and requirements of the human-rating process, ensuring that the design can effectively support human interaction in a way that maximizes the safety of the crew and the potential for successful vehicle operations. A flow chart of NASA's human-rating workflow can be seen below, detailing the necessary path through NASA administration to achieve human-rating certifications.

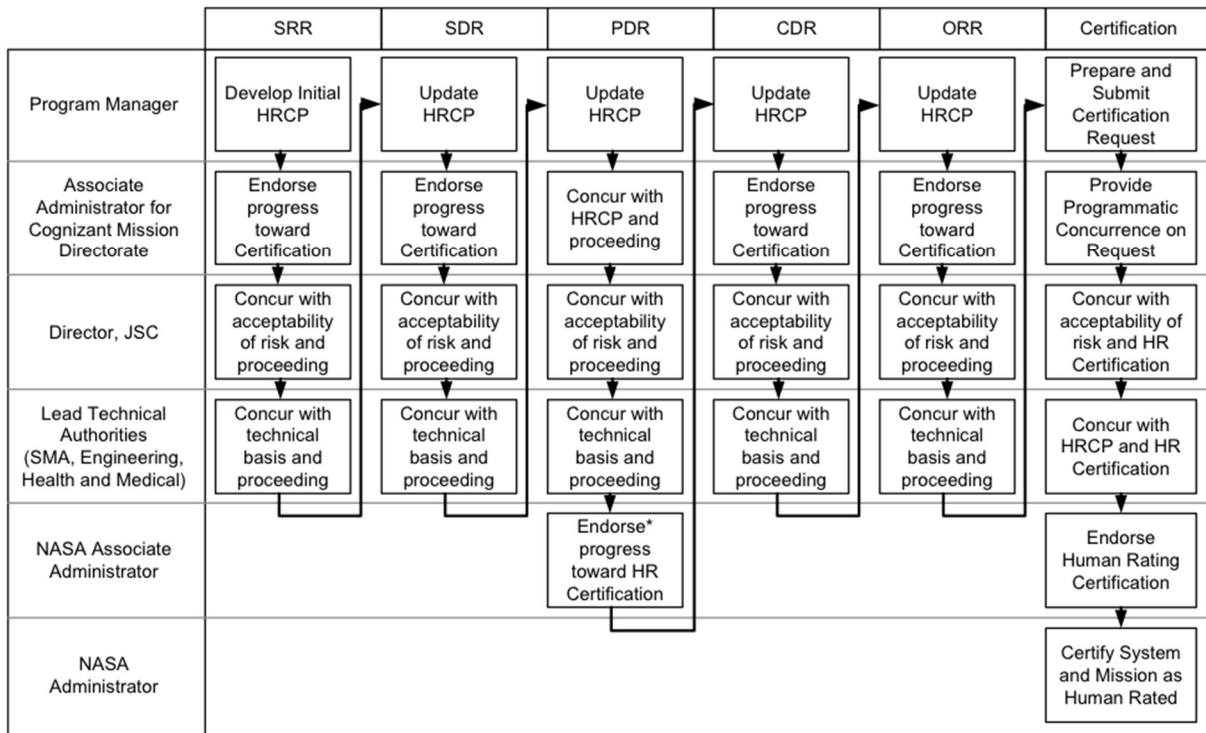


Figure 7: NASA Human-Rating Certification Process Flow Chart [5]

1.6.2. Overall Mission Safety Requirements

The G3LATTO System will adhere to the Loss of Crew (LOC) and Loss of Mission (LOM) requirements detailed in the CCTSCR documentation, including the mean of the LOC probability distribution being no more than 1 in 1000 for the ascent and re-entry phases, and the mean of the LOC probability distribution being no more than 1 in 270 for the overall mission. Additionally, the mean of the LOM probability distribution for the overall mission is to be no more than 1 in 55.

1.6.3. Fault Tolerance

Fault tolerances will be designed in such a way that they prevent total mission failures which could potentially arise from multiple sources, including human error, systems failures, software and electronics malfunctions, and other potentially catastrophic events. These tolerances will be determined through a safety analysis of the G3LLATO System, after which the appropriate fault tolerance levels will be incorporated into the vehicle. These levels exclude the use of emergency systems, as these systems exist to diminish the damage caused by a failure, and do not have the capability to prevent failures before they occur. These fault tolerance features will be designed with the intention of increasing crew capability to correct failures while maintaining their safety in the process.

1.6.4. Vehicle Monitoring and Control Requirements

The G3LATTO System will be designed with human accessibility in mind, especially in regard to vehicle health monitoring and control. The vehicle health systems and vehicle control systems will be subject to manual override systems, with the intention of allowing human control over autonomous systems in the event of a potential or occurring catastrophic failure.

1.6.5. Mission Abort Requirements

The G3LLATO system will allow for the mission to be aborted in the launch, ascent, and orbit phases. Additionally, a crew will be capable of an unassisted exit from the capsule in the event of a catastrophic failure. Mission control will have the ability to abort the mission during the ascent phase, and the G3LATTO System will be provided with the ability to alert recovery forces to its location while maintaining human safety.

1.7. Timeline

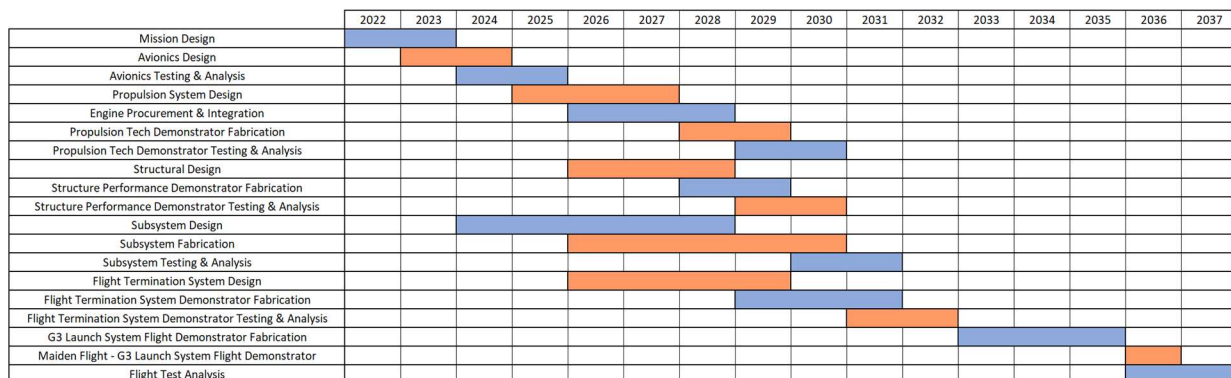


Figure 8: Projected System Development Timeline

2. G3LATTO System Specifications Overview Sheet

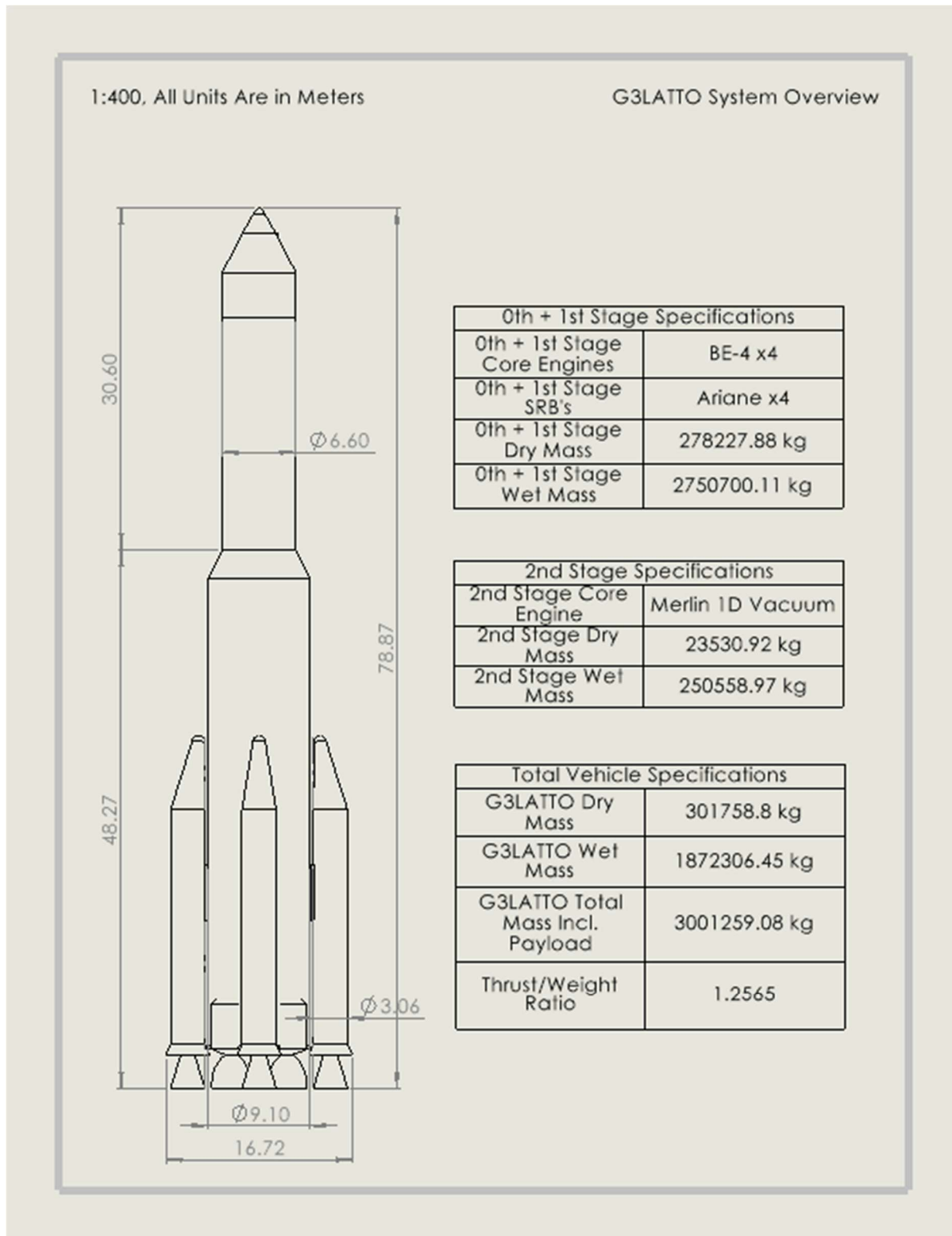


Figure 9: Specifications Overview Sheet for the G3LATTO System

3. Launch-to-Orbit Overview

3.1. Flight Simulation

Using numerical integration as outlined on pages 329-332 of *Design of Rockets and Space Launch Vehicles* [7], the launch can be simulated from liftoff all of the way into orbit. Starting with the initial conditions of $h_0 \approx 0$ meters, $V_0 = 0$ m/s, $a_0 = 2.5204$ m/s 2 , and $\gamma_0 = 90^\circ$, the change in the variables between time steps can be calculated and used to find the other variables (such as acceleration being used to find velocity, which is used to find altitude, etc.) This is accomplished by using a few constants in the equations like thrust values, propellant mass consumption, and gravity to determine the mass, acceleration, velocity, etc. The equations utilized can be seen below:

$$m_i = m_{i-1} - \dot{m}_{stage} * \Delta t \quad (Eq. 3)$$

$$a_i = \frac{T_i - D_i}{m_i} - g_i * \sin(\gamma_i) \quad (Eq. 4)$$

$$V_i = V_{i-1} + a_i * \Delta t \quad (Eq. 5)$$

$$h_i = h_{i-1} + V_i * \Delta t * \sin(\gamma_i) \quad (Eq. 6)$$

$$x_i = x_{i-1} + V_i * \Delta t * \cos(\gamma_i) \quad (Eq. 7)$$

A Δt value of 0.01 was used in the MATLAB simulations of the G3LATTO System. Below are figures showing the flight simulation:

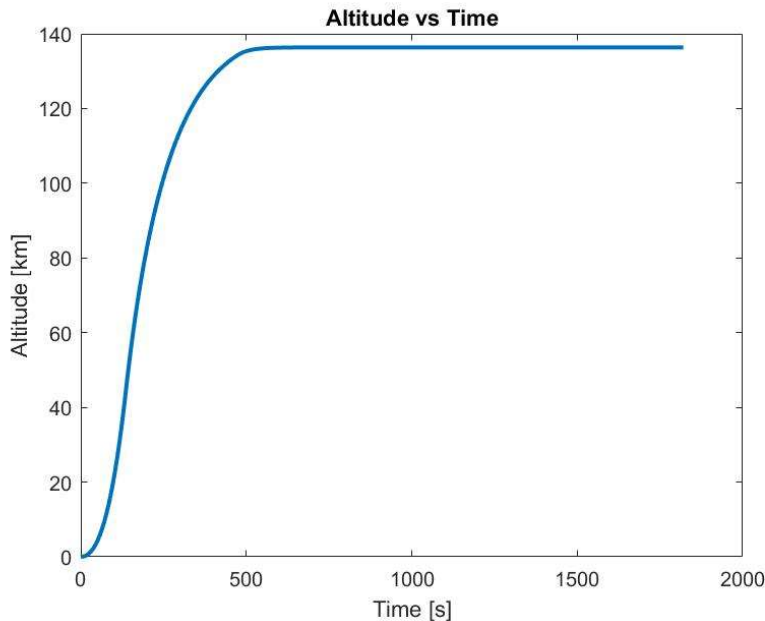


Figure 10: Vehicle Altitude as a Function of Time

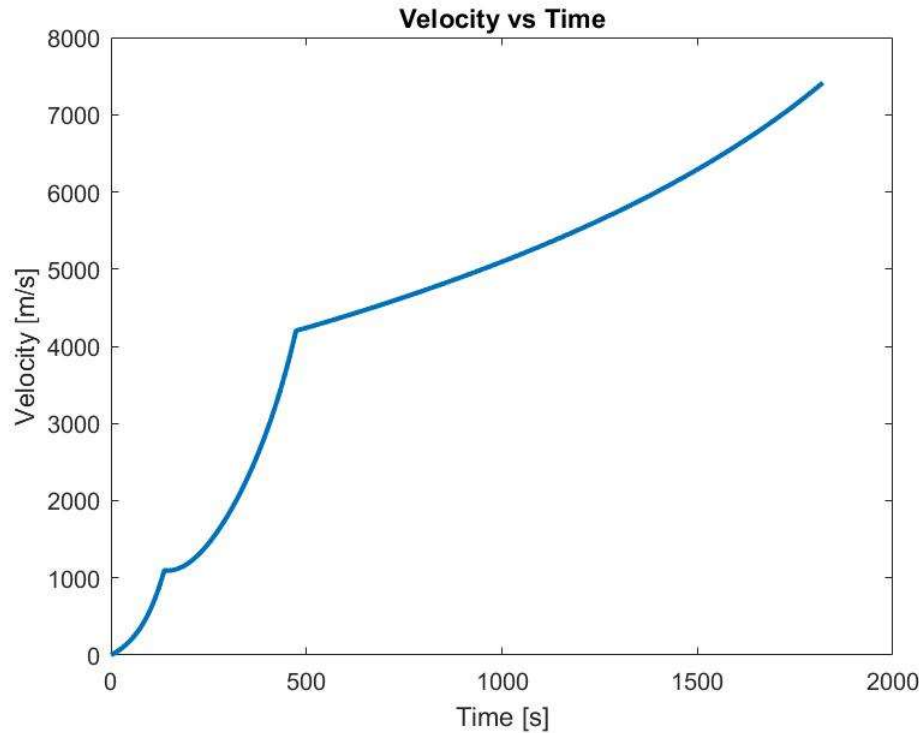


Figure 11: Velocity as a Function of Time

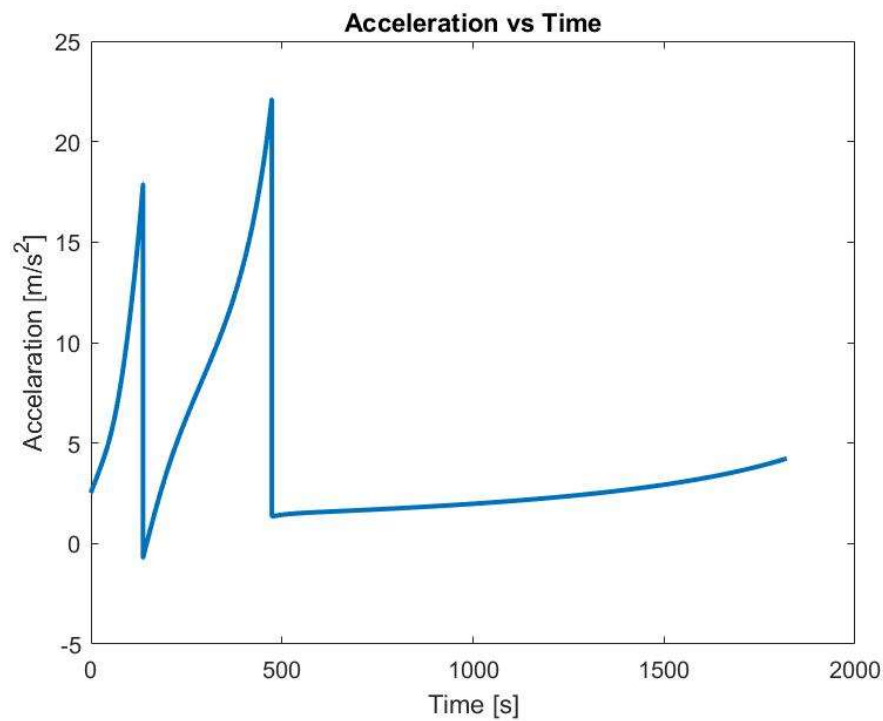


Figure 12: Acceleration as a function of Time

3.2. Gravity Turn

A key component of any launch is reaching a flight path angle (FPA) of 0° in order to achieve orbit. The way this is normally achieved is to give the launch vehicle a small “kick” to change the angle from 90° and give a non-zero cosine. This will then allow gravity to do the work of turning the rocket. This has the added advantage of not inducing any incident angle in the flow over the rocket reducing drag and lateral aerodynamic stresses on the vehicle. The equation used for calculating the angle change is:

$$\dot{\gamma} = - \left(\frac{g}{v} - \frac{v}{r} \right) * \cos(\gamma) \quad (\text{Eq. 8})$$

The G3LATTO uses a relatively steep gravity turn with an initial kick of 2° t+40s into flight putting the vehicle into a transfer orbit of nearly 140km before boosting the rest of the way up to 800km using most of the rest of the second stage. This is done in order to reduce the already steep gravity losses (over 1,800 m/s) seen by the vehicle. Drag losses are relatively minimal and will remain so at the altitude in which the vehicle achieves orbit. Normally a low orbit such as this would decay relatively quickly but the vehicle will be boosted up before this can occur and thus is a non-issue.

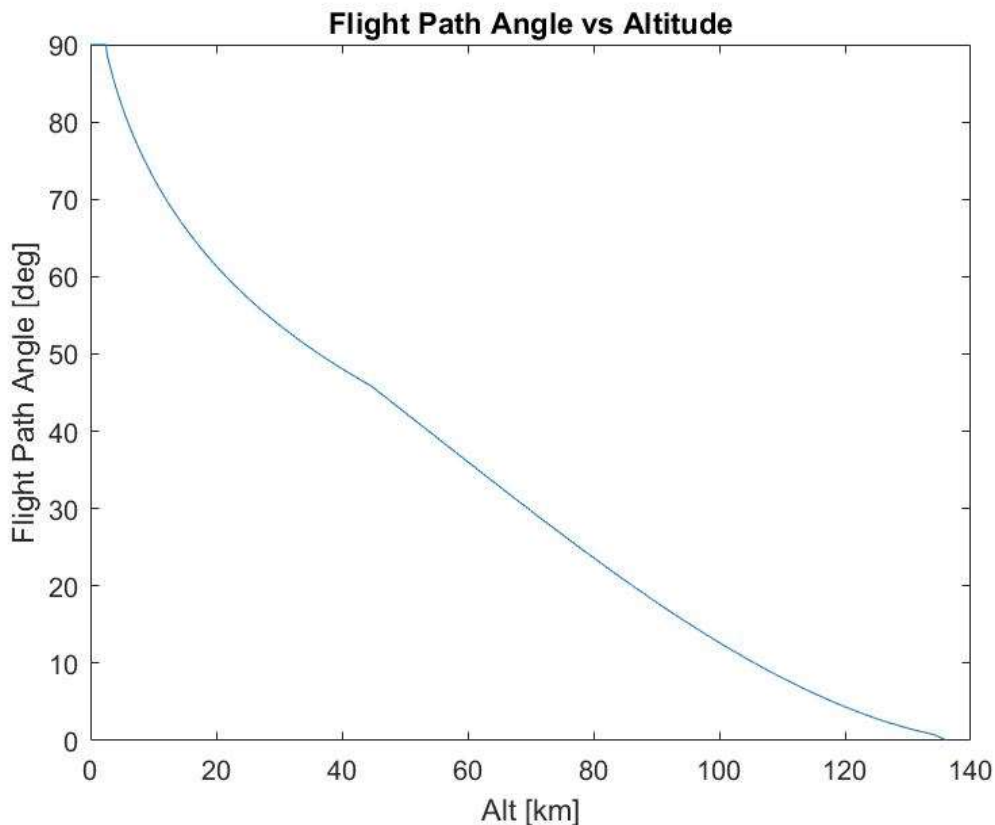


Figure 13: Vehicle Flight Path Angle (FPA) vs Altitude in kilometers

3.3. Delta-V Calculations

The launch vehicle is planned to launch from the Kennedy Space Center located on the Atlantic coast of Florida. This provides the vehicle with an essentially “free” 408 m/s added to its orbital velocity reducing the delta-V requirements of the launch vehicle. The delta-V by stage can be seen in the table below:

Table 5: G3LATTO System delta-V by stage

Stage:	Delta-V
0th Stage (Boosters and part of 1st Stage)	2334.59 m/s
1st Stage (Post Booster Separation)	3648.25 m/s
2nd Stage	3732.16 m/s
Total	9715 m/s

The expended delta-V to get to orbit and then to the target orbit can be seen as losses below:

Table 6: Total delta-V losses

Expense:	Delta-V
Achieve Orbit @ 136 km	7413.64 m/s
Boost to 800 km	370.37 m/s
Drag Losses:	13.43 m/s
Gravity Losses:	1853.4 m/s
Total:	9650.84 m/s

Approximately 9,280 m/s of delta-V is expended getting into orbit at 136 km with another 370 m/s being expended putting the spacecraft into a high orbit. Thus, after achieving orbit, the vehicle is left with approximately 64 m/s of delta-V left. Gravity losses are very high due in part to the relatively low TWR the vehicle has for large portions of the flight. This made it imperative that the vehicle achieve a 0° FPA relatively quickly to avoid the losses becoming unrecoverable. The low drag losses can be owed to the relative speed with which the vehicle exits the thick part of the atmosphere with drag peaking around 515 kN at t+75s into the flight as seen in the figure below.

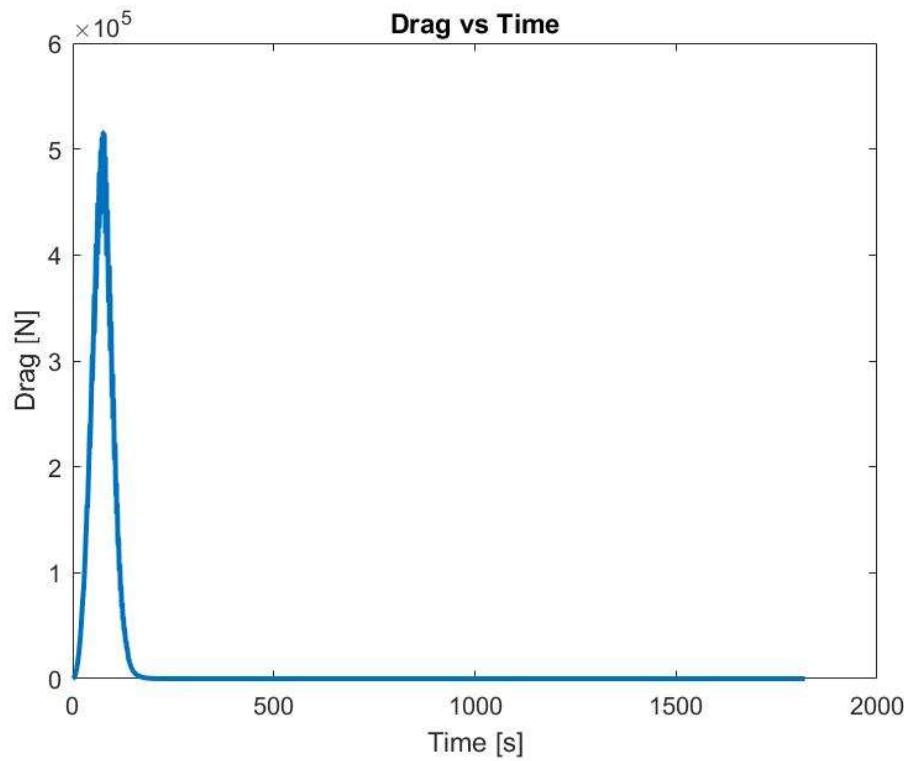


Figure 14: Drag as a Function of Time

Once in orbit, the vehicle will burn to boost apoapsis up to 800 km and then again after reaching the apoapsis to circularize. The burn will take approximately 82 seconds to both boost to the orbit and then circularize.

4. G3LATTO System Staging

4.1. 0th + 1st Stage

4.1.1. CAD Overview

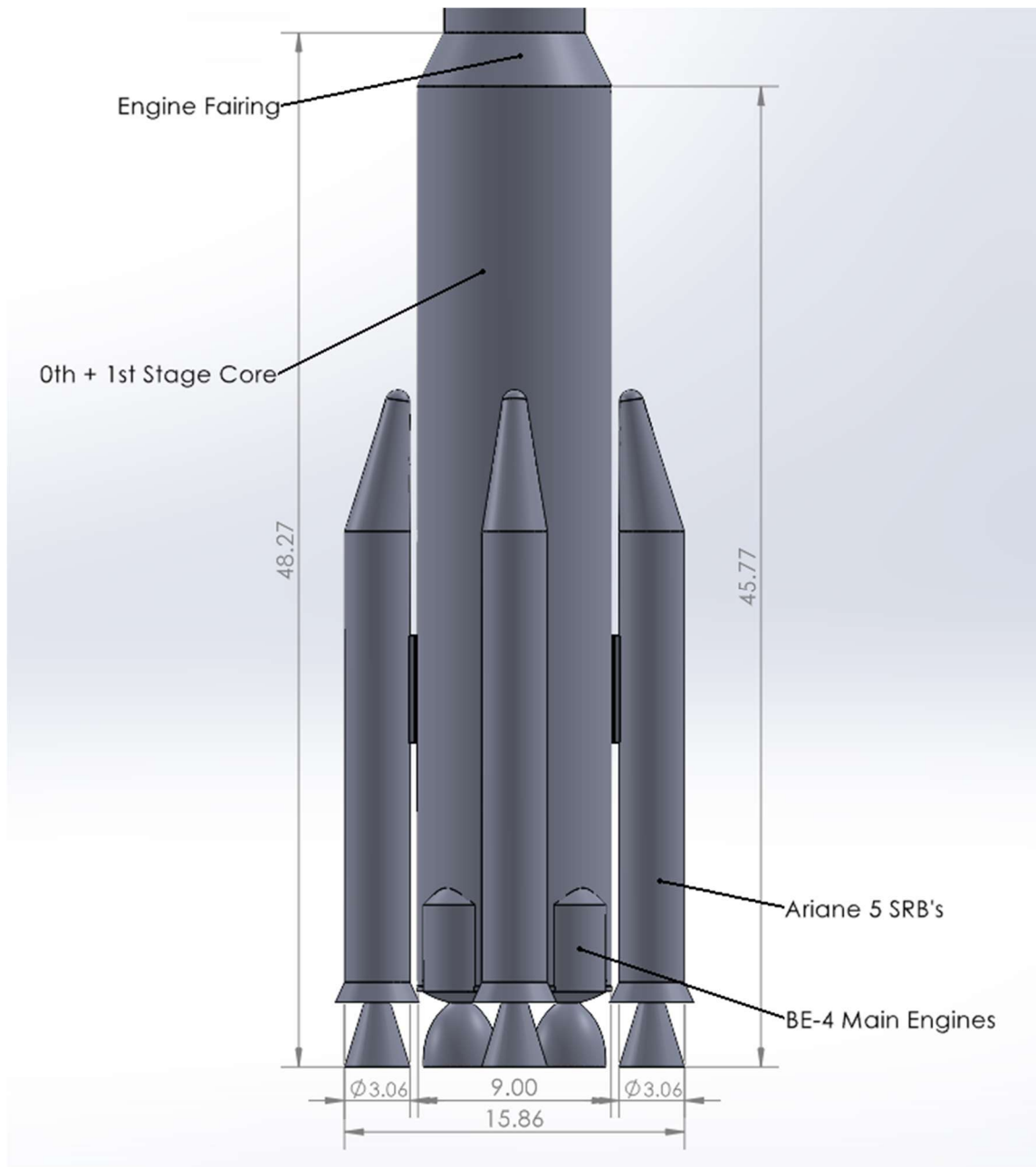


Figure 15: CAD Overview of the 0th + 1st stage of the G3LATTO System

4.1.2. Mass and Volume Requirements/Build Specifications

For the 0th + 1st stage, the vehicle utilizes 4 BE-4 engines and 4 Ariane solid rocket boosters. This design allows for a large amount of thrust produced by the vehicle, while still maintaining a manageable aerodynamic design not provided by other SRB's. This amount of thrust is paramount for a mission to an 800 km orbit, as a large delta-V is necessary to meet this requirement successfully. Due to this configuration, the core segment of the two stages use the same fuel and oxidizer tanks. This simplifies the overall design, allowing the same fuel to be used for much of the early portion of the flight. The mass and volume specifications for the liquid core staging and the Ariane boosters can be found in the following table.

Table 7: Mass and volume specifications for the 0th + 1st stage of the G3LATTO System

0th + 1st stage	Core Oxidizer - LOX	Core Fuel - LCH ₄	Ariane x4 - SRB's
Propellant Mass (kg)	1111474.11	400998.12	960000
Tank Volume (m³)	974.12	945.75	X
Inert Mass Fraction	0.0735		X
Payload Fraction	0.0198		X
Dry Mass (kg)	146227.88		132000
Wet Mass (kg)	1658700.11		1092000

4.2. 2nd Stage

4.2.1. CAD Overview

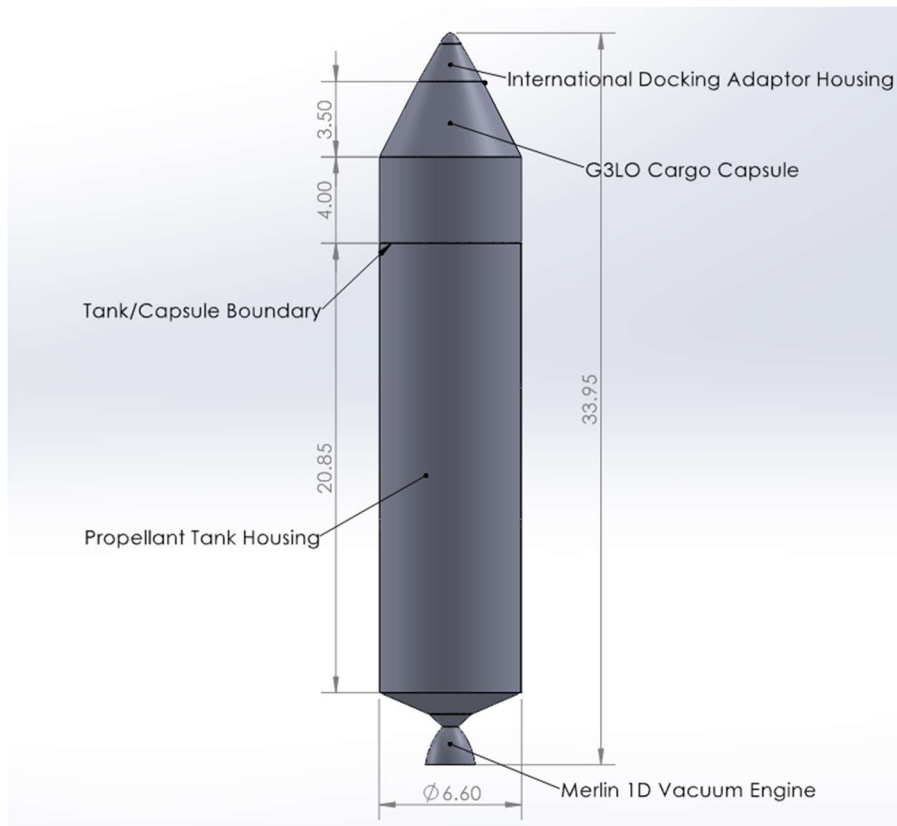


Figure 16: CAD Overview of the 2nd stage of the G3LATTO System

4.2.2. Mass and Volume Requirements/Build Specifications

For the 2nd stage, the vehicle utilizes a Merlin 1D Vacuum engine with associated oxidizer and fuel tanks. The Merlin engine has great throttle ability and can produce sufficient thrust, allowing for the use of only one engine to complete the trip to orbit. The mass and volume specifications for this staging can be found in the following table.

Table 8: Mass and volume specifications for the 2nd stage of the G3LATTO System

2nd stage	Oxidizer - LOX	Fuel - RP-1
Propellant Mass (kg)	156465.92	70562.13
Tank Volume (m³)	137.13	87.11
Inert Mass Fraction		0.0723
Payload Fraction		0.23
Dry Mass (kg)		23530.92
Wet Mass (kg)		250558.97

5. Vehicle Propulsion

5.1. 0th + 1st Stage

5.1.1. 0th + 1st Stage Propulsion Trade Study

It was deemed necessary for this design to construct a lower stage capable of producing extremely large amounts of thrust. Because of this, the efficiency of the propulsion system for both the 0th stage and the 1st stage was much less crucial in the decision-making process. In addition to these two parameters, the ability of the liquid core system to throttle its thrust output was considered a necessary factor to consider in order to meet human-rating acceleration requirements. Due to these parameters, the design and staging detailed in Sections 2 and 4 was determined to be the best option, combining the use of liquid core engines with external SRB's. For the SRB's, the mass and aerodynamics were considered as factors along with the maximum thrust, as increased weight would make reaching the required delta-V more difficult, and the Ariane SRB's more aerodynamic design relative to the overall staging was considered valuable in reducing delta-V loss due to aerodynamic forces. The liquid core engines that were considered were the Blue Origin BE-4, SpaceX Raptor, and the Aerojet Rocketdyne RS-25 engine. The SRB's that were considered were the Space Shuttle 4-Segment SRB's and the Ariane-5's SRB's, specifically in configurations of two Shuttle SRB's and four Ariane SRB's. The results of the weighted values trade studies can be found in the tables below, and the full study can be found in Appendix C.

Table 9: Results of 0th + 1st Stage Core Propulsion Weighted Values Trade Study

Weighted Values			
Items	BE-4	Raptor	RS-25
Max Thrust (kN)	9	3	6
Isp (s)	1	2	3
Throttle Ability	4	6	4
Total	14	11	13

Table 10: Results of 0th + 1st Stage External SRB Propulsion Weighted Values Trade Study

Weighted Values		
Items	Shuttle SRB x2	Ariane SRB x4
Max Thrust (kN)	9	9
Mass (kg)	4	6
Aerodynamics	1	2
Total	14	17

5.1.2. LOX/LCH₄ and APCP Properties

Important properties of the liquid core and external SRB propellants – Liquid Oxygen/Liquid Methane and Ammonium Perchlorate/Hydroxyl-Terminated Polybutadiene + Aluminum – used in this design can be found in the tables below.

Table 11: LOX/LCH₄ Propellant Properties

Items	LOX	LCH ₄
Density (kg/m³)	1141	424
Isp (s)	299	
Density Impulse (kg-s/m³)	235	
Mixture Ratio	2.77:1	

Table 12: AP/HTPB + Aluminum Propellant Properties

Items	AP/HTPB
Isp (s)	277
Density Impulse (kg-s/m³)	474
Mixture Ratio	2.12:1

5.1.3. BE-4 Characteristics

The Blue Origin BE-4 uses a staged-combustion power cycle relatively standard to bipropellant engines capable of producing large amounts of thrust. The preburner stage of this cycle is provided with an oxygen rich environment fed from the propellant tanks by fuel and oxidizer turbopumps, upon which the results of this stage continue to the combustion chamber to produce thrust. Each BE-4 engine is capable of producing 2.4 MN [8] of thrust at a calculated flow rate of 818.22 kg/s, totaling 9.6 MN of thrust at 3272.88 kg/s for the 4 BE-4's in this design. The thrust vector control is managed by the throttle ability and gimbling of the BE-4's engines, with the ability to throttle down to 65% power [9] and a gimbal range of 5° from vertical. The gimbal rate for the BE-4 engines is not published, but based on historical analysis of similar engines, a gimbal rate of 5° per second is a good approximation.

5.1.4. Ariane SRB Characteristics

The Ariane SRB is capable of producing 7.08 MN of thrust at a calculated average flow rate of 1714.29 kg/s. For the 4 SRB's in this design, this totals to 28.32 MN of thrust at a flow rate of 6857.14 kg/s. Each SRB has a 140s burn time, at which point it will separate from the vehicle, marking advancement to the 1st stage. The thrust vector control is managed by a 7.3°-from-vertical gimbal [10] at approximately 5° per second based on historical data, allowing capability for further flight path adjustments.

5.1.5. 0th + 1st Stage Thrust Vector Arc Fan

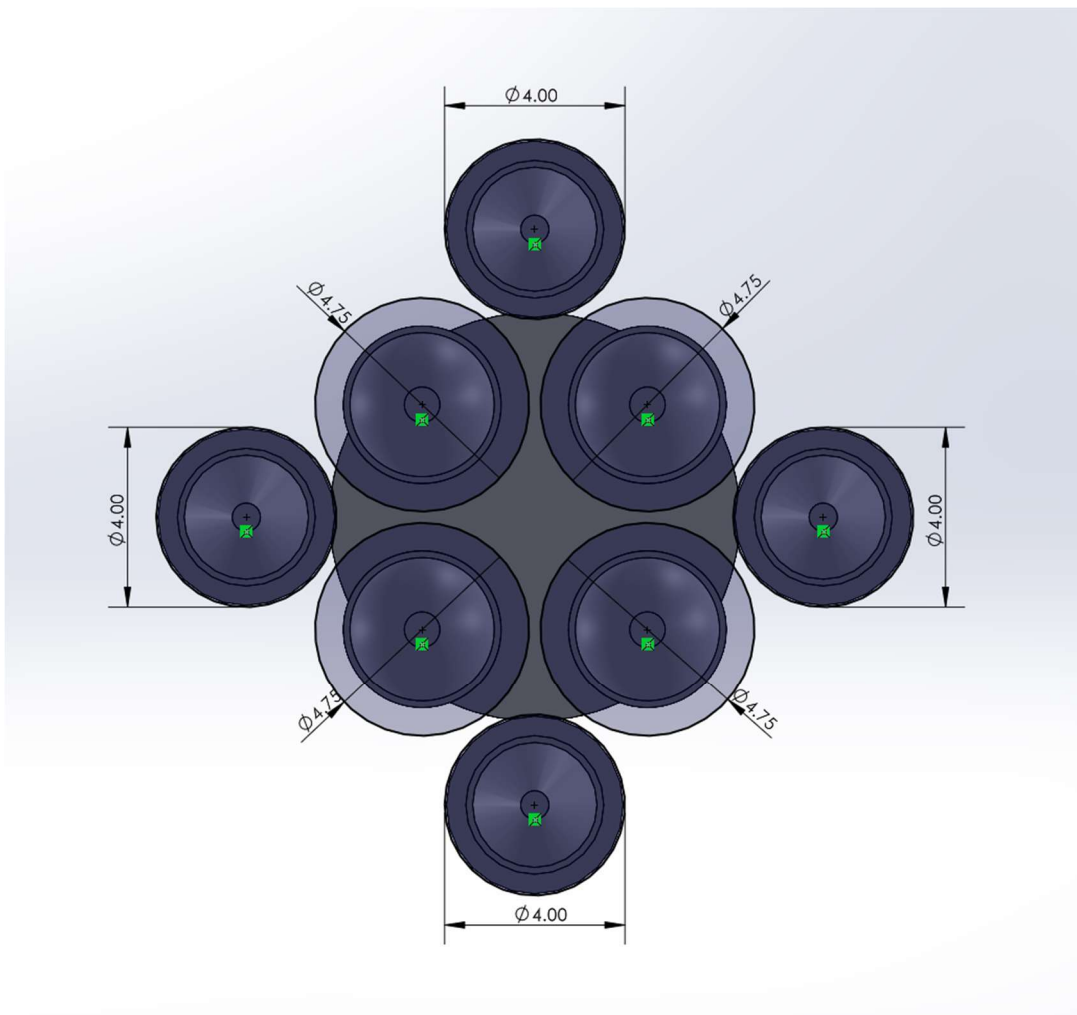


Figure 17: Thrust Vector arc fan diagram for BE-4 main engines and Ariane SRB's with gimble range in meters.

5.2. 2nd Stage

5.2.1. 2nd Stage Propulsion Trade Study

For the design of the second stage, the maximum thrust is much less of a factor than in the previous stages, largely due to the smaller delta-V requirements along with the relatively simpler flight conditions at higher altitudes. Much more important is the Isp of the system, as a higher efficiency will reduce weight and cost allocated to the 2nd stage due to propellant. Like the lower stages, throttle ability is an important factor. The number of engines needed to provide an adequate amount of thrust was also considered, as increasing the number of engines could potentially cause an

increase in cost and weight. The results of the weighted values trade study for 2nd stage propulsion systems can be found in the table below, and the full trade study can be found in Appendix C.

Table 13: Results of 2nd Stage Propulsion Weighted Values Trade Study

Weighted Values			
Items	AJ10	Merlin 1D Vacuum	RL10
Max Thrust (kN)	1	3	2
Isp (s)	4	8	12
Throttle Ability	2	6	4
# of engines needed	3	9	6
Total	10	26	24

5.2.2. LOX/RP-1 Properties

Due to the selection of the SpaceX Merlin 1D Vacuum engine for the second stage of the G3LATTO, it is necessary to detail the properties of the required propellant – Liquid Oxygen/RP-1. A table of these properties can be seen below.

Table 14: LOX/RP-1 Propellant Properties

Items	LOX	RP-1
Density (kg/m3)	1141	810
Isp (s)		289
Density Impulse (kg-s/m3)		294
Mixture Ratio		2.35:1

5.2.3. Merlin 1D Vacuum Characteristics

The SpaceX Merlin 1D Vacuum engine is a highly efficient engine that has successfully been used in and is very well optimized for a space environment. As such, it makes an ideal engine for the 2nd stage of the G3LATTO System. The Merlin 1D Vacuum uses a fuel-rich gas generator to pump the fuel and oxidizer from the propellant tanks to the combustion chamber. The engine is capable of producing 480 kN of thrust at a calculated mass flow rate of 157.33 kg/s. The second stage will manage thrust vector control through the auxiliary propulsion system detailed in Section 7 and through the Merlin's ability to throttle down to 39% of maximum thrust [11].

6. Cargo Module Design

6.1. Overview

The G3LATTO vehicle is designed to carry a payload of 75,000 kg to an orbit of 800km. To carry this payload, the Group 3 Low-Earth Orbiter (G3LO) cargo module will be used. Figure 18 below provides a basic overview of the cargo module.

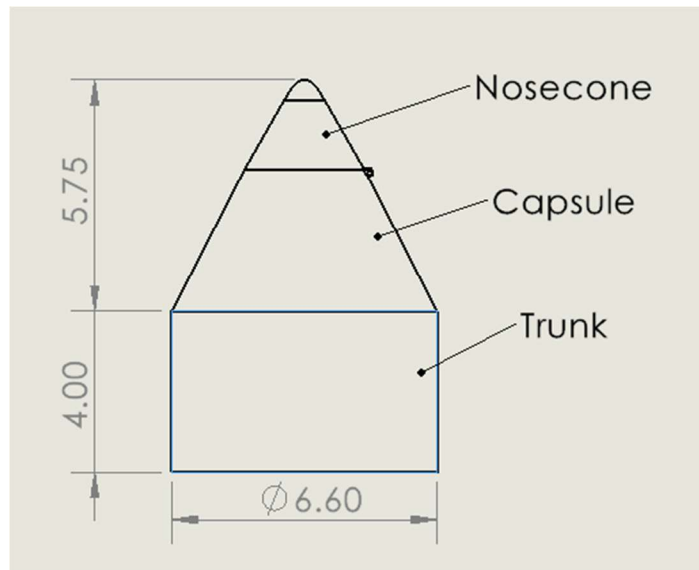


Figure 18: G3LO cargo module exterior diagram. All dimensions are in meters.

The G3LO cargo module consists of three main sections. First is the trunk which contains the G3LATTO's batteries along with the flight control, communications, and data management systems. Further information on these individual systems can be found in Sections 11, 12, 13, and 14.4 of this document, respectively. Keeping these systems grouped together simplifies the electrical system and allows for easier inspection and maintenance. The module's trunk also has four radially mounted reaction control system (RCS) thrusters which provide roll and attitude control for the G3LATTO's second stage. The RCS system is discussed further in Section 7 of this document. The second part of the G3LO cargo module is the capsule. This part of the module primarily contains the payload, and its interior is highly customizable depending on customer needs. The total internal volume of the G3LO cargo module is 205 cubic meters, with about 160 cubic meters of that space being available for cargo depending on customer needs. The third main section is the nosecone. The nosecone is responsible for protecting the docking port while also providing an aerodynamic nose to help minimize the G3LATTO rocket's overall drag during its ascent. The nosecone is equipped with a hinge system similar to the Space-X Dragon capsule which allows it to open and pivot clear of the front of the capsule to enable docking with other spacecraft.

6.2. Docking Equipment

The G3LO Cargo Module is equipped with a NASA standard International Docking Adaptor (IDA) to facilitate docking with other spacecraft once in orbit. An example of one of these docking ports can be found in Figure 19 below.



Figure 19: NASA International Docking Adaptor [12]

The G3LO Cargo Module's IDA is located underneath the capsule's nosecone which protects the docking port during ascent and can pivot clear to provide access to the IDA as needed both before launch and once in space. This operation is visualized in Figure 20 below.

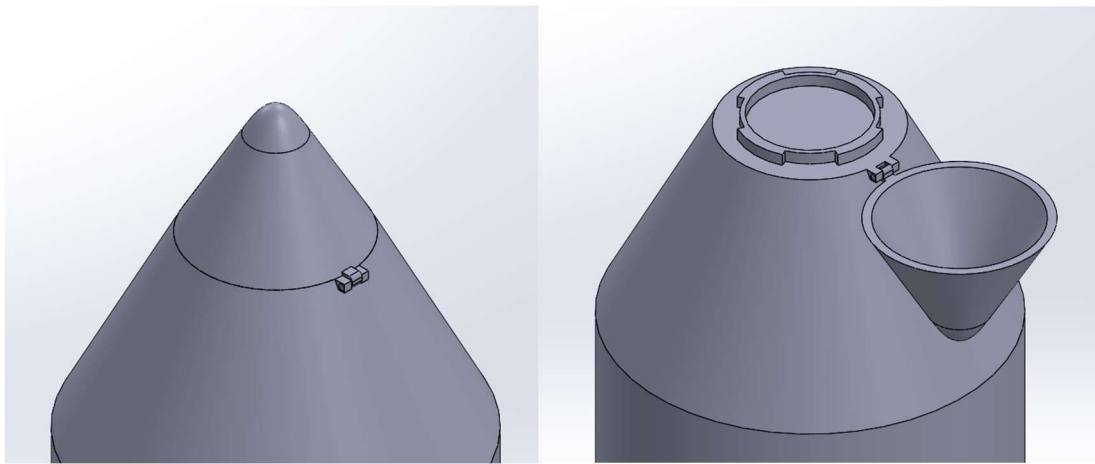


Figure 20: The G3LO cargo module's nosecone pivots to provide access to its IDA

6.3. Docking Methodology

The docking methodology for the International Docking Adaptor is fairly standardized thanks to its usage of sophisticated sensor systems that guide the docking spacecraft's flight control computer automatically [12]. The G3LO's RCS thruster system will be critical for this component of the mission, as precise adjustments must be made in both roll and attitude to facilitate successful docking. The docking procedure for the G3LO capsule will entail four basic steps once the spacecraft has set up an orbital encounter with its docking target. The first step is to open the nosecone to allow access to the IDA. The second step is to use the RCS thrusters to bring the vehicle close enough to the targeted docking port so that the IDA's sensors can begin to operate. The third step is to make precise adjustments to the vehicle's attitude and roll as determined by the IDA's sensor suite and slowly close the distance to the targeted docking port until contact is made. Finally, the two docking ports must lock together to create an airtight seal between the two spacecraft. Once the time has come to disengage from the second spacecraft, the G3LO must follow a similar sequence in reverse. First the two IDAs must be unlocked from each other. Then the G3LO must slowly back away from the second spacecraft until a sufficient distance has been established between them. Next the G3LO capsule's nosecone must be closed, and from there the G3LO can continue its mission freely.

7. Auxiliary Propulsion Systems

The main attitude control of the vehicle will be from the gimbaling of the main propulsion system. There will be additional thrusters for finer adjustments of attitude and flight path trajectory. A trade study was performed on different reaction control systems utilized on similar launch vehicles. The systems that will be analyzed are advanced hydrogen/oxygen reaction control system utilizing current Space Shuttle data, the R-4D thrusters used on the Apollo and Space Shuttle missions, and the orbital maneuvering system's aft reaction control system. The weight, specific impulse, thrust, and propellant are all included in the trade study, which can be seen in the following table.

Table 15: Results of Auxiliary Propulsion Systems Weighted Values Trade Study

Weighted Values			
Items	ARCS	R-4D	OMS Aft Primary RCS
Weight	2	3	1
Isp	6	9	6
Thrust	4	4	6
Propellant	H/O	NTO/MMH	MMH/N2O4
Total	12	16	13

In the previous study, the ISP, thrust, and propellants were the criteria of most interest due to the necessity of weight reduction with limited tanks and total number of thrusters. The R-4D thrusters were found to be the most optimal of the analyzed systems due to the high ISP of 312s and thrust of 490 N [13]. Additionally, these thrusters utilize nitrogen tetroxide and hydrazine as the propellant with an oxidizer to fuel ratio of 1.65. Because of this, the R-4D thrusters were chosen for this design. Specifications for the R-4D thrusters can be seen below.

Table 16: Notable specifications for the R-4D thrusters to be used in the G3LATTO System

R-4D Specifications	
Weight (kg)	4
ISP	312
Thrust (N)	490
Propellant	NTO/MMH

These thrusters are ideal as the propellant used is hypergolic, requiring no ignition. There will be twelve thrusters arranged in the configuration seen in the figure below. This configuration will allow for roll control firing thruster tangent to the surface of the rocket. Additional attitude control can be achieved by the four thrusters perpendicular to the skin surface in the event of needed attitude control outside of thrust vector gimbaling from the main engines. These thrusters will utilize six degrees of freedom to maintain the intended trajectory. Additionally, this design does not call for ullage motors for use in settling propellant in tanks. The NTO/MMH tank is configured in a securely divided manner, in order to preserve radial space in the second stage structure while ensuring that the hypergolics do not mix unintentionally. The total wet mass of the auxiliary propulsion system including the propellant and tank is 26,400 kg.

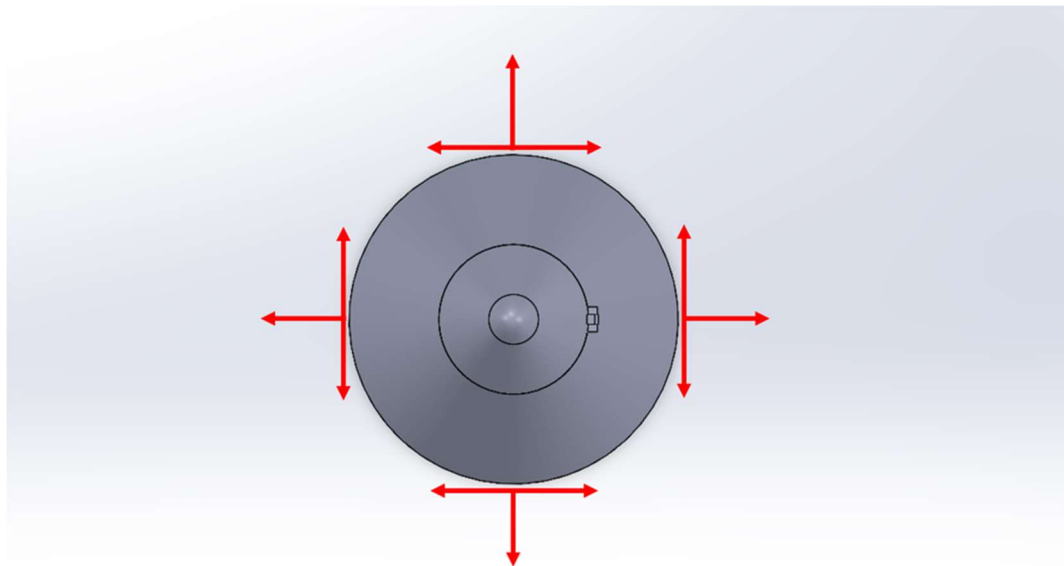


Figure 21: Auxiliary propulsion system vector control diagram

8. Liquid Propellant Tank Pressurization

As the G3LATTO's first and second stage main engines are burned, the liquid propellant tanks will need to remain pressurized as the propellant is drained. The G3LATTO rocket's first stage will accomplish this for its cryogenic liquid methane and liquid oxygen tanks by recycling boil-off gases [14]. This requires the redirection of evaporated methane and oxygen gas back into the top of their respective tanks to maintain overall tank pressurization. Utilizing these evaporated vapors for cryogenic tank pressurization is a highly efficient and practical process because no additional gas must be stored and carried by the launch system, making these types of systems weigh significantly less than other pressurization systems. The cold vapors can also act as a coolant to help maintain the cryogenic conditions within the propellant tanks.

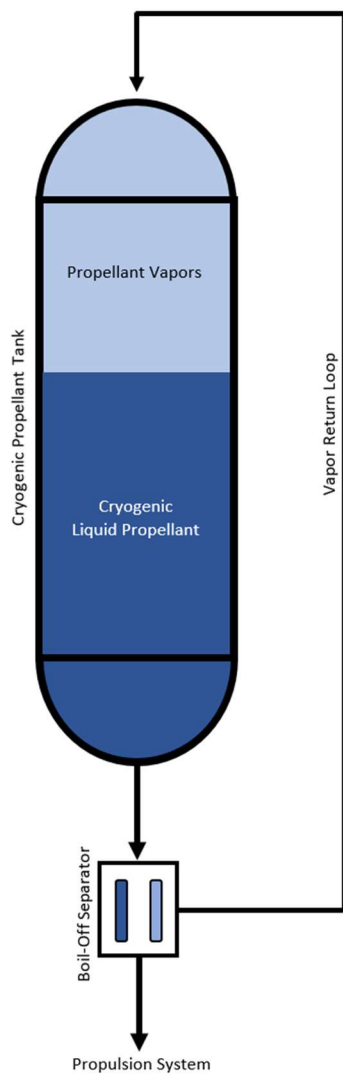


Figure 22: Cryogenic tank self-pressurization system diagram

The rocket's second stage will use a similar system for its cryogenic liquid oxygen tank; however a different approach will be required for the RP-1 tank since the propellant is non-cryogenic. The boiled-off vapors will not be sufficient to maintain tank pressurization, so another gas must be stored and carried to pump into the RP-1 tank as it drains. Helium is an ideal choice for this role since it is both lightweight and inert and has a proven track record of successful deployment in launch vehicles such as the Space Shuttle [14]. Similar to the cryogenic propellant tanks, the helium will be allowed to enter the top of the RP-1 tank as the propellant is expended in order to maintain tank pressurization.

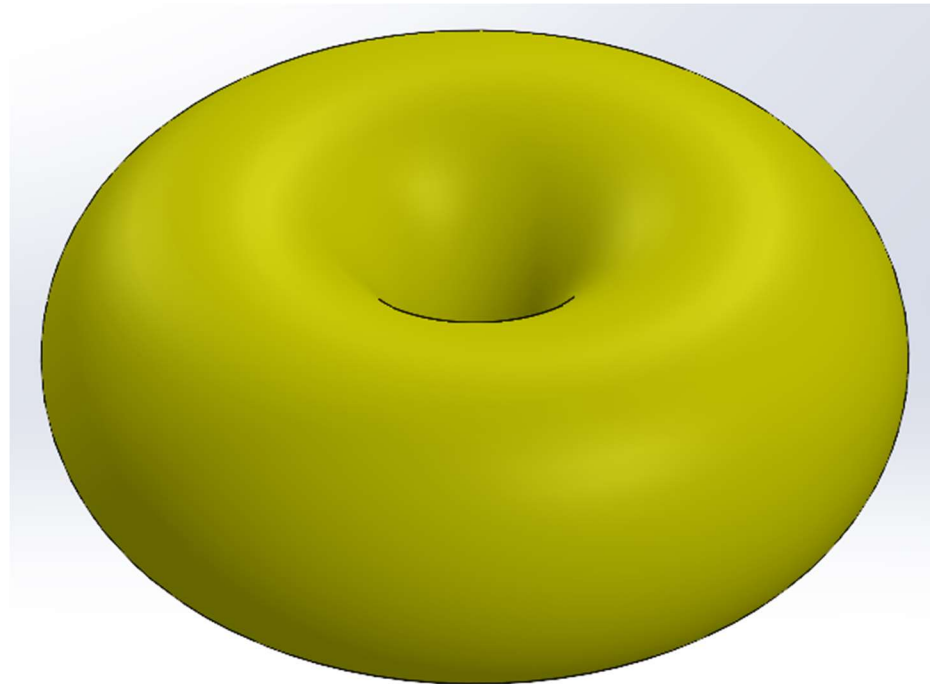


Figure 23: Helium tank for RP-1 tank pressurization system

With both systems, the pressurant will be fed into the propellant tanks from the top. This arrangement is beneficial because it helps mitigate slosh within the tanks as the vehicle's acceleration changes.

9. Structural Design

9.1. Vehicle Stability

Calculating the center of gravity (CG) and center of pressure (CP) are crucial for determining the stability of the vehicle. Since the rocket will rotate around the center of gravity, the net air pressure needs to be behind the CG such that the resulting force from the air stream will be in the opposite direction of the rotation. If the CP is too far in front of the CG, the vehicle will not be as stable, and any disturbance could cause it to lose control. The CG was calculated using the equation below.

$$CG * W = d_n w_n + d_b w_b + d_e w_e \quad (Eq. 9)$$

Where d is the location of the local centroid, w is weight of the part, W is the weight of the entire vehicle, and the subscript n is nosecone, b is body, and e is engine. The center of gravity for the entire launch vehicle was calculated from the top of the nose cone to be 34.25 m wet and 21.79 m dry.

Next, the CP was calculated using the following equation:

$$CP * A = d_n a_n + d_b a_b + d_e a_e \quad (Eq. 10)$$

Where a is now the surface area of the part and A is the total surface area of the vehicle. It is important to note that this is a simplified method for calculating the CP and a more accurate approach is used in Section 10.3. From this method, the center of pressure was determined to be 36.47 m from the nose cone. Therefore, the difference between the two was 2.22 m when wet and 14.68 m when dry. Since an increase in the distance leads to a more stable vehicle, the launch vehicle will become more stable as the propellant is burned.

9.2. Structural Methodology

The G3LATTO Vehicle will use a series of four circumferentially spaced stringers over the length of both the 0th + 1st stage and the 2nd stage. This will support the overall stacked structure of the vehicle and ensure the rigidity of the overall structure throughout the entire ascent phase. Additionally, these stringers support the tanks, serving as a mount to keep the tanks static within the vehicle during flight. The tank mounts are to be manufactured in halves so the tanks can be laid inside before the whole structure is secured together. The tanks will be a combination of capsule-shaped and spherical tanks, with the semi-spherical caps of the capsule-shaped tanks having the same radius as the cylindrical portion of the tank to ensure ideal design. The tanks will be equipped with internal slosh baffles in order to aid in preventing propellant slosh in flight.

9.3. Materials

9.3.1. Material Trade Study Overview

To select materials for the different components of the design, it was deemed necessary to conduct trade studies to find the appropriate material for each component. The materials that were considered were Aluminum 2024-T4 [15], Aluminum A2219-T62 [16], Steel (AISI 4140) [17], Titanium [18], Mild/Low Carbon Steel (AISI 1018) [19], and Aluminum 6061-T6 [20]. The properties of each material were assembled into a table of values, and a set of normalization values was generated to better compare the benefits and detriments of each material. These were combined into a table of unweighted values to be weighted on a component basis. The tables of actual, normalization, and unweighted values can be seen below. In the following sections, tables containing weighting factors and the final weighted values result will be detailed for each considered structural component.

Table 17: Properties of materials considered for G3LATTO Structural Design

Items	Aluminum 2024-T4	Aluminum A2219- T62	Steel (AISI 4140)	Titanium	Mild/low Carbon Steel (AISI 1018)	Aluminum 6061-T6
Corrosion Resistance	Low	Med	High	High	High	High
Density (lb/in³)	0.1	0.103	0.284	0.163	0.284	.0975
Cost	4	4	4	10	4	3
Yield Strength (psi 10³)	42	42	60.2	20.3	53.7	56
Thermal Expansion Coefficient (micro in/in- F)	12.9	12.4	6.78	4.94	6.39	13.1
Thermal Conductivity (BTU-i/hr- ft²-F)	840	833	296	118	360	1160

Table 18: Normalization values for materials considered for G3LATTO Structural Design

Items	1	2	3	4	5	6
Corrosion Resistance	Poor	Low	Low-Med	Med	Med-High	High
Density (lb/in³)	>0.25	>0.225	>0.2	>0.15	>=0.1	<0.1
Cost	>3000	>2000	>900	>700	>250	<250
Yield Strength (psi 10³)	<10	<20	<40	<50	<60	>60
Thermal Expansion Coefficient (micro in/in-F)	>13	>12	>10	>6.5	>5	<5
Thermal Conductivity (BTU-i/hr-ft²-F)	<200	<300	<400	<800	<1000	>1000

Table 19: Unweighted values for materials considered for G3LATTO Structural Design

Items	Aluminum 2024-T4	Aluminum A2219	Steel (AISI 4140)	Titanium	Mild/low Carbon Steel (AISI 1018)	Aluminum 6061-T6
Corrosion Resistance	2	4	6	6	6	6
Density	5	5	1	4	2	6
Cost	3	6	4	1	5	4
Yield Strength	4	4	6	3	5	5
Thermal Expansion Coefficient	2	2	4	6	5	1
Thermal Conductivity	5	5	2	1	3	6

9.3.2. Propellant Tanks

The weighting factors and final weighted values result can be seen in the tables below.

Table 20: Weighting factors for materials considered for propellant tank design

Item	Factor	Reason
Corrosion Resistance	3	Material needs to withstand corrosion from the fuel/oxidizer.
Density	6	The material needs to be lightweight ease take off and save on costs.
Cost	3	Quality is more important than cost.
Yield Strength	4	Strength is important to withstand strong forces, but a good structural design can compensate for strength.
Thermal Expansion Coefficient	4	There will be a lot of temperature variation in space.
Thermal Conductivity	2	The tanks themselves should not reach high temperatures.

Table 21: Result of weighted values study for materials considered for propellant tank design

Items	Aluminum 2024-T4	Aluminum A2219	Steel (AISI 4140)	Titanium	Mild/low Carbon Steel (AISI 1018)	Aluminum 6061-T6
Corrosion Resistance	6	12	18	18	18	18
Density	30	30	6	24	12	36
Cost	9	18	12	3	15	12
Yield Strength	16	16	24	12	20	20
Thermal Expansion Coefficient	16	16	24	12	15	15
Thermal Conductivity	10	10	4	2	6	12
Total	87	102	88	71	86	113

As can be seen from the above table, Aluminum 6061-T6 was chosen for the propellant tanks due to its high strength to low weight, as well as its reasonable cost.

9.3.3. Skin and Structural Components

Table 22: Weighting factors for materials considered for skin and structural component design

Item	Factor	Reason
Corrosion Resistance	1	Corrosion not very important for LEO
Density	6	The material needs to be lightweight ease take off and save on costs.
Cost	3	Quality is more important than cost.
Yield Strength	4	Strength is important to withstand strong forces, but a good structural design can compensate for strength.
Thermal Expansion Coefficient	6	There will be a lot of temperature variation in space.
Thermal Conductivity	4	The skin will face high temperatures when exposed in the sun.

Table 23: Result of weighted values study for materials considered for skin and structural component design

Items	Aluminum 2024-T4	Aluminum A2219	Steel (AISI 4140)	Titanium	Mild/low Carbon Steel (AISI 1018)	Aluminum 6061-T6
Corrosion Resistance	2	4	6	6	6	6
Density	30	30	6	24	12	36
Cost	9	18	12	3	15	12
Yield Strength	16	16	24	12	20	20
Thermal Expansion Coefficient	12	12	24	36	30	6
Thermal Conductivity	20	20	8	4	12	24
Total	89	100	80	85	95	104

From this trade study, it was determined that Aluminum 6061-T6 was the best option for the material of the skin and structural components.

9.3.4. Engine Mounts

Table 24: Weighting factors for materials considered for engine mount design

Item	Factor	Reason
Corrosion Resistance	1	Corrosion not very important for LEO
Density	5	The material needs to be lightweight ease take off and save on costs.
Cost	3	Quality is more important than cost.
Yield Strength	6	The strength of the material is the most important near the engines due to the very large thrust force.
Thermal Expansion Coefficient	4	There will be a lot of temperature variation in space.
Thermal Conductivity	5	The engine mounts will face high temperatures.

Table 25: Result of weighted values study for materials considered for engine mount design

Items	Aluminum 2024-T4	Aluminum A2219	Steel (AISI 4140)	Titanium	Mild/low Carbon Steel (AISI 1018)	Aluminum 6061-T6
Corrosion Resistance	2	4	6	6	6	6
Density	25	25	5	20	10	30
Cost	9	18	12	3	15	12
Yield Strength	24	24	36	18	30	30
Thermal Expansion Coefficient	8	10	16	24	20	4
Thermal Conductivity	25	25	10	5	15	30
Total	93	106	85	76	96	112

As can be seen from the above table, Aluminum 6061-T6 was chosen for the engine mounts for similar reasons as the propellant tanks, namely its high strength to low weight, as well as its reasonable cost.

9.4. Structural Manual Calculations

The primary structure of the vehicle is from the pressurized tanks. After the tank sizing for propellant volumes and masses, this data can be used to find the thickness of the tanks which will enable analysis of the substructure. The calculations used to find the wall thickness is the same for each tank. First, the ullage pressure of the tank needs to be known, for this, data from previous missions and flights will be used as a measure for the pressurization of each of the tanks [21]. Utilizing the volume of propellant as well as known diameter of the pressure vessel, the height of the propellant in the tank can be found. The hydrostatic pressure of the fluid can be found from the product of propellant density, acceleration due to gravity, and height of propellant in tank from earlier. Now, the thickness of the pressure vessel can be found. This is done by assuming the internal pressure to be the ullage pressure and hydrostatic pressure, and the hoop stress as the tensile strength of the material of the tank, Aluminum 6061-T6. The hoop stress can be seen from the following relation:

$$\sigma_H = \frac{Pr}{t} \quad (\text{Eq. 11})$$

Where P is the internal pressure, r is the radius of the pressure vessel, and t is the wall thickness of the pressure vessel. From this, the thickness can be solved. Then the actual hoop stress can then be solved for with the thickness of the tanks after the factor of safety has been added. Additionally, the longitudinal stress of the tanks can be found using the relation:

$$\sigma_L = \frac{Pr}{2t} \quad (\text{Eq. 12})$$

This process is repeated for each tank to obtain the wall thickness of each tank and internal stresses. Further analysis needs to be done utilizing the wall thickness to obtain structural masses to simulate interstage structural loadings. Below is a table of values for each tank which includes wall thickness and internal stresses. In the table, the wall thickness has an included factor of safety of 1.5.

Table 26: Results of Manual Calculations for G3LATTO System Propellant Tank Structures

Tank	Wall Thickness (mm)	Hydrostatic Pressure (MPa)	Hoop Stress (MPa)	Longitudinal Stress (MPa)
CH4 (0th + 1st Stage)	6.359	0.376	250.835	125.418
LOX (0th + 1st Stage)	10.481	0.619	271.188	135.594
RP1 (2nd Stage)	2.907	0.300	204.484	102.242
LOX (2nd Stage)	6.652	0.481	234.419	117.209
Helium	35.066	2.899	297.283	148.642
NTO/MMH	1.735	0.143	166.257	83.128

No stresses exceed the maximum yield strength for this alloy of aluminum, 470 MPa. Thus, the tank geometry should be able to withstand the loadings. The helium tank has much larger wall thickness, which is due to the large hydrostatic pressure, ensuring that the propellant tank pressure is larger than that of the chamber pressure. Additionally, the buckling of the tank support structure can be analyzed. This will be done by utilizing the critical buckling formula:

$$P_{crit} = \frac{\pi^2 EI}{L^2} \quad (Eq. 13)$$

The analysis will be made for the stringers on each of the fuel tanks for the first and second stage. This is due to the arrangements of the tanks, allowing for the analysis of the tank structure with the larger loads. The stringer geometry is used to calculate the moment of inertia in the final analysis. The critical buckling is for two possible modes of failure – buckling in the x-direction and z-direction. Aluminum 6061-T6 is used as the material for the stringers. To know if the structure will buckle, the second stage is loaded with the payload and first stage oxidizer and oxidizer tank mass while the first stage is the total weight of the second stage, payload and first stage oxidizer mounts. Both are analyzed using the maximum launch accelerations and tank structure top area to obtain the launch loadings. The table below shows the critical buckling as well as launch loadings for the stringers on the 0th + 1st and 2nd stage tank structures. Note that these calculations are an approximation, as the full geometry of the stringers cannot be encapsulated within this equation. A more detailed analysis can be found in the following section.

Table 27: Stringer buckling and launch loading

Stage	Stringer X-Buckling (MPa)	Stringer Z-Buckling (MPa)	Launch Loading (MPa)
0th + 1st	2.666	4.166	1.68
2nd	30.994	78.588	0.736

9.5. Finite Element Analysis

In order to verify that the structural design of the vehicle was sufficient, Finite Element Analysis was conducted within Solidworks. The inertial relief method was used to perform the FEA, since inertial relief is used for accelerating, free bodies that are not fixed in space. The loads applied were the inertial loadings, which included the maximum force due to gravity and the mass of the vehicle including the payload. Along with the inertial loadings, the max thrust and max dynamic pressure were applied to simulate the largest possible loads the vehicle would experience. Due to the small thicknesses of the propellant and oxidizer tanks, they were not able to mesh correctly while analyzing the full stack assembly. The tanks were analyzed individually, but their masses were still included within the full stack analysis.

The figures below represent the pseudocolor plots for the displacement and von Mises stress. The left image of each figure has the skin hidden within Solidworks to better visualize the internal structure. The analysis showed a maximum displacement of 6.47 mm and a maximum stress of 18.78 MPa, verifying that the structural components of the vehicle will be capable of sustaining the largest loading conditions it will face.

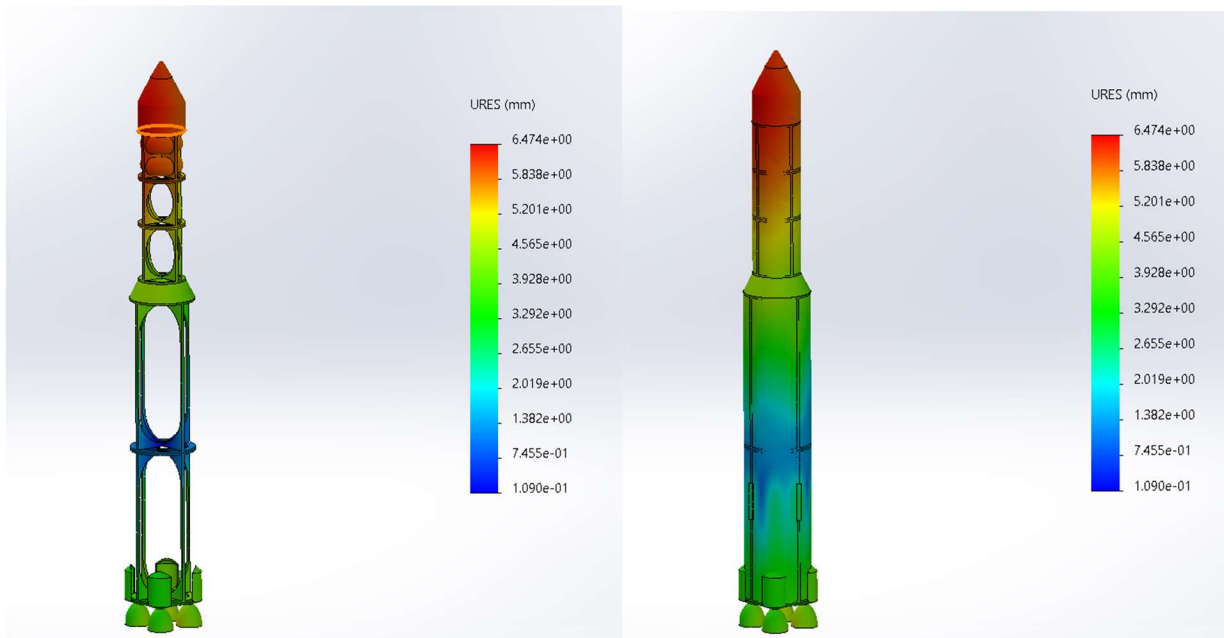


Figure 24: G3LATTO System Displacement Plot

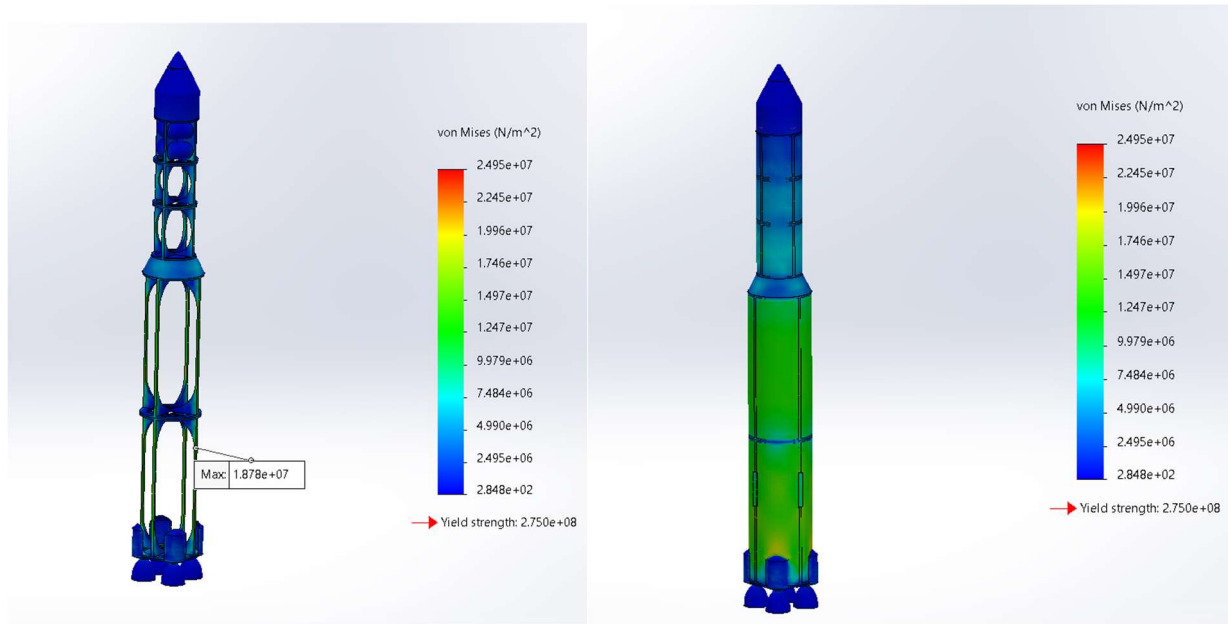


Figure 25: G3LLATO System von Mises Stress Plot



Figure 26: Structural components undergoing largest loading conditions

In the figure above, it is noted that the stringers carry the largest portion of the load. With this information, it would be reasonable to suggest that the other structural components could be modified such that the overall structure is lighter and still be able to remain intact. However, it is best that the stringers remain as designed, since they are shown to be the most responsible for carrying the bulk of the loading.

Due to the limited capabilities to analyze the full stack, some individual components need to be analyzed further to ensure safety, primarily the propellant tanks for each stage. There are three main assumptions to make, namely fixtures, loadings, and meshing. For fixtures, the tanks were fixed by the projected centerline axis and edges. The constraints were for the rotation about and translation from the centerline axis. It was not constrained by expansion. The loadings were a 3g maximum acceleration on the structure of the tank, each tank's respective internal pressure, and the mass of each tank's respective fuel or oxidizer at the maximum acceleration. Due to the thin walls of the pressure vessel, a mesh control had to be added to ensure the finest meshing in Solidworks for the analysis. Below are figures for the displacements and stress on the propellant tanks, in order to analyze the loadings for the propellant tanks.

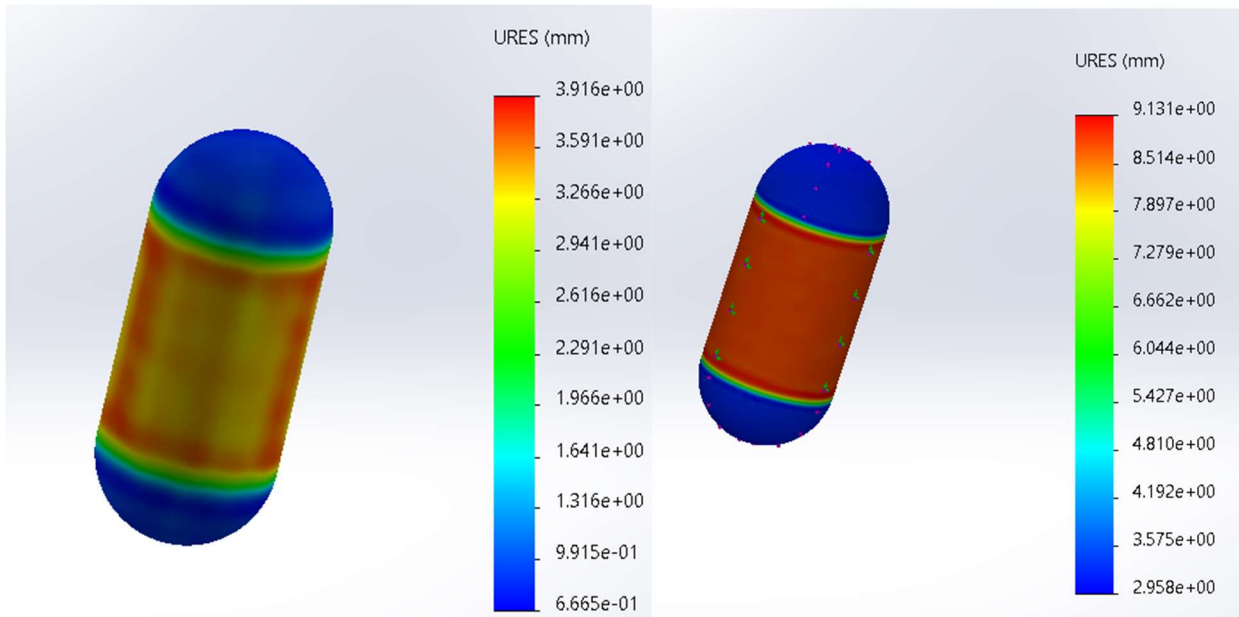


Figure 27: 0th + 1st stage LOX (left) and LCH₄ (right) tank displacements

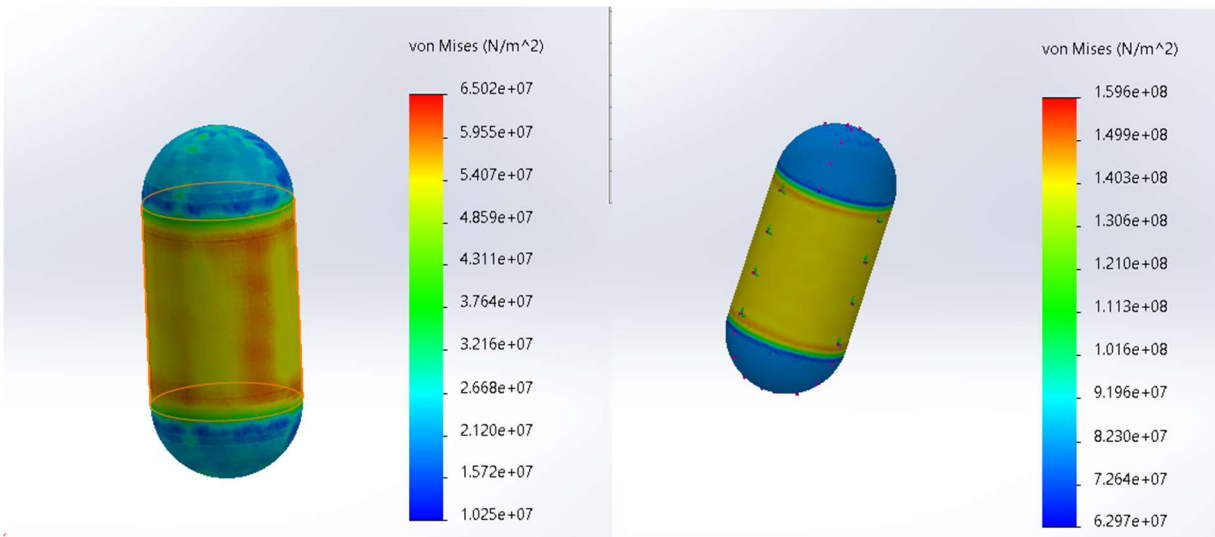


Figure 28: 0th + 1st stage LOX (left) and LCH₄ (right) tank von Mises stresses

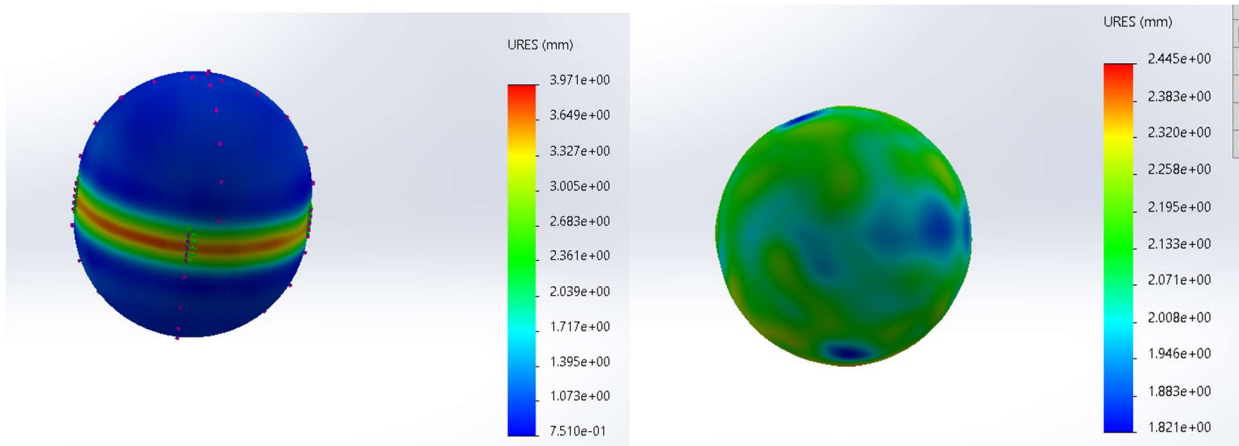


Figure 29: 2nd stage LOX (left) and RP-1 (right) tank displacements

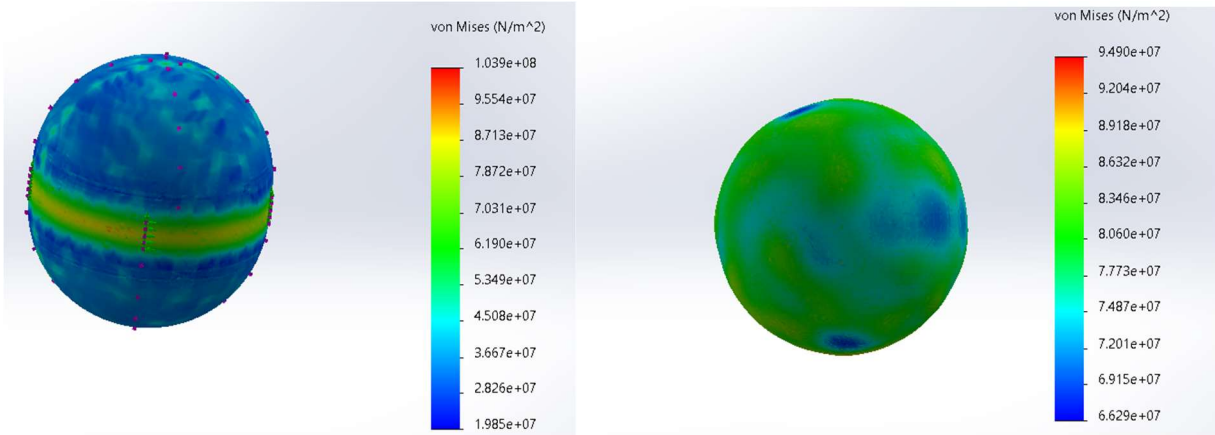


Figure 30: 2nd stage LOX (left) and RP-1 (right) tank von Mises stresses

Additionally, it is beneficial to analyze the components that carry majority of the loadings – the tank mounts. To analyze the tank mounts, the inertial solver is used to simulate loadings during launch. For each mount. The masses of the payload, upper mounts, tanks, and propellant are included with the 3g acceleration on the upper surface of the tank mounts. Additionally, the maximum thrust is applied to the lower surface of the mounts. The figures below show the analysis of the tank mounts.

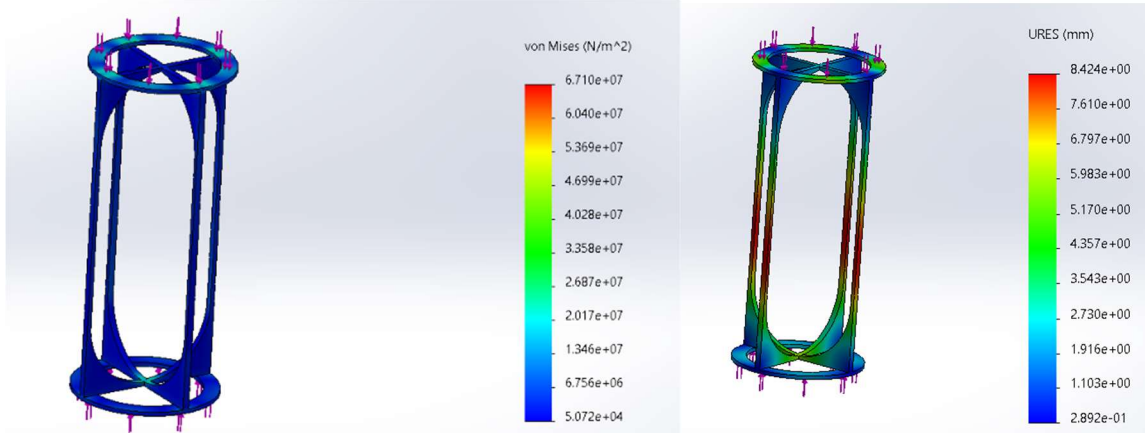


Figure 31: 0th + 1st stage LOX mount von Mises stresses (left) and displacements (right)

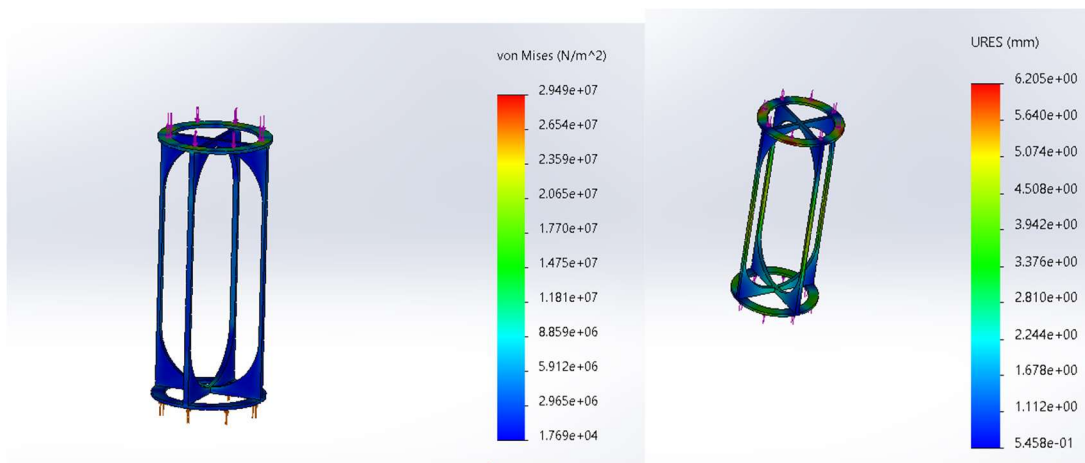


Figure 32: 0th + 1st stage LCH₄ mount von Mises stresses (left) and displacements (right)

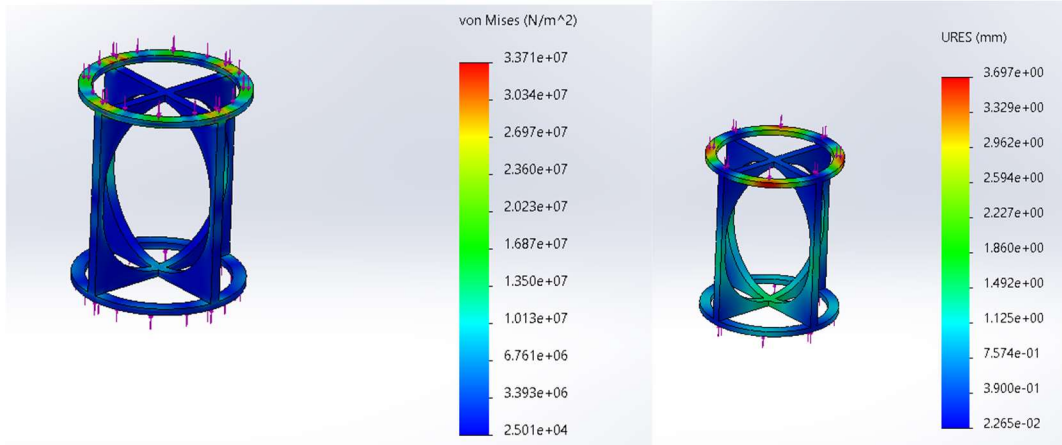


Figure 33: 2nd stage LOX mount von Mises stresses (left) and displacements (right)

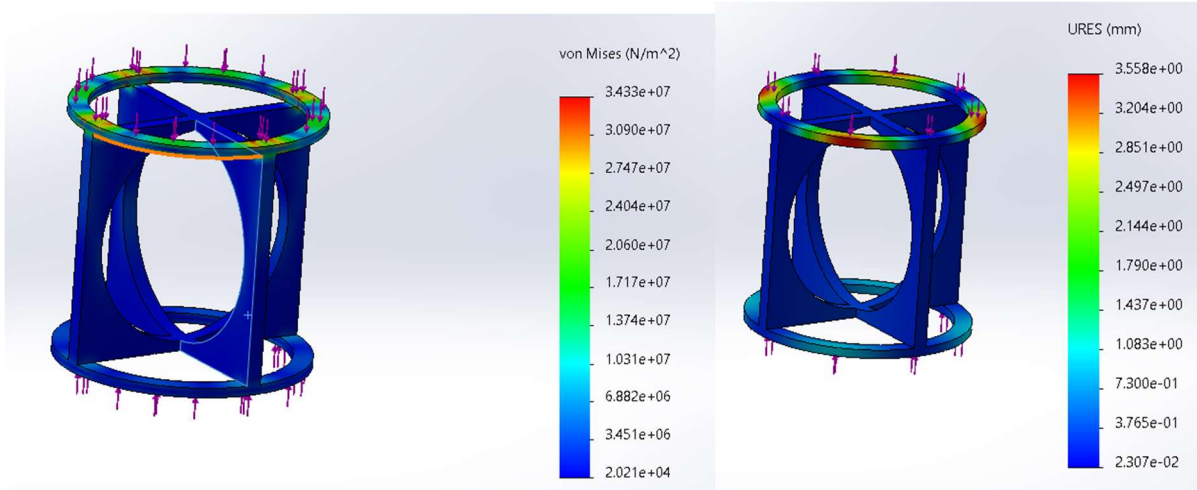


Figure 34: 2nd stage RP-1 mount von Mises stresses (left) and displacements (right)

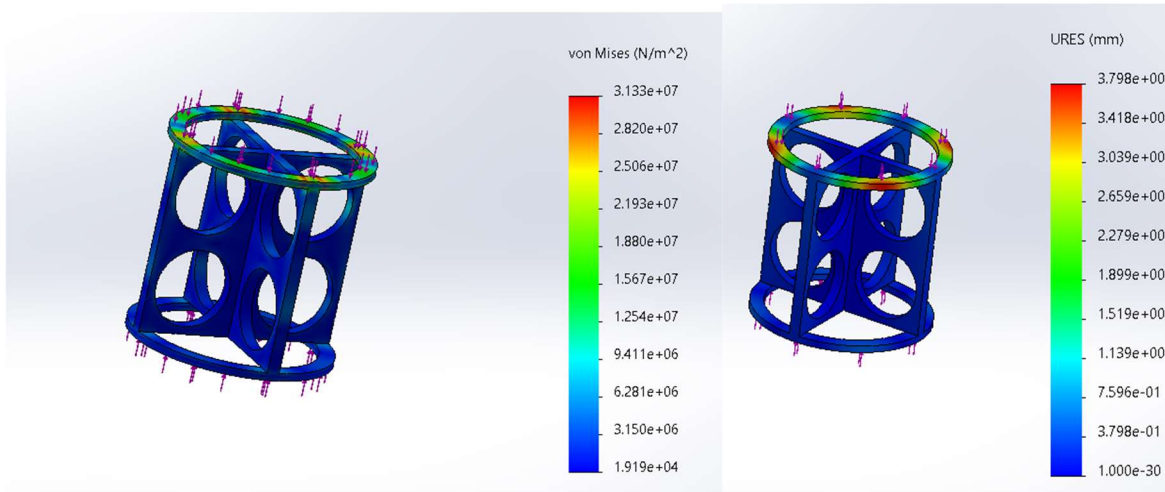


Figure 35: 2nd stage auxiliary tank mount von Mises stresses (left) and displacements (right)

In order to better analyze this data, the table below includes each component that was analyzed along with its respective minimum factor of safety, maximum displacement, and maximum stress.

Table 28: Component factors of safety, maximum displacement, and maximum stress.

Component	Minimum Factor of Safety	Maximum Displacement (mm)	Maximum Stress (Pa)
Stage 1 LOX Mount	4.1	8.424	6.71E+07
Stage 1 Prop Mount	9.1	6.205	3.02E+07
Stage 1 Engine Mount	3.4	12.97	8.06E+07
Stage 1 LOX Tank	3.4	4.943	8.16E+07
Stage 1 Prop Tank	1.7	9.131	1.60E+08
Stage 2 LOX Mount	8.2	3.697	3.37E+07
Stage 2 Prop Mount	8	3.558	3.43E+07
Stage 2 LOX Tank	2.6	3.971	1.04E+08
Stage 2 Prop Tank	2.9	2.445	9.49E+07
Stage 2 AUX Mount	8.8	3.798	3.13E+07

As detailed previously, the yield strength of Aluminum 6061-T6 is 2.75×10^8 Pa. There are no members where the von Mises stress reaches that of 2×10^8 Pa. Additionally, the lowest factor of safety of any component is 1.7 for that of the first stage propellant tank. For the mounts, which bear majority of the load, the factors of safety range upwards of 9.1 at the maximum possible loadings for the launch. It can be noted again that the stresses are slightly higher than that for the full stack. This is likely due to slightly inaccurate masses from above stages. This however does result in larger loadings to show the strength of the tank mounts. Thus, this ensures that the structures will endure the loadings.

9.6. Structural Design CAD Overview

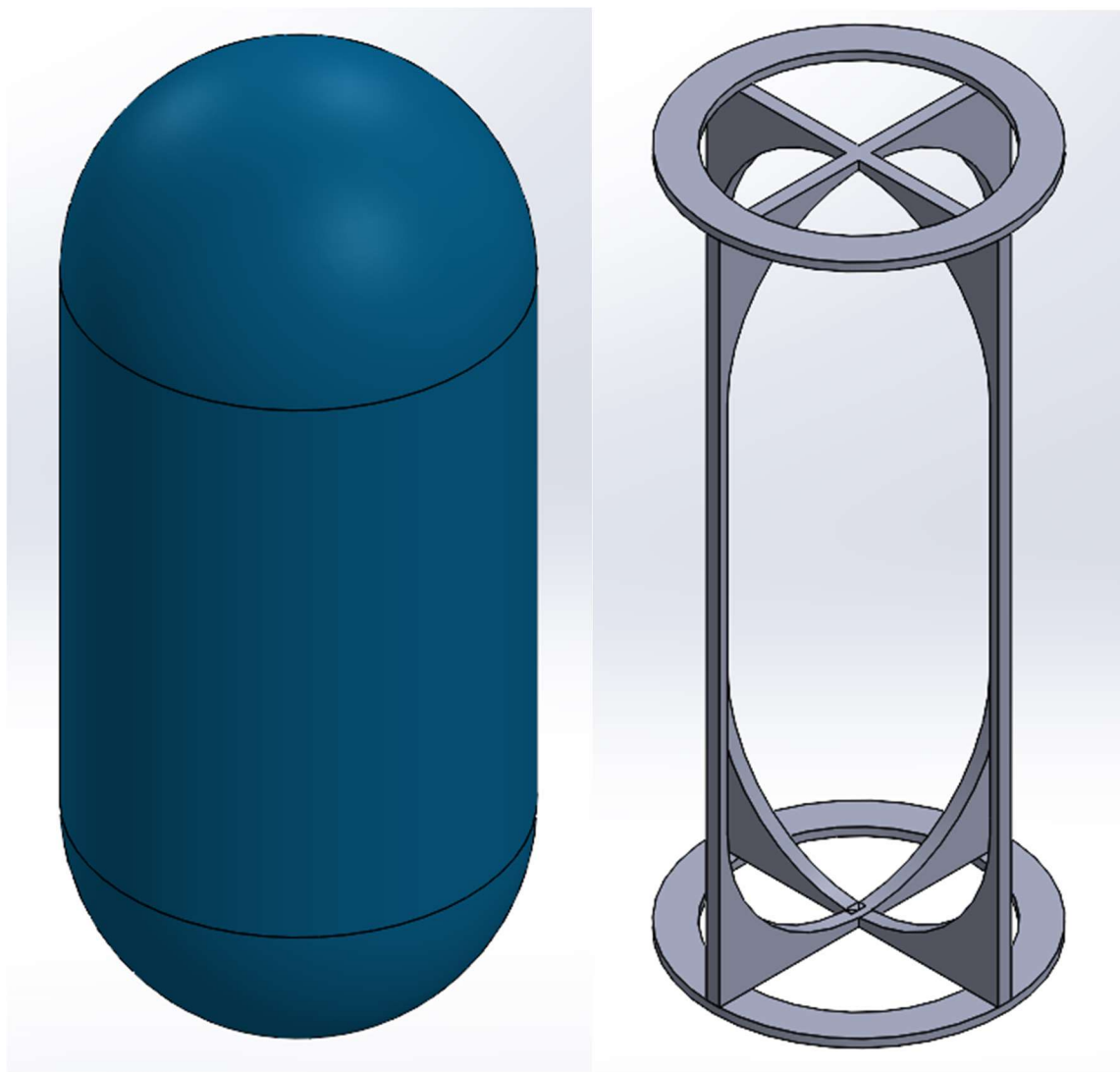


Figure 36: G3LATTO System 0th + 1st stage Oxidizer Tank (Left) and Oxidizer Tank Mount (Right)

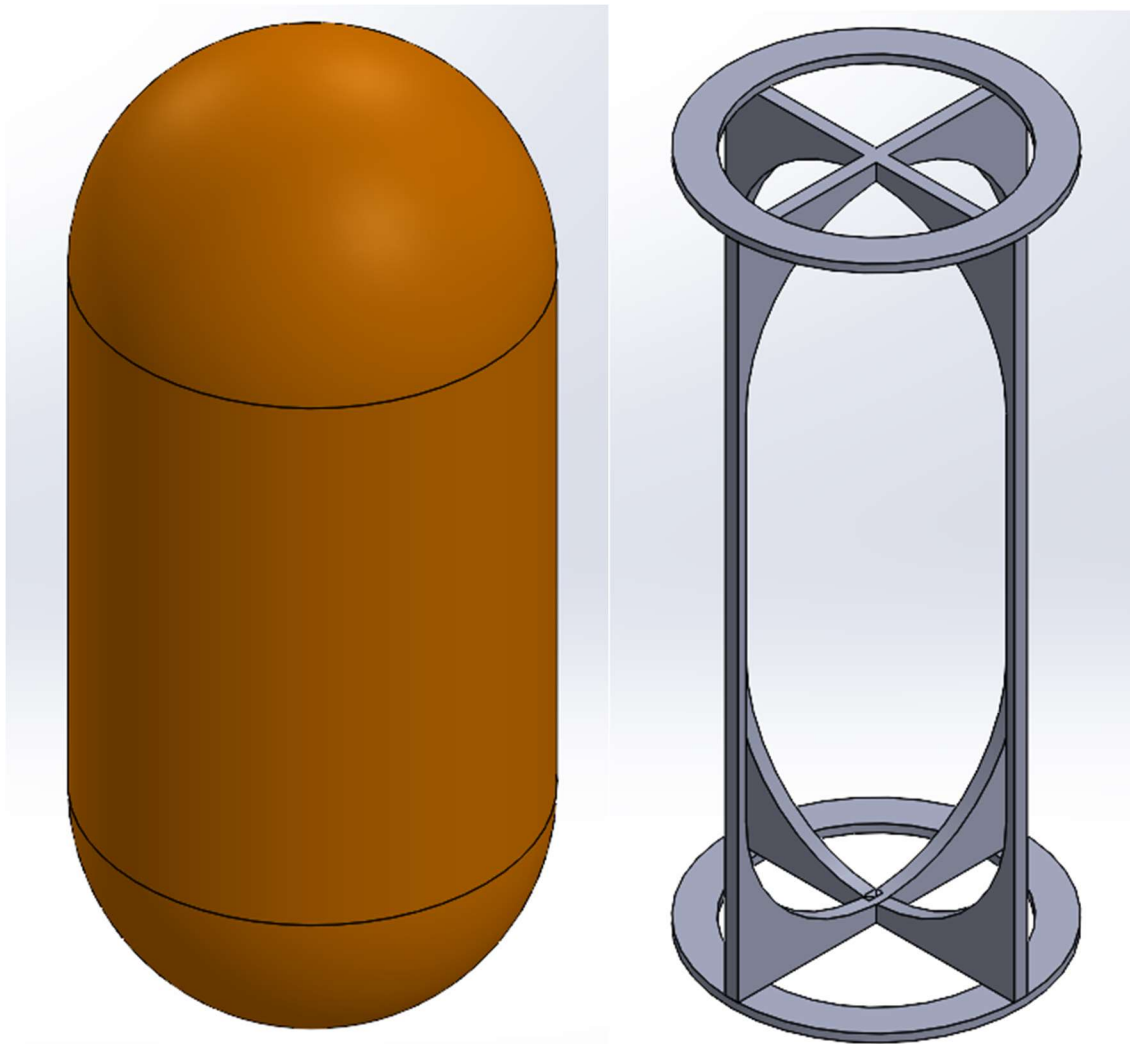


Figure 37: G3LATTO System 0th + 1st stage Fuel Tank (Left) and Fuel Tank Mount (Right)

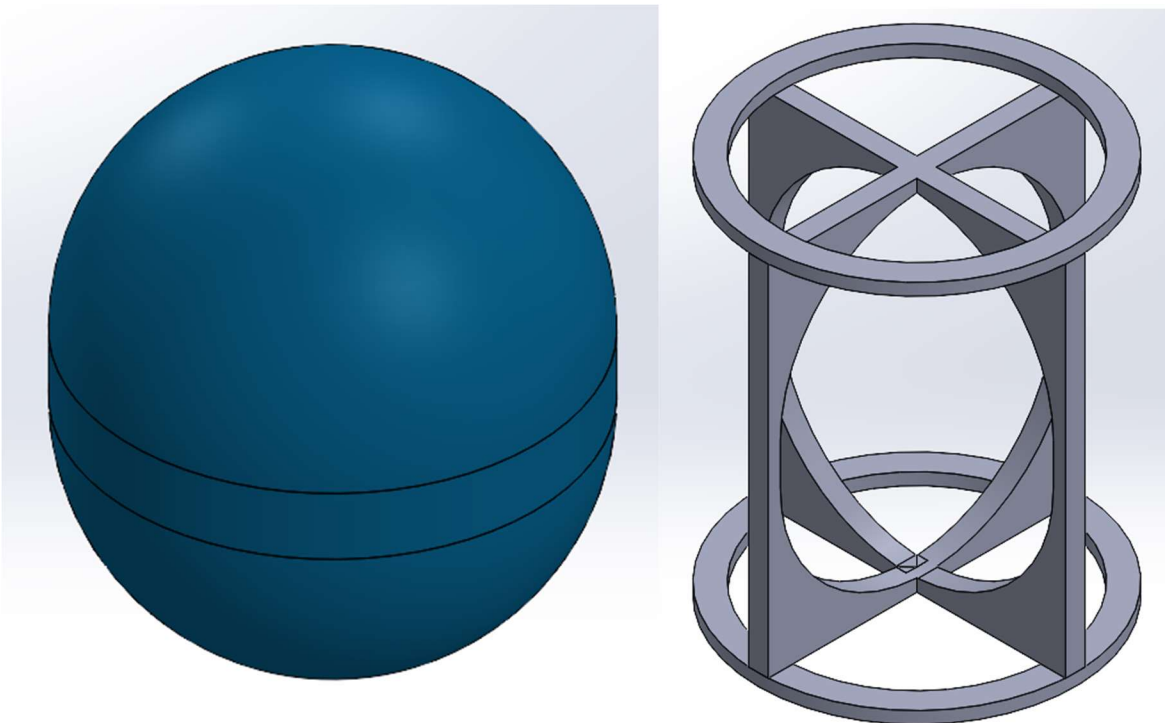


Figure 38: G3LATTO System 2nd stage Oxidizer Tank (Left) and Oxidizer Tank Mount (Right)

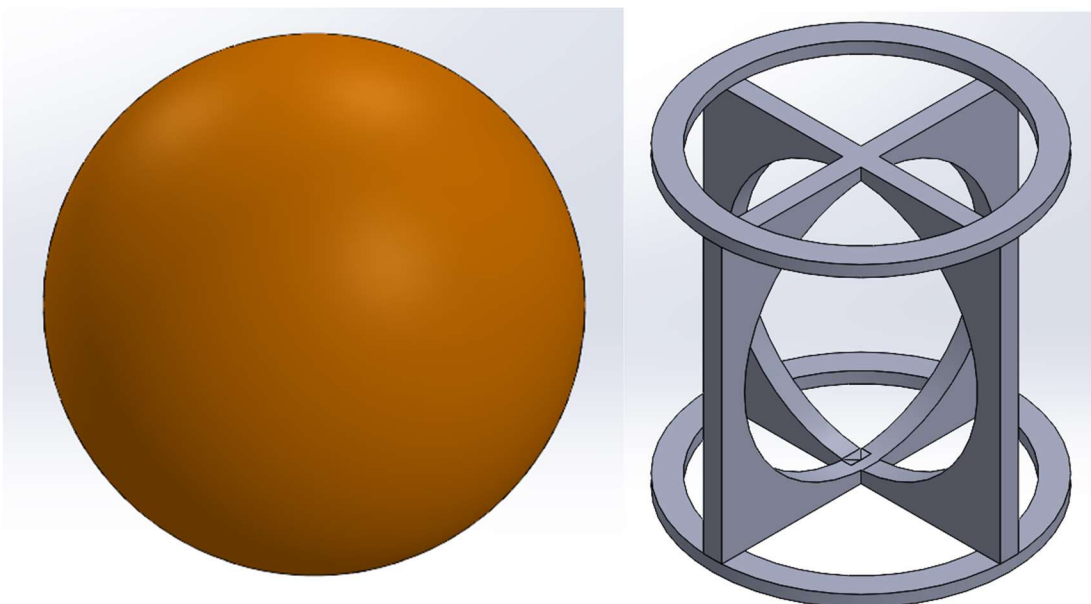


Figure 39: G3LATTO System 2nd stage Fuel Tank (Left) and Fuel Tank Mount (Right)

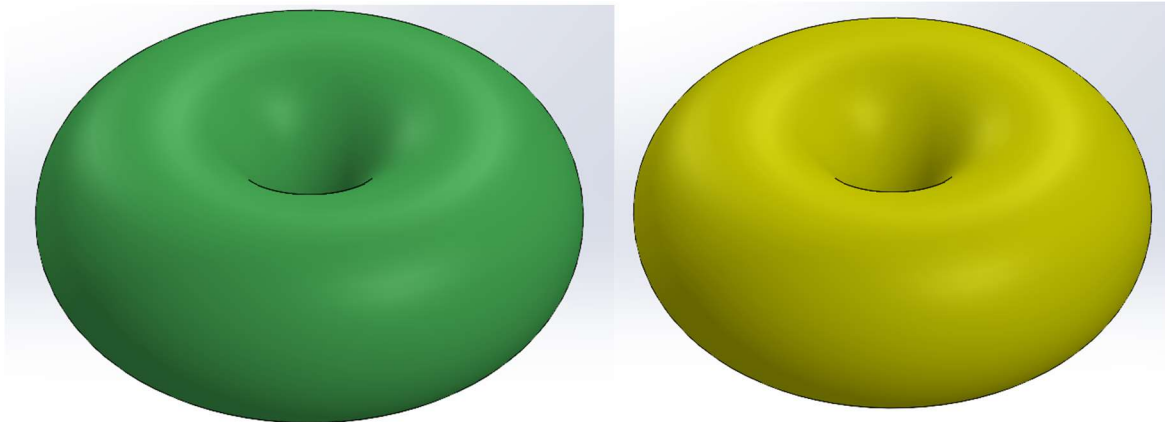


Figure 40: G3LATTO System NTO/MMH (left) and helium (right) tanks for auxiliary propulsion and tank pressurization

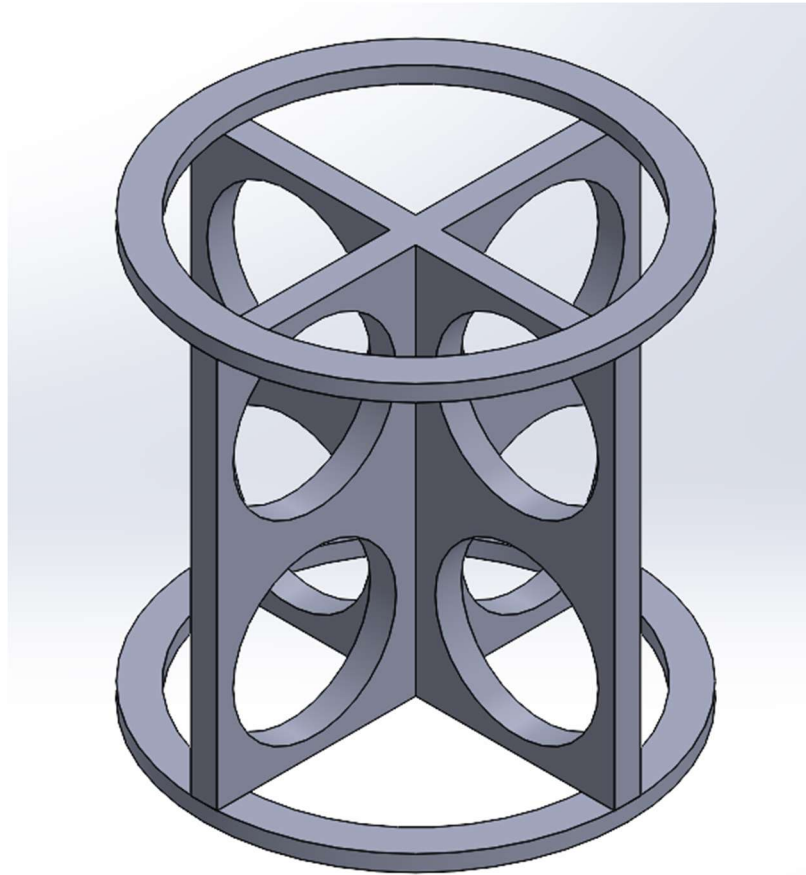


Figure 41: G3LATTO System NTO/MMH and helium tank mount

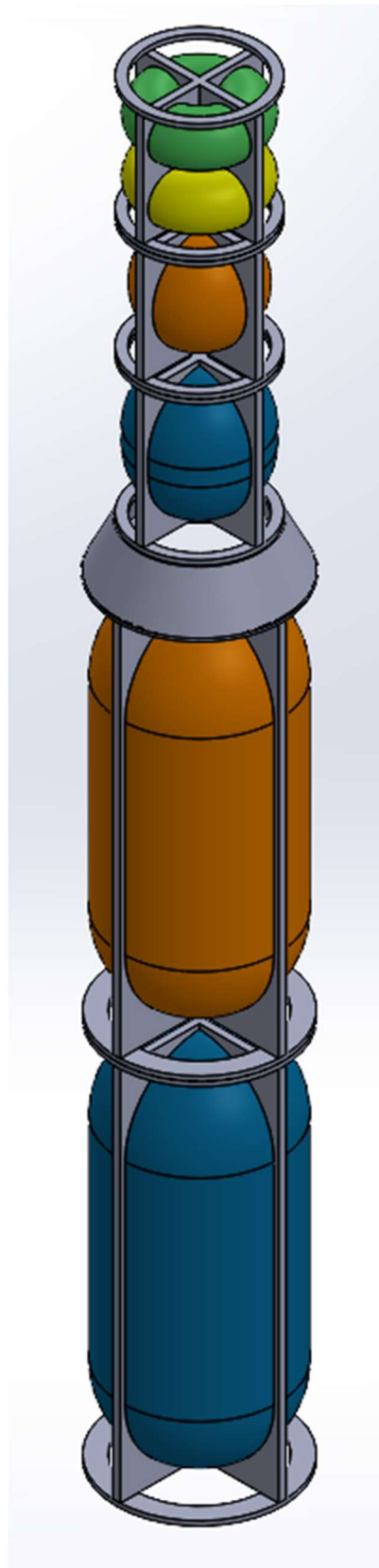


Figure 42: Assembled internal structure for all stages of the G3LATTO vehicle

10. Aerodynamic Analysis

10.1. Drag

As one of the fundamental aerodynamics forces, drag is present with any object moving through a fluid, rockets included. Thus, it is important to consider any delta-v losses that might be induced through drag on the vehicle. For the purposes of this cursory analysis, hand and MATLAB calculations based on a constant C_D will be done to get an idea of the magnitude of these losses.

For this preliminary analysis, a C_D of 0.27 is used based on historical rocket data from the NASA data on the Saturn C-1 rocket [7]. This coefficient can then be plugged into the equation:

$$D = 0.5 * C_D * S_{ref} * \rho * V^2 \quad (\text{Eq. 14})$$

Where D is the drag force, S_{ref} is the reference area of the rocket, ρ is the density of air, and V is the velocity of the rocket. An atmospheric model is utilized in order to provide accurate density numbers to provide a more accurate drag assessment. Since the drag is a function of density, it begins to fall off sharply as altitude increases. In the calculations, the drag peaked at around t+76 seconds after launch with a magnitude of just over 515kN at an altitude of 11 km and velocity of nearly 357.19 m/s. The total drag losses to delta v are calculated to be around 14 m/s.

According to the CFD calculations, at max q, the launch vehicle experiences a drag of 150kN. This is much less than expected when comparing to historical data and is potentially due to the much more aerodynamic shape of the nose when compared to some historical rockets. It could also be due to the limitations of the solver. The pressure distribution can be seen in Figure 43.

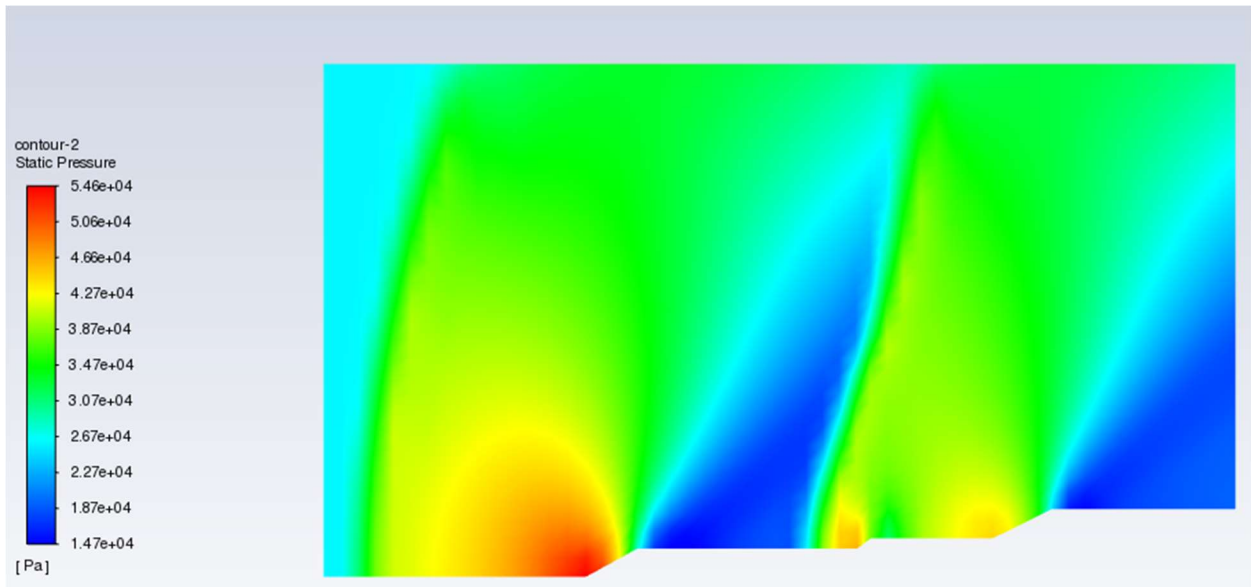


Figure 43: Pressure distribution over the vehicle and in the flowfield

10.2. Ascent Heating

The heating during ascent was calculated utilizing CFD analysis in ANSYS Fluent. The aerodynamic heating at max q was approximately 60 Kelvin above ambient. The heating was most intense in the conic sections at the nose, interstage, and booster as seen in Figure 44.

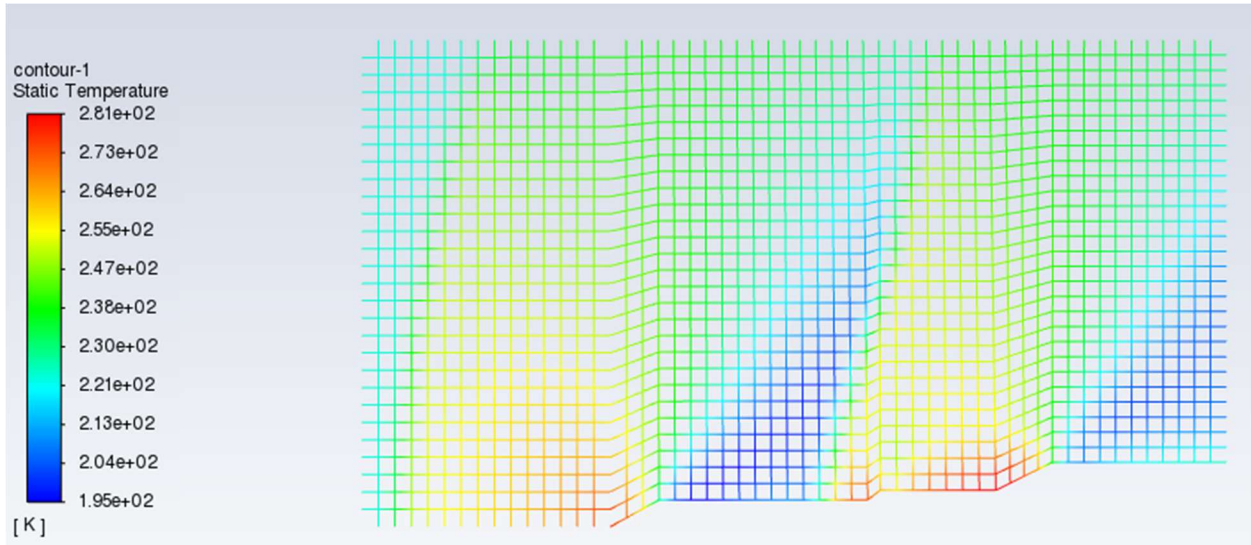


Figure 44: 2D CFD of the aerodynamic heating on the launch vehicle and flowfield

10.3. Center of Pressure

An important consideration for the stability of the rocket is the location of the Center of Pressure (CP). In order to ensure stable flight, it is recommended for the location of the CP to be at least one diameter behind the center of mass. The method developed by Barrowman is used to find the distance of the cp from the nose of the rocket:

$$\bar{X}_{cp} = \frac{C_N \bar{X}_N + C_{CS1} \bar{X}_{CS1} + C_{CS2} \bar{X}_{CS2}}{C_N + C_{CS1} + C_{CS2}} \quad (Eq. 15)$$

Where \bar{X}_N distance to the center of pressure of the nosecone, \bar{X}_{CS1} is the distance to the center of pressure for the conical shoulder separating the first and second stages, \bar{X}_{CS2} is the distance to the center of pressure of the second conical shoulder that is taken to be from where the tip of the SRB nosecone starts to where it ends, and the C_X values are the coefficients of pressure for each of the locations. As the SRB's won't be released until after the launch vehicle gets into the thinner portions of the atmosphere, the CP after their release won't be considered due to the negligible aerodynamic forces in the upper atmosphere. The calculations for the variables above can be seen below.

Nose:

$$\bar{X}_N = \frac{2}{3} * L_N = 3.66 \text{ m} \quad (\text{Eq. 16})$$

$$C_N = 2 \quad (\text{Eq. 17})$$

First Conical Shoulder (Second-to-First Stage Transition):

$$\bar{X}_N = X_{CS} + \frac{L_{CS1}}{3} \left[\frac{1 - \frac{d_{CS1,1}}{d_{CS1,2}}}{1 - \left(\frac{d_{CS1,1}}{d_{CS1,2}} \right)^2} \right] = 31.92 \text{ m} \quad (\text{Eq. 18})$$

$$C_{CS1} = 2 \left[\left(\frac{d_{CS1}}{d_R} \right)^2 - \left(\frac{d_R}{d_R} \right)^2 \right] = 1.72 \quad (\text{Eq. 19})$$

Second Conical Shoulder (First Stage Diameter-to-Booster Diameter Transition):

$$\bar{X}_N = X_{CS2} + \frac{L_{CS1}}{3} \left[\frac{1 - \frac{d_{CS2,1}}{d_{CS2,2}}}{1 - \left(\frac{d_{CS2,1}}{d_{CS2,2}} \right)^2} \right] = 49.28 \text{ m} \quad (\text{Eq. 20})$$

$$C_{CS} = 2 \left[\left(\frac{d_{CS}}{d_R} \right)^2 - \left(\frac{d_R}{d_R} \right)^2 \right] = 7.83 \quad (\text{Eq. 21})$$

With all of the variables calculated, the location of the cp can be found:

$$\bar{X}_{cp} = \frac{2 * 3.66m + 1.72 * 31.91m + 7.83 * 49.28m}{2 + 1.72 + 7.83} = 38.8m \quad (\text{Eq. 22})$$

Thus, the location of the CP is 38.8 meters from the nose of the launch vehicle.

10.4. Flight Dynamics Analysis

In addition to the temperature and pressure distributions, the distributions for the velocity and density were plotted. These reveal the shock waves that form in the flow in front of the nose and on the different conical transitions on the vehicle.

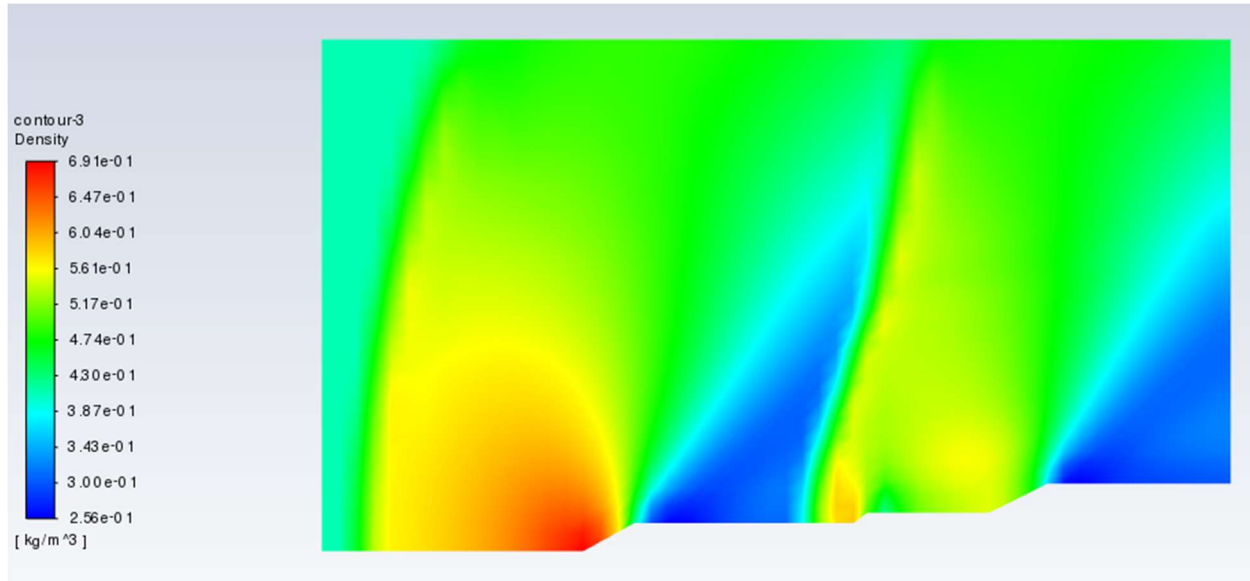


Figure 45: Density distribution over the vehicle and in the flowfield

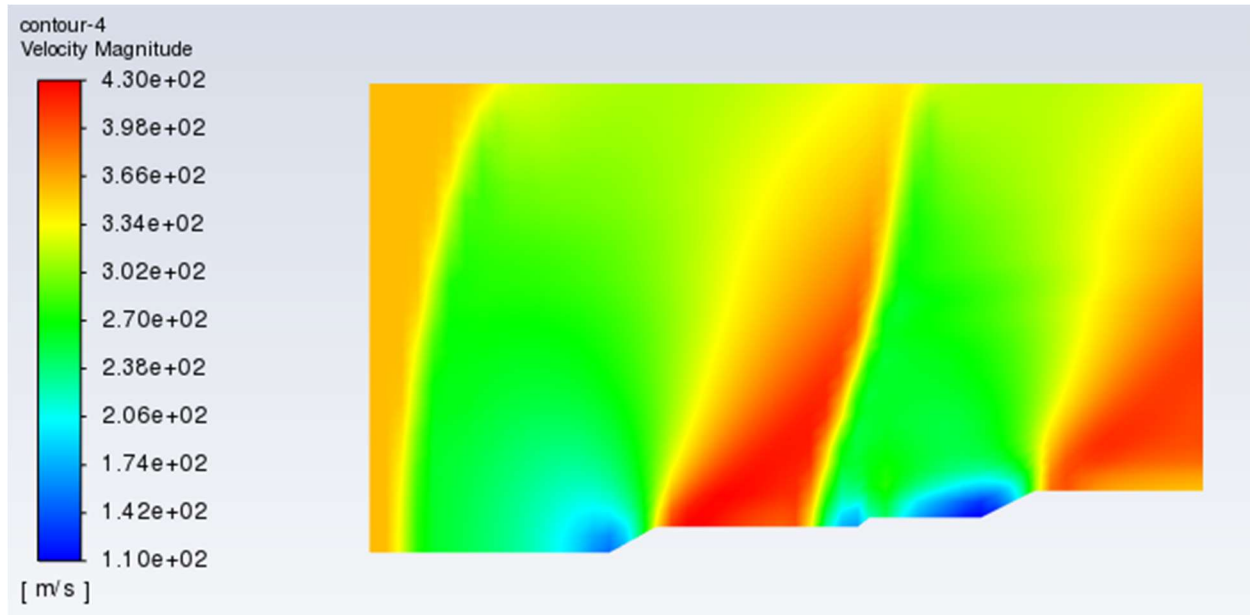


Figure 46: Velocity field around the vehicle

11. Electrical Systems

11.1. Power Supply

Modern spacecraft require the utilization of a wide variety of digital systems that all must have access to reliable power for the duration of the mission in order to function properly, and the G3LATTO launch vehicle is no exception. Long term energy production will not be required for G3LATTO's intended mission duration, so lithium-ion batteries will store all the power needed to operate the electrical systems for the duration of the mission. However, solar panels could be retrofitted to the G3LO capsule in the future to enable longer duration missions.

The lithium-ion batteries to be deployed in the G3LATTO are the Space Information Laboratories' 8S2P 52 Ah Spacecraft Batteries. These batteries will be used because they have a proven track record of successfully powering spacecraft from other launch providers such as United Launch Alliance. They also are relatively small and lightweight with a high energy density and are housed in rugged aluminum casings to prevent damage to the battery cells [22]. The manufacturer's specifications chart for this battery is shown below. The G3LO upper stage will carry 100 of these battery cells for a total battery capacity of 5 kWh.

Battery Specification	SIL 52 Ah 8S2P Li-Po Battery
Cell Chemistry	Ultra High Energy NMC Cell 243Wh/Kg
Voltage Range (J1 and J2 Out)	33.6 – 22.4 Vdc
Capacity (BOL)	52 Ah at C/2 continuous discharge 50 Ah at 1C continuous discharge
Cycle Life	25,000 Cycles to 80% capacity at C/2 discharge and charge, 20-30% DOD
Estimated Weight	26.2 lbs
Dimensions	14.0 inch (L) by 7.0 inch (W) by 5.5 inch (H)
Steady State Load	104A (2C)
Pulse Load	208A (4C), 10 Seconds
Telemetry and Monitoring	RS-422 J1 and J2 Connectors
Protection	Full cell protection, disabled in Discharge Protection Override
Operational Temp Range (no heater)	-10 to +60°C (+14 to +140°F)
Temp Range with Heaters	-40 to +60°C (-40 to +140°F)

Power: 1539.2 Watt-hrs

Weight Estimate: 26.2 lbs
Mil Alum 6061-T6 Enclosure

Figure 47: Manufacturer specifications for the 8S2P 52Ah Spacecraft Lithium Ion-Polymer Battery

11.2. Voltage System

The G3LATTO's overall electric command system is based heavily on the Arianespace Ariane 5 launch vehicle. This decision was made because of the Ariane 5's excellent performance and track record, and also simplifies the G3LATTO's integration of the Ariane 5 EAP P241 external solid rocket boosters. The G3LATTO's electrical system will run at 28Vdc, and the power distribution diagram is shown below in *Figure 48*. The electrical system's command diagram will also be similar to the Ariane 5's, which is shown in *Figure 49* below.

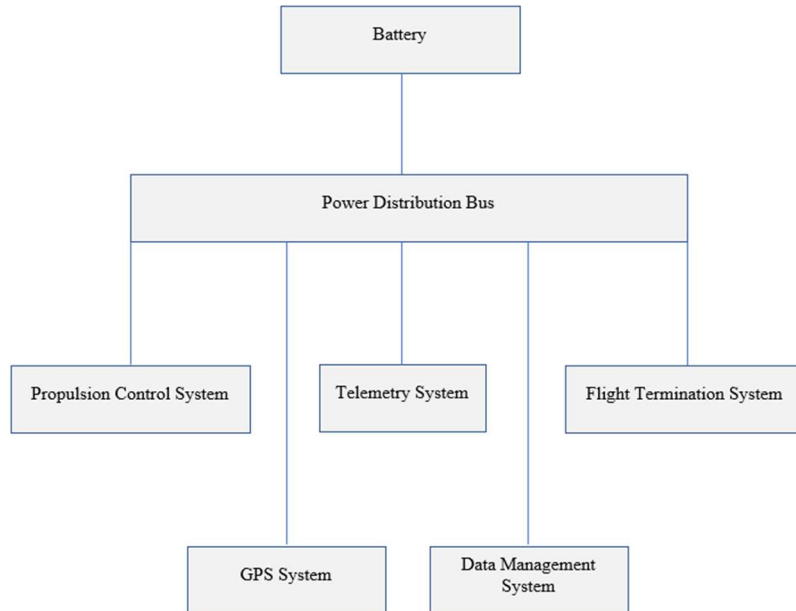


Figure 48: Electric power distribution diagram.

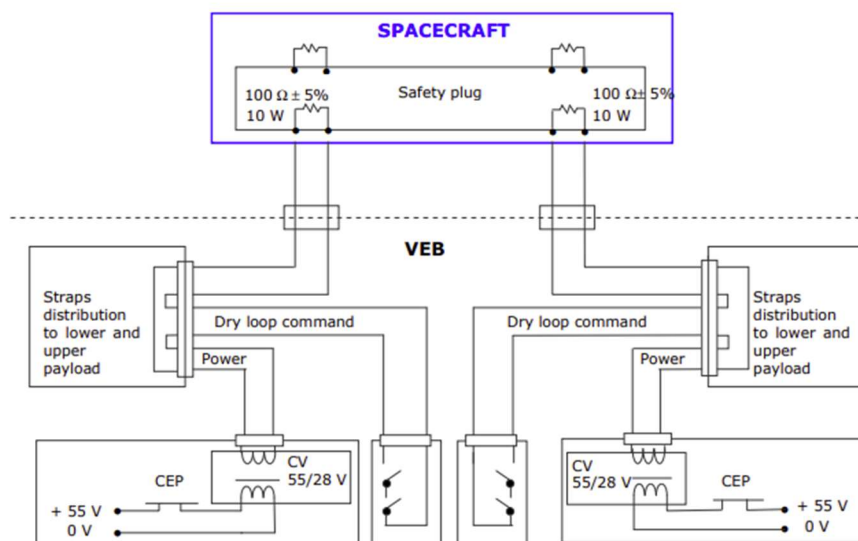


Figure 49: Ariane 5 electrical system command diagram [23].

While on the ground, the G3LATTO will employ standard umbilical links to supply power to the vehicle's systems and payload while keeping the batteries at full charge. This system will once again be adopted from the Ariane 5 launch vehicle, whose umbilical link system is shown in *Figure 50*.

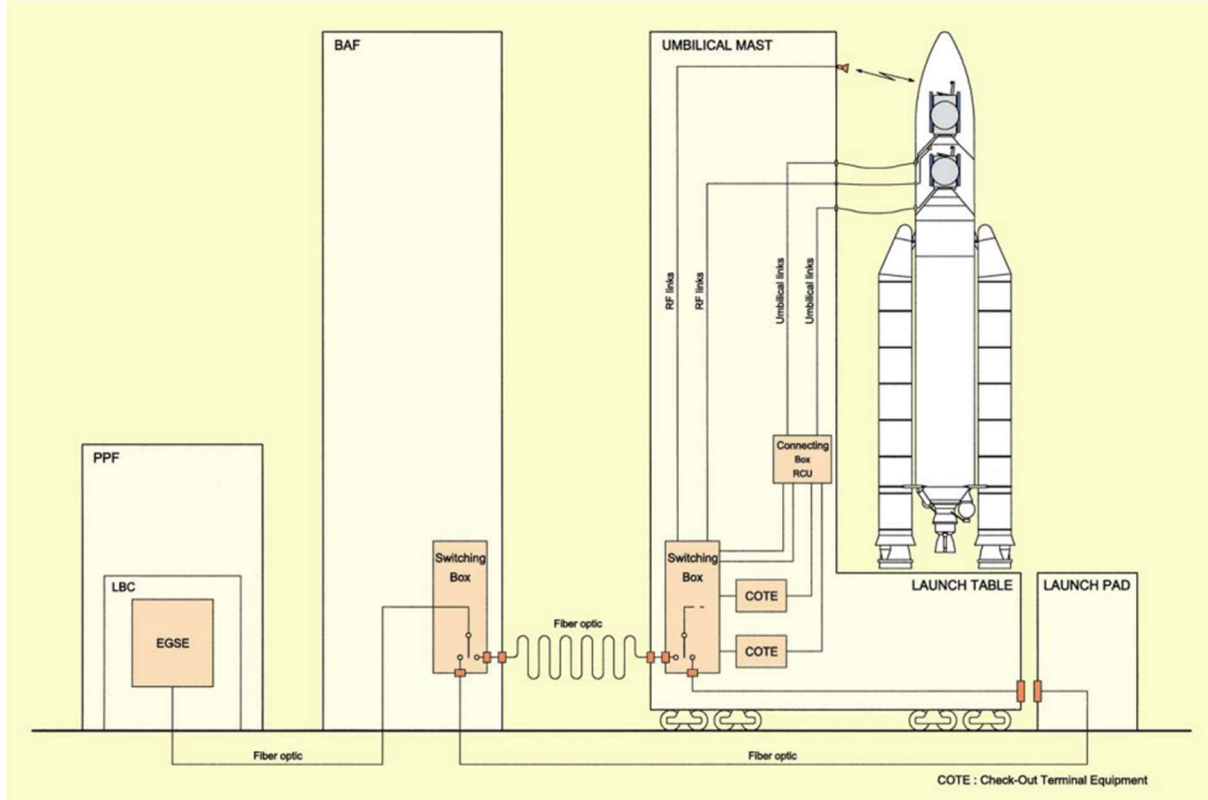


Figure 50: Ariane 5 launch pad umbilical linkage interface diagram [23].

11.3. Stage Separation and Fault Tolerance

In addition to standard vehicle operations, the G3LATTO's electrical system is also responsible for transmitting the stage separation commands to the pneumatic bolts that secure the four solid rocket boosters to the central core of the rocket. This system is single-fault tolerant for each booster to ensure reliable separation of the SRBs from the main core. The diagram for this system is shown in *Figure 51* below.

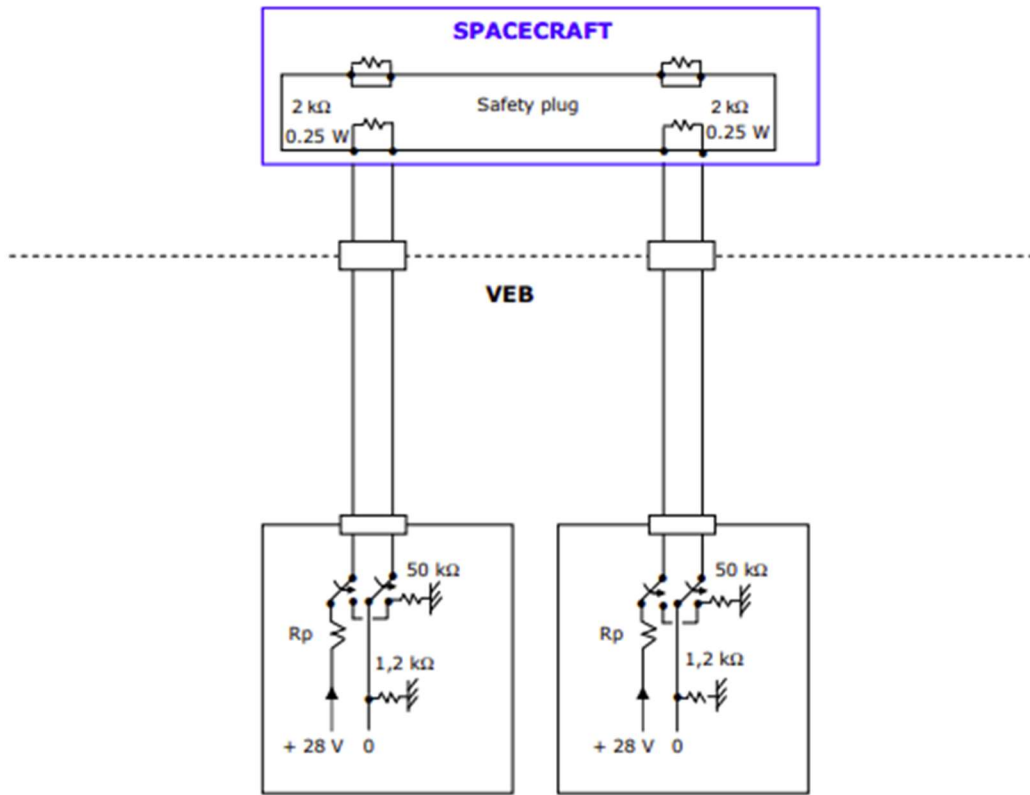


Figure 51: Ariane 5 pyrotechnical command diagram [23].

12. Avionics and Guidance, Navigation, and Control

12.1. Overview and Avionics Systems Diagram

For the launch vehicle to fly autonomously, a guidance, navigation, and control system needs to be implemented to keep the vehicle on its nominal flight path, provide stability, and control the rocket during maneuvers. Navigation is the process of determining the location of the vehicle using sensors. Guidance takes the input from the navigation system and then sends data to the control system to determine where the vehicle needs to go. Lastly, the control system uses the data from the guidance system to direct the movement of the vehicle. This is done by changing the velocity vector through engine gimbaling or activating the R-4D thrusters. A diagram of this avionics system can be seen in the figure below.

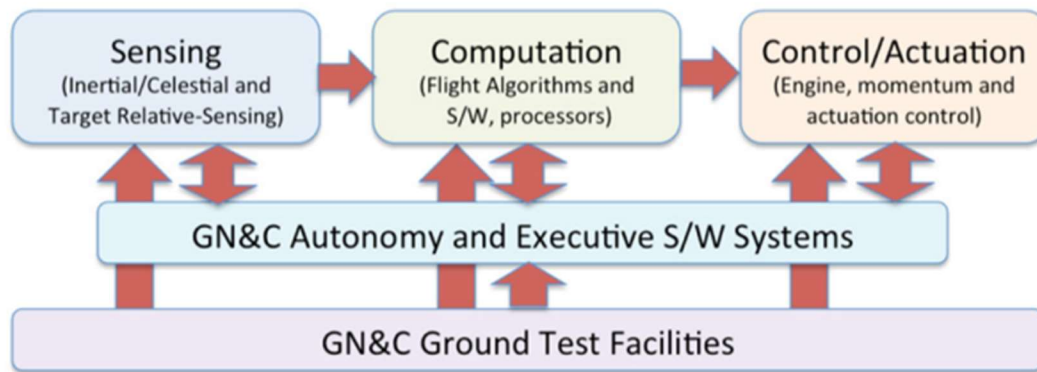


Figure 52: Avionics and GN&C Systems Diagram [24]

12.2. GN&C Sensors

12.2.1. Overview

The purpose of sensors within the GN&C system is to provide the system with data recorded during flight. Sensors will provide the flight computer with data such as orientation, position, velocity, acceleration, etc. The sensors onboard the launch vehicle will consist of inertial measurement units and a star tracker system [25].

12.2.2. Inertial Measurement Units

Inertial Measurement Units (IMUs) use the combination of gyroscopes and accelerometers to measure position, linear velocity, attitude, and angular rates relative to a global frame. It consists of three gyroscopes and three accelerometers, one for each axis of the launch vehicle. The accelerometers of an IMU measure the inertial acceleration or the change in velocity over time of a body, while the gyroscopes operate based off the principles of angular velocity and momentum and can estimate the orientation of the launch vehicle for periods when the star tracker is not able to. Below is a figure demonstrating a gyroscopic instrument.

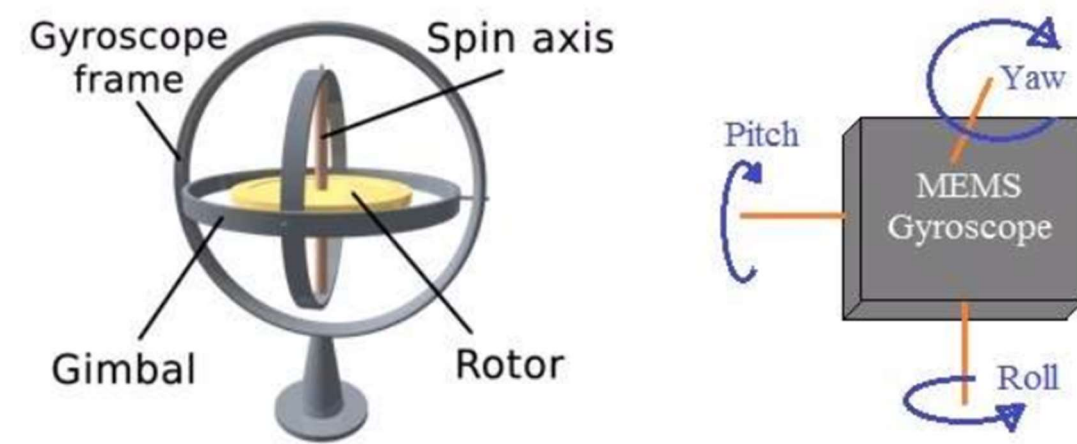


Figure 53: Gyroscope used in IMU sensor

12.2.3. Star Tracker Systems

A star tracker system is used to determine the orientation of the vehicle based on where the Sun, Earth, and Mars are, and can determine which direction to point during maneuvers. The system consists of a camera to capture a picture of the stars, then uses this picture to compare to other stars which have previously been uploaded to the system. Once the star in the picture is matched with a star in the memory, it can know exactly which star it is to then determine where the vehicle is pointing. However, if the launch vehicle is turning too fast for the camera to function, the orientation will be left solely to the IMUs. The figure below is what the camera feed of a star tracking system would look like.

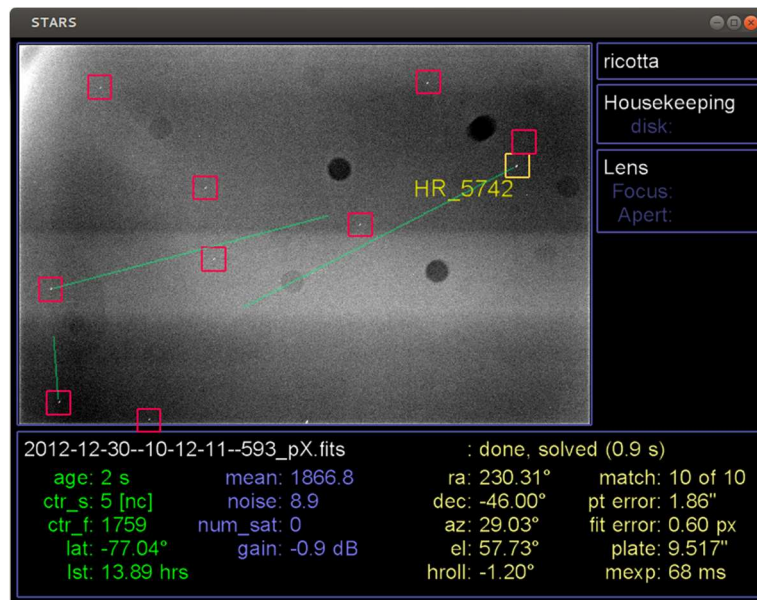


Figure 54: Star tracker camera view

12.3. Navigation

Navigation is the process of determining the location of the vehicle using the sensors mentioned above. Since the sensors can have slight errors and will be taken hundreds to thousands of measurements per second, a Kalman Filter [26] will be incorporated into the navigation system. A Kalman Filter is an algorithm that determines the current position by using a combination of its previous position and calculated future positioning. Within the Kalman Filter, all the previous data is stored to compare the actual position to the estimated. Through this comparison, the error can be better accounted for to determine more precise data for the positioning. Figure 55 provides a visual for how the Kalman Filter uses its previous and current estimated state to compare with the measured state.

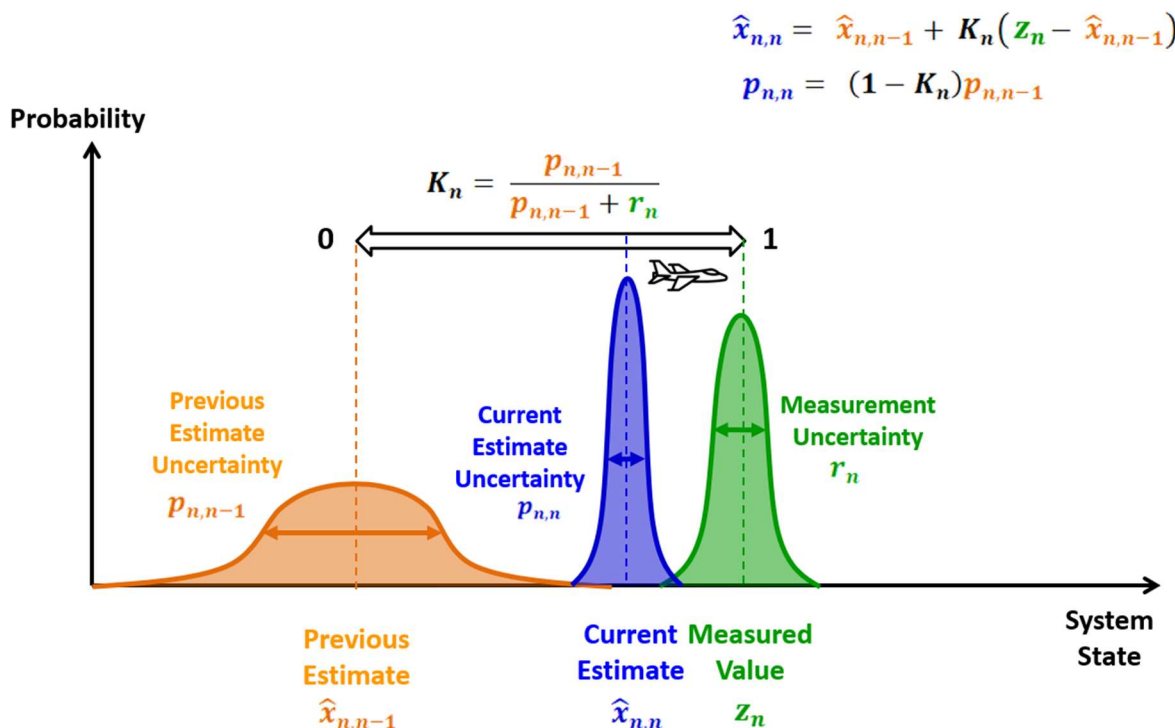


Figure 55: Kalman Filter system diagram

12.4. Control

The purpose of the controller is to recognize error with respect to the ideal flight path and perform corrections. The controller used for this launch vehicle will be a Proportional Integral Derivative (PID) Controller. A PID controller is a control loop that continuously measures error (how far off from trajectory) and corrects for this error. For this launch vehicle, the controller will compensate for the error through gimballing the rocket engines to change the velocity vector. The PID controller will allow for the system to return to its planned trajectory with minimal overshoot and delay. A block diagram of this system can be found in the figure below.

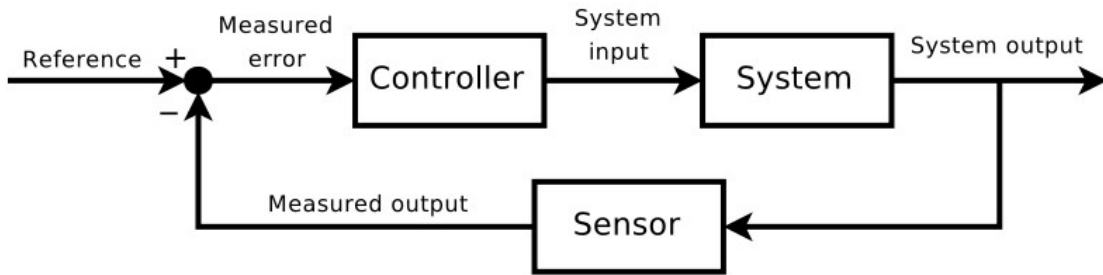


Figure 56: Avionics and GN&C Control System Block Diagram

12.5. Redundancy

In order for this system to be considered human rated, it will have a single fault tolerance. If a part of this system were to fail and be deemed a catastrophic failure it will have multiple backups for redundancies. As such, there will be two-star tracker systems and two IMUs to provide backup.

13. Communications

13.1. Objectives

The communications system will utilize NASA's Space Communications and Navigation (SCaN). This includes the Tracking and Data Relay Satellite System (TRDSS) as well as the Near Space Network (NSN). The NSN is a series of ground stations that support direct-to-Earth services and relays as well as orbiting satellites that assist in relays and coverage through the launch and ascent phase [27]. These network systems are viable in low Earth orbit, geosynchronous orbit, highly elliptical orbit, and lunar orbit. The third generation TRDSS includes a multiple access antenna for thirty-two receive elements and 15 transmit elements for S-band communications. It also utilizes two single-access antennas for S-band, Ku-band, and Ka-band communications, and a forward and aft omni-antenna for S-band telemetry and commands [28].

13.2. Requirements

The communications systems standards will adhere to the same standards for NASA's space data systems. NASA has an active membership in the Consultative Committee for Space Data Systems (CCSDS). NASA is one of the eleven member agencies of this committee that work to develop the international standards to reduce mission complexity and risk among space agencies [29]. There are standard protocols that will be used for telemetry, TM, telecommand, TC, and advanced orbiting systems AOS. The table below shows the services and security of the different space data linking protocols from the CCSDS [30].

Space Data Link Protocol	Service	Authentication	Encryption	Authenticated Encryption
TM	Packet	Protected	Protected	Protected
	VC Access	Protected	Protected	Protected
	VC FSH	Protected	Not protected	Authentication only
	VC OCF	Not protected	Not protected	Not protected
	VC Frame	Not protected	Not protected	Not protected
	MC FSH	Not protected	Not protected	Not protected
	MC OCF	Not protected	Not protected	Not protected
	MC Frame	Not protected	Not protected	Not protected
TC	MAP Packet	Protected	Protected	Protected
	MAP Access	Protected	Protected	Protected
	VC Packet	Protected	Protected	Protected
	VC Access	Protected	Protected	Protected
	COP Management	Not protected	Not protected	Not protected
	VC Frame	Not protected	Not protected	Not protected
	MC Frame	Not protected	Not protected	Not protected
AOS	Packet	Protected	Protected	Protected
	Bitstream	Protected	Protected	Protected
	VC Access	Protected	Protected	Protected
	VC OCF	Not protected	Not protected	Not protected
	VC Frame	Not protected	Not protected	Not protected
	MC Frame	Not protected	Not protected	Not protected
	Insert	Not protected	Not protected	Not protected

Figure 57: Security standards for communications data systems [30]

The communications will mimic those used in satellites and the International Space Station, utilizing S-band RF antennas for uplink and downlink [31]. This is due to the proven reliability of the systems through years of practical use, as well as the smaller size which will reduce weight and costs. The main components of the communications system are the uplink and downlink stations and radio transponders. The uplink station includes a gain amplifier for sending signals while the downlink station includes a low pass amplifier for receiving signals. The radio modules are used for modulation and amplification of the electromagnetic waves to create or receive signals. Each of the bandpass filters and RF filters are included to alter the frequencies of the signals to transition frequencies to the desired range. Below is a block diagram of this communications system.

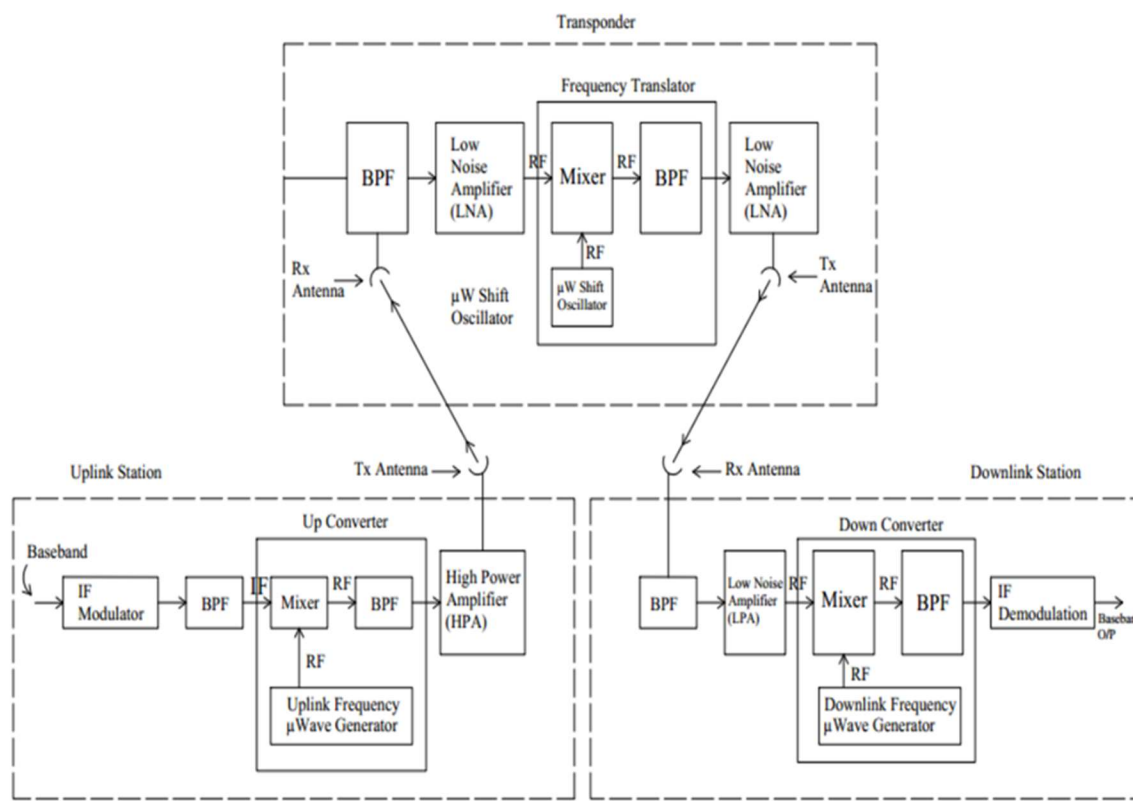


Figure 58: Communications system diagram for the G3LATTO System [31]

13.3. Uplink/Downlink

NASA has developed a various method of communications for different missions, namely Ground Stations, the Tracking and Data Relay Satellites (TDRS), and the Deep Space Network. For this mission, the ground stations and TDRS will be utilized due to the proximity of the mission. There are nineteen ground satellites in different locations, which can be seen in *Figure 59*.



Figure 59: Space Network ground satellite locations [32]

In addition to the ground stations, the TDRS will be used while in orbit. This will aid in the availability of ground stations and aid in opening more avenues for more consistent uplinks and downlinks for data transmission. The purpose of these satellites was to provide almost continuous transmission of data for missions. Below shows the forward and return transmission bands as well as the maximum data rate for each.

	Forward			
	Multiple Access S-band	Single Access S-band	Single Access Ku-band	Single Access Ka-band
Number of user spacecraft per TDRS	1*	2	2	2
3 dB RF Channel BW, MHZ	6	20	50	50
Users Guide Max Data Rate	300 kbps	7 Mbps	25Mbps	25Mbps
	Return			
	Multiple Access S-band	Single Access S-band	Single Access Ku-band	Single Access Ka-band
Number of user spacecraft per TDRS	5*	2	2	2
3 dB RF Channel BW, MHZ	6	10	225	225 or 650
Users Guide Max Data Rate	300 kbps	6 Mbps	300 Mbps	300 Mbps**

- *Direct Spread Spectrum, details available upon request
- **The TDRS channel is capable of higher data rates with user supplied ground equipment. It has been characterized up to 3Gbps.

Figure 60: TRDS forwards and return bands and data rates [33]

The vehicle will carry two S-band antennas at the 2 GHz frequency for uplinks and downlinks. The TDRS architecture as well as antenna architecture are depicted below in Figure 61.

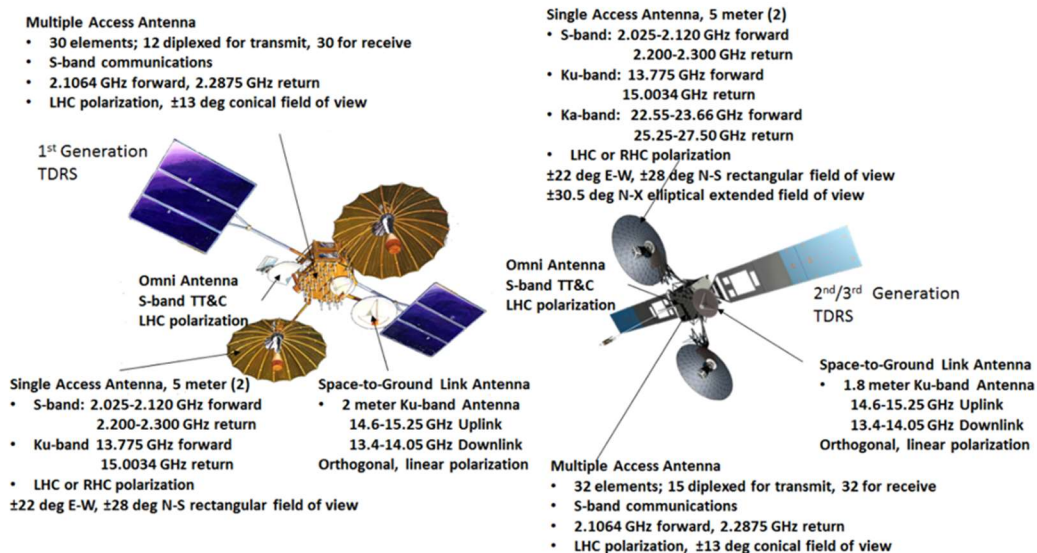


Figure 61: First, second, and third generation TDRS architecture [33]

14. Vehicle Health Monitoring

14.1. Overview

Vehicle health monitoring is a critical aspect of any modern launch vehicle. These systems are responsible for gathering, storing, and interpreting data and making that information available to the rest of the G3LATTO vehicle's systems as needed. It is also able to swiftly identify potential problems and pass the information along to controllers on the ground. The G3LATTO rocket is equipped with a suite of these sensor systems all linked together by a central Data Management System (DMS). The basis for the G3LATTO's sensor array are Fiber Optic Sensing Systems (FOSS) which allows many sensors to be integrated together efficiently while minimizing the added mass of the system [34].

14.2. Structural Monitoring

The monitoring of the G3LATTO rocket's structural performance is handled by advanced structural FOSS sensors developed by NASA. These fiber optic sensors use a variety of optical techniques to measure stress, strain, temperature, and overall displacement of the components they are attached to. The FOSS sensor systems are robust and modular, allowing for significant improvements in efficiency over legacy structural sensor systems [34]. These systems can also detect potential vehicle damage when the fiber optic connections are severed, allowing for immediate measures to be taken by the ground crew if needed.

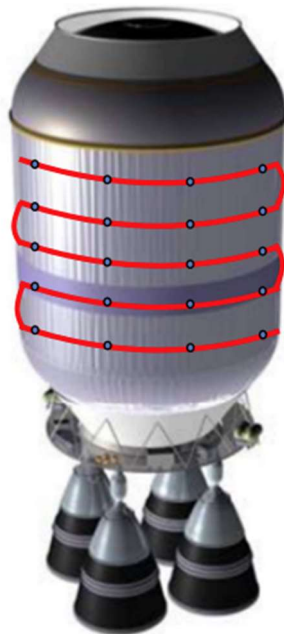


Figure 62: Example FOSS structural sensor system layout [34]

14.3. Engine and Tank Monitoring

One of the most important roles of this system is to monitor the performance of the G3LATTO's engines, turbopumps, and fuel tanks. This is a complicated task due to the presence of extreme temperatures and pressures, so robust technologies must be employed that can withstand those conditions.

The G3LATTO's engines will be monitored by an Optical Combustion Analysis System (OCAS) which is able to detect potential engine damage by analyzing spectral emissions of the combustion process to detect trace amounts of metals and contaminants. The presence of contaminants and metals in the exhaust plume is a good indicator that the engine has been damaged or is beginning to succumb to wear. The OCAS system is valuable because its sensitivity allows for early identification of potential engine issues and allows for appropriate measures to be taken to prevent complete engine failure [35].

The condition of the G3LATTO's turbopumps and fuel tanks will be monitored by a combination of standard FOSS structural sensors and optical cryogenic liquid level sensors. This combination allows the DMS to ascertain the condition of the tanks and turbopumps both in terms of structural rigidity and fuel levels [34].

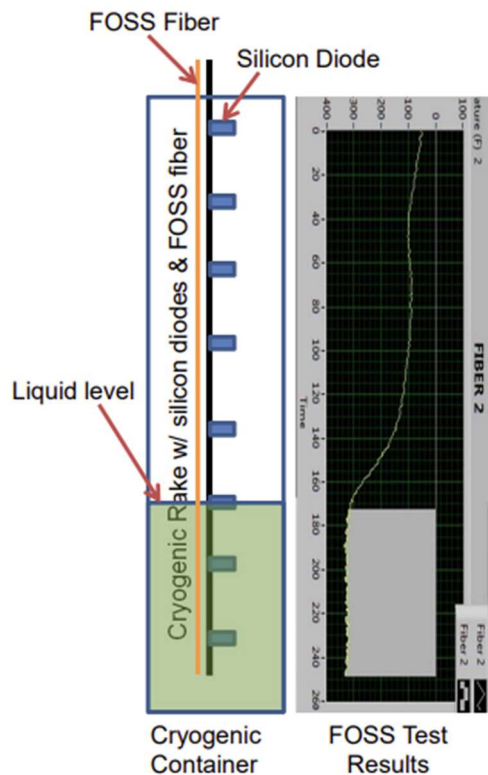


Figure 63: Cryogenic liquid level sensor operation example [34]

14.4. Data Management System

G3LATTO's Data Management System is responsible for recording and interpreting the data collected by the vehicle's FOSS and OCAS so that it can be used by the rest of the launch vehicle's systems such as the flight computer, while also making the data available to the ground crew in real time. While the DMS is capable of providing a variety of valuable information about the health and condition of the vehicle, it is not solely responsible for triggering the G3LATTO's Flight Termination System (FTS) since the FTS must be capable of operating fully independently of the DMS and flight computer.

15. Flight Termination System

15.1. System Requirements and Overview

Onboard the G3LATTO System is a flight termination system designed to terminate the vehicle and ensure that as much of the remaining propellant is safely discarded before impact safely and reliably and minimize or eliminate the risk to protected areas. In the event of a crewed launch, the vehicle also has systems in place to ensure their safety. These objectives are achieved by removing any ability of the rocket to produce thrust and through the safe ejection of the capsule away from the rocket. The order of operations for flight termination are as follows:

1. The vehicle begins to leave the allowable operational envelope and/or experiences critical system failures
2. Ground control is notified of this deviation/failure in the launch and allows for a decision by the range safety officer in the event that the launch vehicle can still make it to orbit.
3. If the flight termination sequence is initiated, then the vehicles thrust is terminated via closing the turbopumps to the main liquid engines and the destruction of the SRB bulkheads (thus destroying their pressure integrity) before jettisoning them from the vehicle.
4. In the event of a crewed launch, the capsule is then jettisoned from the vehicle.
5. The propellant tanks are then “unzipped” via charges that run the length of the tanks on at least 2 sides of the vehicle. This allows for the safe dispersion of the cryogenic propellant.
6. If crewed, the capsule will perform a water landing via parachutes and be recovered by USN personnel.

To increase the redundancy of the system, if the vehicle detects a deviation from the flight path and has lost contact with ground control for more than a couple of seconds, the system will automatically terminate the flight to prevent unnecessary loss of life. The system also uses redundant sensors, power supplies, termination charges, and communications devices in order to maximize system reliability and avoid crippling system failures. The flight termination system complies with all requirements of reliability and safety as outlined in the NASA Flight Termination Systems Commonality Standard (Doc. 319-10).

15.2. Components, Locations, and Potential Outcomes

Given the launch location and direction, any flight termination will likely result in the capsule landing somewhere in the Atlantic Ocean. In the event that the second stage fails to achieve orbit, the vehicle will burn up on reentry and thus pose minimal risk to protected areas. Locations of flight system termination components can be seen in the figure below.

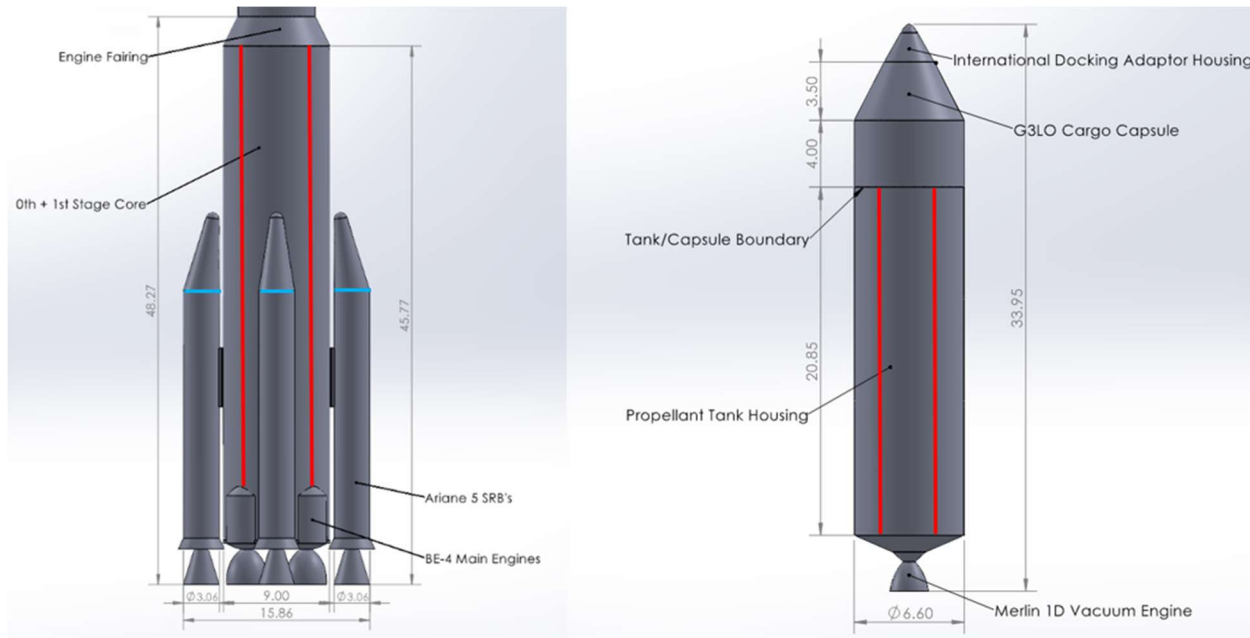


Figure 64: Locations of the charges for unzipping the propellant tanks (red) and blowing the SRB bulkheads (blue).

15.3. Failure Mode and Effect Analysis

A Failure Mode and Effects Analysis (FMEA) is used to describe the potential failures of an item and evaluate the effects that failure introduces [36]. This is critical to the mission as it is important in identifying critical components, likely sources of failure, and areas that need extra precautions or redundancy. For the initial analysis of failure modes, the most known critical failures will be examined to ensure redundancy and precautions are in place. Initially, the main engines, the solid rocket boosters, and the second stage assembly are examined for critical or catastrophic failures, namely leakages, hydraulic failures, gimbaling faults, separation failure, and GN&C errors. Further analysis on other components that have an ability to impose critical or catastrophic failures as well as the incorporate occurrences are critical in reducing unexpected failures.

Table 29: FMEA for BE-4 Liquid Core Main Engine

Subsystem/ Component Name	Potential Failure Modes	Potential Causes of Failure	Potential Effects of Failure	Severity	Severity Category
BE-4 Main Engines	Ignition Fault	Leakage	- Failure at site - Area risk	10 10	1R 1
		Interlock failure	- Failure to ignite - Possible loss of mission	5 10	3 1
	Gimballing Error	Hydraulic malfunction	- Unable to gimble - Loss of control	10 10	1 1
	Combustion Instability	Pressure variations	- Vibrations - Thrust variation	7 7	1R 1R
		Excess fuel delivery	- Vibrations - Thrust variation	7 7	1R 1R

Table 30: FMEA for Ariane SRB's

Subsystem/ Component Name	Potential Failure Modes	Potential Causes of Failure	Potential Effects of Failure	Severity	Severity Category
Ariane SRB's	Separation failure	System command failure	- Early separation - No separation	9 10	1R 1
		Interlock failure	- Structural deficiency - No separation	8 10	1R 1
	Case breach	Impact during ascent	- Possible mission loss - Unbalanced thrust	10 7	1 2
		Structural failure	- Possible mission loss	10	1
	Controls failure	GN&C failure	- Inability to vector/throttle	8	1R
		Hardware failure	- Inability to vector/throttle	8	1R

Table 31: FMEA for 2nd Stage Assembly

Subsystem/ Component Name	Potential Failure Modes	Potential Causes of Failure	Potential Effects of Failure	Severity	Severity Category
2 nd Stage Assembly	Separation failure	System command failure	- Early separation - No separation	9 10	1R 1
		Interlock failure	- Structural deficiency - No separation	8 10	1R 1
	Nose cone release	Hydraulic failure	- Decreased efficiency - Inability to dock	5 10	3 1
		Structural failure	- Decreased efficiency - Inability to dock	5 10	3 1
	Inner structural failure	Structural buckling	- Decreased maneuverability	8	1R
			- Decreased stability	8	1R
			- Additional structural damage	8	1R

16. Flight Test Plan

Prior to the first operational launch of the vehicle, a series of prototypes must be built in order to test critical systems as well as the overall structure of the launch system. This must be done in order to ensure each part of the system functions properly and integrates smoothly into the rocket as a whole. To accomplish this, four prototypes will be manufactured and tested in the order shown in the following table:

Table 32: Launch system prototype descriptions and objectives

Prototype	Description	Objectives	Location
Propulsion Tech Demonstrator	Full propulsion and tankage assemblies for the first and second stage main engines	<ul style="list-style-type: none"> -Perform pressure tests to ensure tankage assemblies can withstand the required pressures and cryogenic conditions -Perform static firing to ensure the main engines and their control systems operate nominally in their G3LATTO System configuration 	Marshall Space Flight Center, Huntsville, AL
Structural Performance Demonstrator	Full structural assembly for first and second stages	<ul style="list-style-type: none"> -Perform vibration and vibro-acoustic tests with simulated loads to ensure the overall structure remains sound under anticipated operational conditions 	Marshall Space Flight Center, Huntsville, AL
Flight Termination System Demonstrator	Full prototype including all stages and systems with a simulated payload	<ul style="list-style-type: none"> -Perform full flight termination system tests to ensure the system can safely abort mid-flight in case of emergency 	Cape Canaveral Space Force Station, Cape Canaveral, FL
G3LATTO System Flight Demonstrator	Full prototype of all stages and systems with a simulated payload	<ul style="list-style-type: none"> -Perform a full test flight including launch, ascent, orbital injection, and cargo deployment 	Cape Canaveral Space Force Station, Cape Canaveral FL

17. Final Vehicle System Overview

The Group 3 Launch Alliance has created the G3LATTO system, a launch vehicle that is more than capable of transporting a 75 metric ton payload to an 800 km equatorial orbit. The design is structured in such a way to maximize seamless integration with existing technology and architecture while prioritizing human safety for secondary manned configurations. This concept design is capable of meeting all the necessary technical and human rating requirements while operating as a platform capable of a range of mission profiles, including transporting payloads smaller than the design specifications and sending a human crew up to 800 km orbit. With the final design documentation, this design will become even further refined, providing an excellent foundation to prevent requirement creep and deliver a successful vehicle within the expected timeline.

18. CAD Modeling of Vehicle Segments

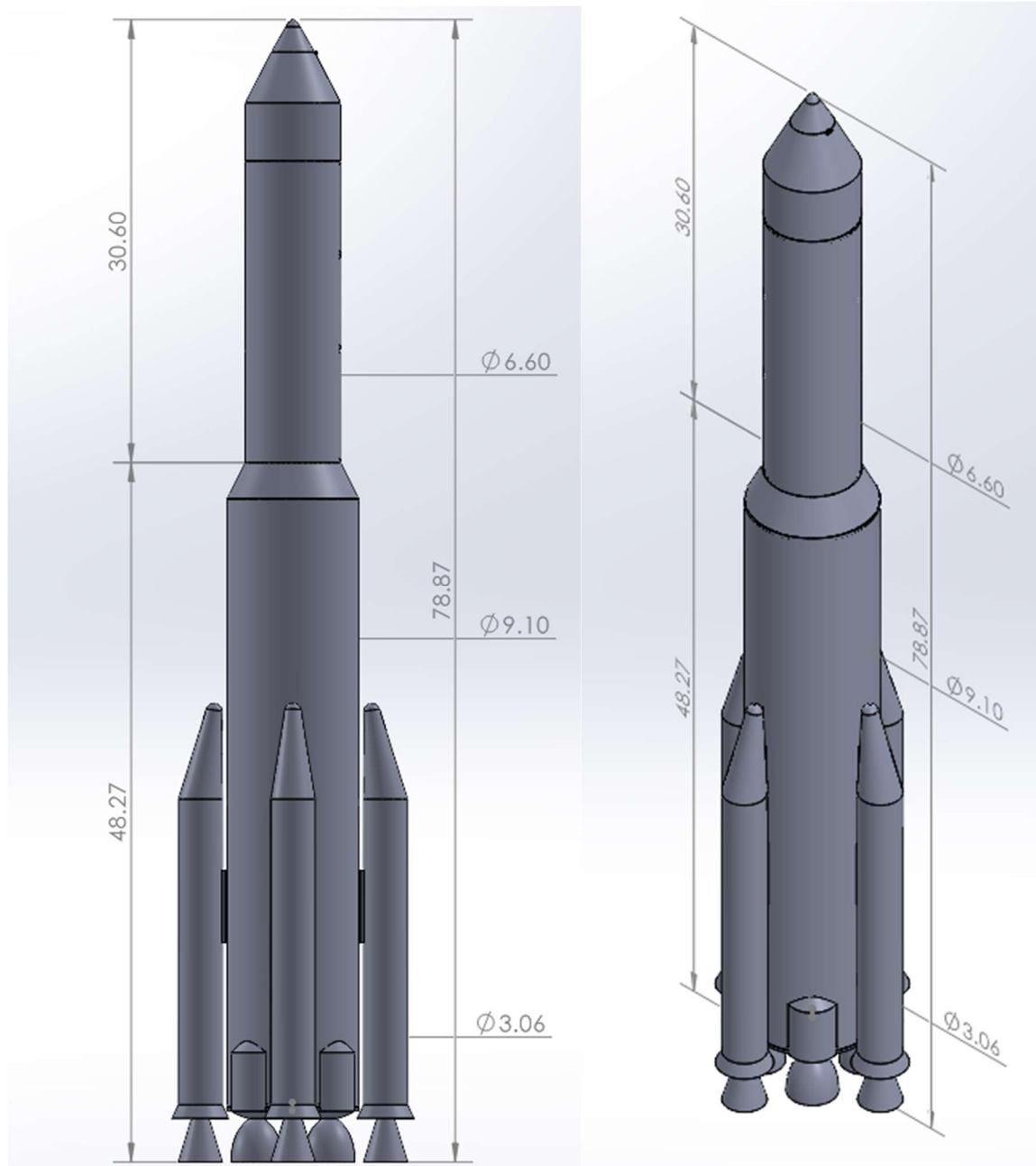


Figure 65: Full-Stack launch configuration of G3LATTO system, all dimensions are in meters

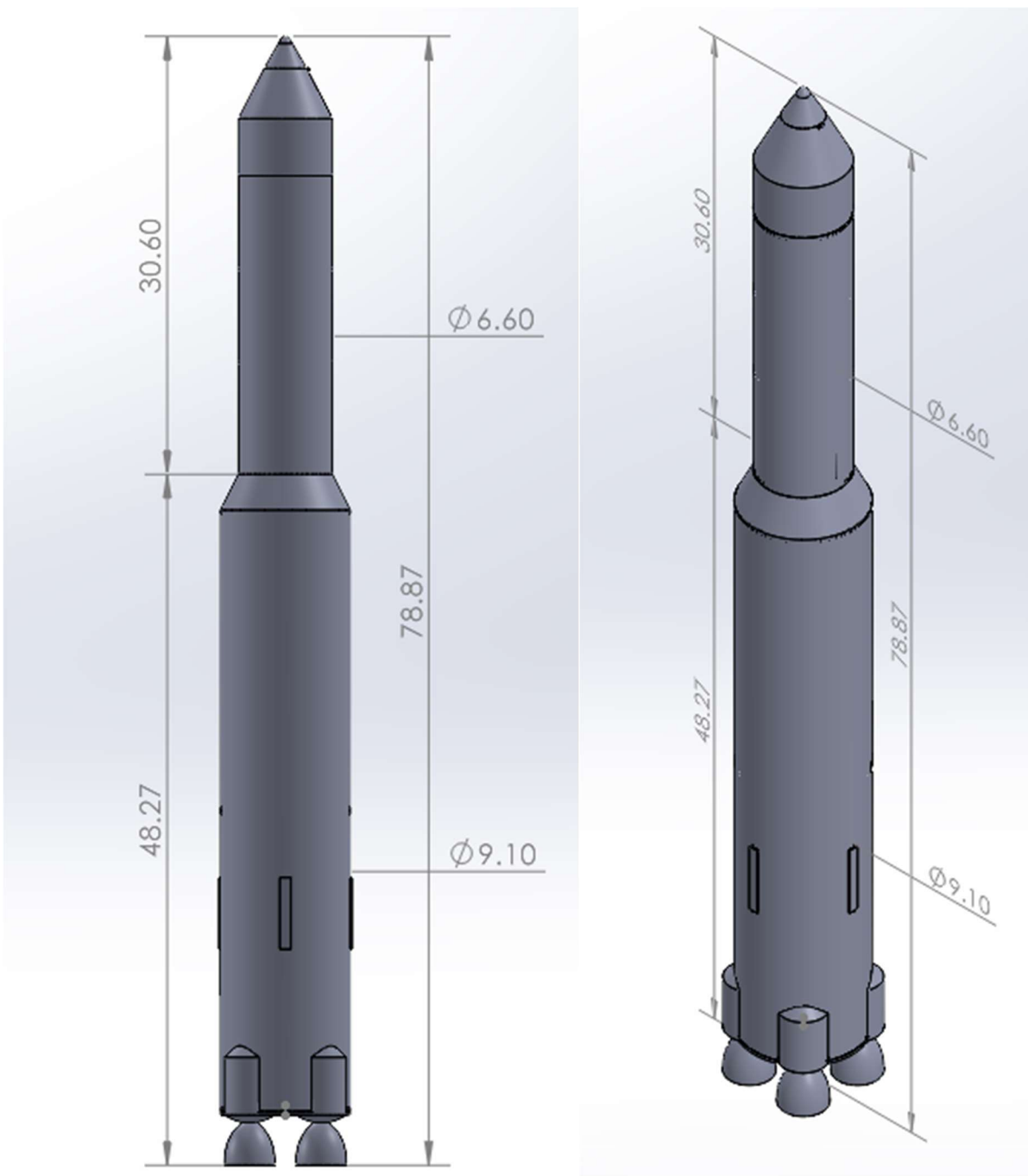


Figure 66: 1st stage of G3LATTO system – Post SRB separation, all dimensions are in meters

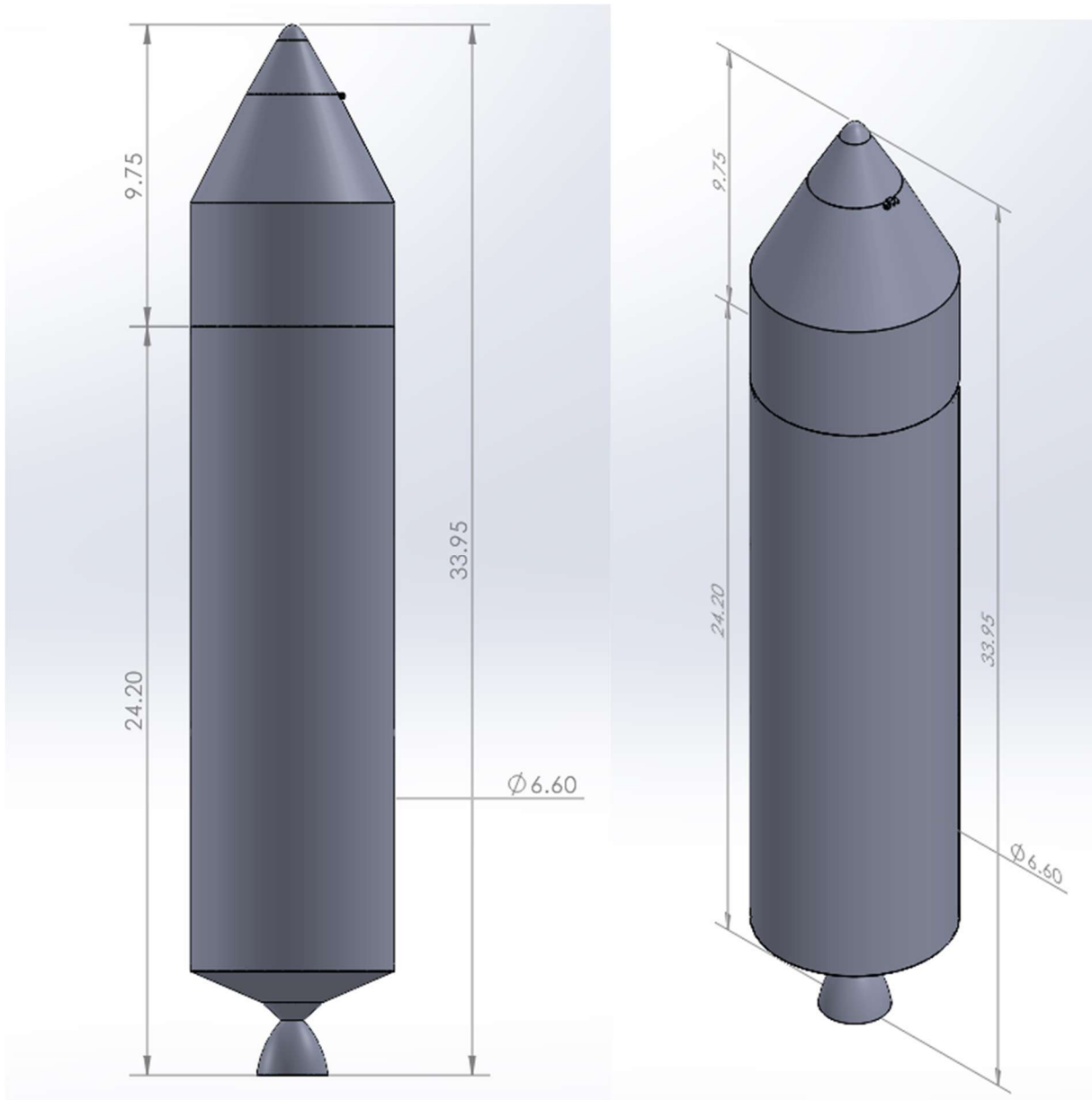


Figure 67: 2nd stage of G3LATTO system – Post 1st stage separation, all dimensions are in meters

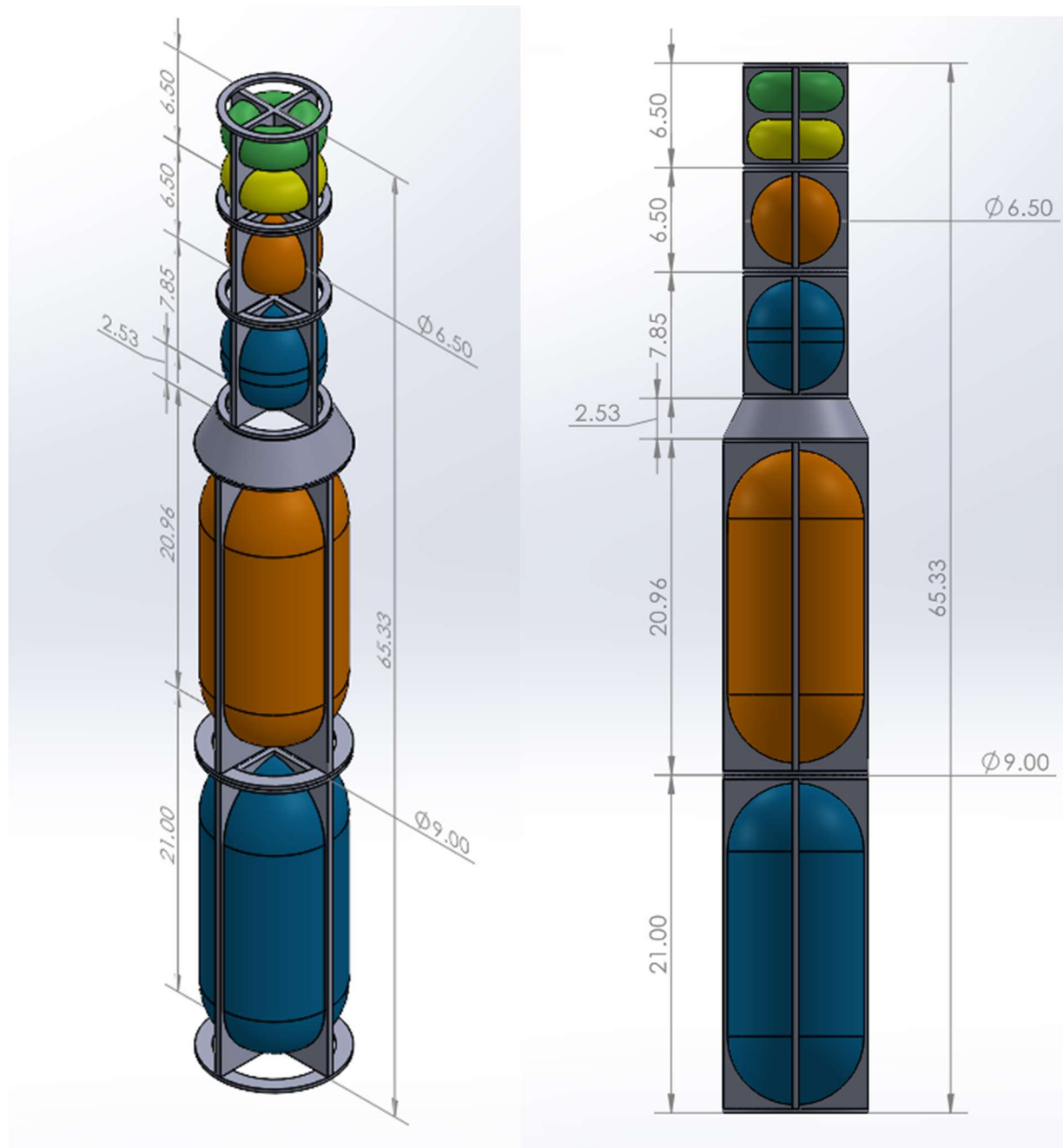


Figure 68: Full-Stack internal structural design, all dimensions are in meters

Appendix A. – References

Conceptual Overview and Design Philosophy

- [1] “NASA FY 2022 BUDGET REQUEST,” NASA.
https://www.nasa.gov/sites/default/files/atoms/files/fy2022_nasa_fact_sheet.pdf. Accessed Mar. 20, 2022.
- [2] “Consumer Price Index Summary - 2022 M02 Results,”
<https://www.bls.gov/news.release/cpi.nr0.htm>. Accessed Mar. 20, 2022.
- [3] Bureau of Labor Statistics Data.
https://data.bls.gov/timeseries/CUUR0000SA0L1E?output_view=pct_12mths. Accessed Mar. 20, 2022.
- [4] “ESAS Cost Analysis Context,” NASA.
https://www.nasa.gov/pdf/140643main_ESAS_12.pdf. Accessed Apr. 23, 2022
- [5] “NASA Procedural Requirements 8705.2C,” July 2017, NASA.
https://nodis3.gsfc.nasa.gov/displayDir.cfm?Internal_ID=N_PR_8705_002C_&page_name=Chapter1&search_term=human%20rating. Accessed Apr. 25, 2022
- [6] “Commercial Crew Transportation System Certification Requirements for NASA Low Earth Orbit Missions,” December 2010, NASA.
https://www.nasa.gov/pdf/504982main_CCTSCR_Dec-08_Basic_Web.pdf. Accessed Apr. 25, 2022

Launch-to-Orbit Overview

- [7] Edberg, D. and Costa, W., “Design of Rockets and Space Launch Vehicles,” AIAA Education Series, 2020.

Propulsion

- [8] “BE-4,” Blue Origin. <https://www.blueorigin.com/engines/be-4>. Accessed Mar. 19, 2022.
- [9] “BE-4 Engine Test: 65% Power Level and 114 Seconds” - YouTube.
<https://web.archive.org/web/20180928235910/https://www.youtube.com/watch?v=Fp0WgodhR7s>. Accessed Mar. 19, 2022.
- [10] “Boosters (EAP),”
https://www.esa.int/Enabling_Support/Space_Transportation/Launch_vehicles/Boosters_EA_P. Accessed Mar. 19, 2022.

- [11] “Falcon 9 Launch Vehicle – Payload User’s Guide Rev 2,” SpaceX.
https://web.archive.org/web/20170314002928/http://www.spacex.com/sites/spacex/files/falcon_9_users_guide_rev_2.0.pdf. Accessed Mar. 19, 2022.

Cargo Module Design

- [12] “Meet the International Docking Adapter,” NASA. <https://www.nasa.gov/feature/meet-the-international-docking-adapter>. Accessed Apr. 24, 2022.

Auxiliary Propulsion

- [13] “Marquardt R-4D Apollo Spacecraft Attitude Control Engine,” Apollo Artifacts.
<https://www.apolloartifacts.com/2013/11/marquardt-r-4d-apollo-spacecraft-attitude-control-engine.html>. Accessed Mar. 17, 2022.

Tank Pressurization

- [14] “Space Shuttle Use of Propellants and Fluids,” NASA.
https://www.nasa.gov/centers/kennedy/pdf/167433main_Propellants08.pdf. Accessed Mar. 17, 2022

Structural Design

- [15] “ASM Material Data Sheet,”
<https://asm.matweb.com/search/SpecificMaterial.asp?bassnum=ma2024t4>. Accessed Mar. 20, 2022.
- [16] “ASM Material Data Sheet,”
<https://asm.matweb.com/search/SpecificMaterial.asp?bassnum=MA2219T62>. Accessed Mar. 20, 2022.
- [17] “AISI 4140 Alloy Steel (UNS G41400),” AZoM.com.
<https://www.azom.com/article.aspx?ArticleID=6769>. Accessed Mar. 20, 2022.
- [18] “Titanium, Ti,”
<https://www.matweb.com/search/DataSheet.aspx?MatGUID=66a15d609a3f4c829cb6ad08f0dafc01&ckck=1>. Accessed Mar. 20, 2022.
- [19] “AISI 1018 Steel, Cold Drawn,”
<https://www.matweb.com/search/DataSheet.aspx?MatGUID=3a9cc570fbb24d119f08db22a53e2421&ckck=1>. Accessed Mar. 20, 2022.

[20] “ASM Material Data Sheet,”
<https://asm.matweb.com/search/SpecificMaterial.asp?bassnum=ma6061t6>. Accessed Mar. 20, 2022.

[21] “A History of Collapse Factor Modeling and Empirical Data for Cryogenic Propellant Tanks,” NASA.
<https://ntrs.nasa.gov/api/citations/20100026018/downloads/20100026018.pdf>. Accessed Mar. 16, 2022.

Electrical Systems

[22] Burke, E. “Li-Ion Intelligent and Safe Battery Technology Innovation Leader,” NASA MSFC. Li-Ion Battery Workshop, 2020. <http://www.spaceinformationlabs.com/wp-content/uploads/2021/01/SIL-Li-Ion-Polymer-Intelli-Pack-Battery-NASA-Workshop-2020.pdf>. Accessed Mar. 19, 2022

[23] Lagier, R. “Ariane 5 User’s Manual,” 2020. pp. 93-105. <https://www.arianespace.com/wp-content/uploads/2016/10/Ariane5-users-manual-Jun2020.pdf>. Accessed Mar. 19, 2022.

Avionics and GN&C

[24] “Guidance, Navigation, and Control Technology Assessment for Future Planetary Science Missions,” January 2013, NASA.
https://solarsystem.nasa.gov/system/downloadable_items/155_GNC_Tech_Assess_Part_II_Onboard_GNC_130228_soo.pdf. Accessed Mar. 19, 2022.

[25] “Sensors,” NASA. <https://mars.nasa.gov/mro/mission/spacecraft/parts/gnc/sensors/>. Accessed Mar. 20, 2022.

[26] “How to land a Spaceship,” <http://www.ilanman.io/blog/2016/4/29/kalman>. Accessed Mar. 20, 2022.

Communications

[27] “What is the Near Space Network,” NASA.
https://www.nasa.gov/directorates/heo/scan/services/networks/near_space_network/about. Accessed Mar. 20, 2022.

[28] “Tracking and Data Relay Satellite (TDRS) Third Generation Capabilities,” NASA.
https://www.nasa.gov/directorates/heo/scan/services/networks/tdrs_third_gen. Accessed Mar. 20, 2022.

- [29] “Data Standards,” NASA.
<https://www.nasa.gov/directorates/heo/scan/engineering/datastandards/index.html>. Accessed Mar. 20, 2022.
- [30] “Space Data Link Security Protocol,” pp. 5-3. CCSDS.
<https://public.ccsds.org/Pubs/355x0b1.pdf>. Accessed Apr. 23, 2022
- [31] Caldwell, S. “9.0 Communications,” NASA. <http://www.nasa.gov/smallsat-institute/sst-soa/communications>. Accessed Apr. 23, 2022.
- [32] “Where Are The NSN Complexes Located?” NASA.
https://www.nasa.gov/directorates/heo/scan/services/networks/near_space_network/complexes. Accessed Mar. 20, 2022.
- [33] Sobchak, T., Shinners, D.W., and Shaw, H., “NASA Space Network Project Operations Management: Past, Present and Future for the Tracking and Data Relay Satellite Constellation,” SpaceOps 2018.
<https://ntrs.nasa.gov/api/citations/20180003338/downloads/20180003338.pdf>. Accessed Mar. 20, 2022.

Vehicle Health Monitoring

- [34] Chan, P., “Fiber Optics Sensing System (FOSS) at NASA Armstrong Flight Research Center (AFRC): Summary and Recent Deployments,” 3rd Edward Technical Symposium, 2018. <https://ntrs.nasa.gov/citations/20180007391>. Accessed Mar. 20, 2022.
- [35] Opto-Knowledge, “Spectral Measurement System for Health Monitoring of Liquid Rocket Engines,” Air Force SBIR STIR, 2018.
https://media.defense.gov/2018/May/16/2001918253/-1/-1/1/OPTO-KNOWLEDGE_AF093-187.PDF. Accessed Mar. 20, 2022.

Flight Termination System

- [36] “Standard for Performing a Failure Mode and Effects Analysis (FMEA) and Establishing a Critical Items List (CIL) (DRAFT),” NASA. <https://rsdo.gsfc.nasa.gov/documents/rapid-iii-documents/mar-reference/gsfc-fap-322-208-fmea-draft.pdf>. Accessed Mar. 20, 2022.

Appendix B. – List of Abbreviations

Table 33: List of Abbreviations and Acronyms

AMCM	Advanced Mission Cost Model
ANSI	American National Standards Institute
ASTM	American Society for Testing and Materials
CAD	Computer-Aided Design
CCSDS	Consultative Committee for Space Data Systems
CCTSCR	Commercial Crew Transportation System Certification Requirements
CDR	Concept Design Review
CFD	Computational Fluid Dynamics
CG	Center of Gravity
CONOPS	Concept of Operations
CP	Center of Pressure
DMS	Data Management System
DOT	Department of Transportation
EAP	Etage d'Accélération à Poudre
ECLSS	Environmental Control and Life Support System
FAA	Federal Aviation Administration
FEA	Finite Element Analysis
FMEA	Failure Modes and Effects Analysis
FOSS	Fiber Optic Sensing Systems
FPA	Flight Path Angle
FTS	Flight Termination System
FY	Fiscal Year
G3LA	Group 3 Launch Alliance
G3LATTO	Group 3 Launch and Transfer to Orbit
G3LO	Group 3 Low-Earth Orbiter
GN&C	Guidance, Navigation, and Control
IDA	International Docking Adapter
IEEE	Institute of Electrical and Electronics Engineers
IMU	Inertial Measurement Unit
Isp	Specific Impulse
LCH₄	Liquid Methane
LEO	Low Earth Orbit
LOC	Loss of Crew
LOM	Loss of Mission
LOX	Liquid Oxygen

MATLAB	Matrix Laboratory
MECO	Main Engine Cutoff
MMH	Monomethylhydrazine
NASA	National Aeronautics and Space Administration
NPR	NASA Procedural Requirements
NSN	Near Space Network
NTO	Nitrogen Tetroxide
OCAS	Optical Combustion Analysis System
PID	Proportional Integral Derivative
RCS	Reaction Control System
RP-1	Rocket Propellant-1
SCaN	Space Communications and Navigation
SECO	Secondary Engine Cutoff
SRB	Solid Rocket Booster
STD	Standard
TDRS	Tracking and Data Relay Satellites
TRDSS	Tracking and Data Relay Satellite System
TWR	Thrust-to-Weight Ratio
USN	United States Navy

Appendix C. – Propulsion Trade Study

Main Engines

Table 34: Main engine actual values

Actual Values			
Items	BE-4	Raptor	RS-25
Max Thrust (kN)	2400	1810	1860
Isp (s)	299	330	366
Throttle Ability	Medium	High	Medium

Table 35: Main engine normalization values

Normalization Values			
Items	1	2	3
Max Thrust (kN)	< 1850	< 1900	> 2000
Isp (s)	< 300	< 350	< 400
Throttle Ability	Low	Medium	High

Table 36: Main engine normalized values

Normalized Values			
Items	BE-4	Raptor	RS-25
Max Thrust (kN)	3	1	2
Isp (s)	1	2	3
Throttle Ability	2	3	2

Table 37: Main engine weighting factors

Weighting Factors		
Items	Factor	Reason
Max Thrust (kN)	3	Large amounts of thrust are imperative for first stage engines
Isp (s)	1	Efficiency is less important in first stage flight
Throttle Ability	2	Control of thrust output aids in managing structural and human requirements

Table 38: Final weighted values result for the main engines

Weighted Values			
Items	BE-4	Raptor	RS-25
Max Thrust (kN)	9	3	6
Isp (s)	1	2	3
Throttle Ability	4	6	4
Total	14	11	13

Solid Rocket Boosters

Table 39: SRB actual values

Actual Values		
Items	Shuttle SRB x2	Ariane SRB x4
Max Thrust (kN)	2940	2832
Wet Mass (kg)	1182000	1092000
Aerodynamics	Medium	High

Table 40: SRB normalization values

Normalization Values			
Items	1	2	3
Max Thrust (kN)	< 2000	< 2500	> 2500
Wet Mass (kg)	> 1200000	< 1200000	< 1100000
Aerodynamics	Low	Medium	High

Table 41: SRB normalized values

Normalized Values		
Items	Shuttle SRB x2	Ariane SRB x4
Max Thrust (kN)	3	3
Wet Mass (kg)	2	3
Aerodynamics	2	3

Table 42: SRB weighting factors

Weighting Factors		
Items	Factor	Reason
Max Thrust (kN)	3	Large amounts of thrust are imperative for first stage engines
Wet Mass (kg)	2	SRB mass makes up much of the first stage
Aerodynamics	1	Good aerodynamics will prevent drag and delta-V losses

Table 43: Final weighted values result for the solid rocket boosters

Weighted Values		
Items	Shuttle SRB x2	Ariane SRB x4
Max Thrust (kN)	9	9
Mass (kg)	4	6
Aerodynamics	2	3
Total	15	18

2nd Stage Engines

Table 44: Actual values for the 2nd stage engines

Actual Values			
Items	AJ10	Merlin 1D Vacuum	RL10
Max Thrust (kN)	43.7	981	110.5
Isp (s)	319	348	465.5
Throttle Ability	Medium	High	Medium
# of engines needed	High	Low	Medium

Table 45: Normalization values for the 2nd stage engines

Normalization Values			
Items	1	2	3
Max Thrust (kN)	< 100	< 250	> 500
Isp (s)	< 325	< 350	> 400
Throttle Ability	Low	Medium	High
# of engines needed	High	Medium	Low

Table 46: Normalized values for the 2nd stage engines

Normalized Values			
Items	AJ10	Merlin 1D Vaccum	RL10
Max Thrust (kN)	1	3	2
Isp (s)	1	2	3
Throttle Ability	2	3	2
# of engines needed	1	3	2

Table 47: Weighting factors for the 2nd stage engines

Weighting Factors		
Items	Factor	Reason
Max Thrust (kN)	1	Large amounts of thrust are not as important for upper stage flight
Isp (s)	4	Efficiency is highly important in upper stage flight
Throttle Ability	2	Control of thrust output aids in managing human and structural requirements
# of engines needed	3	Less total engines can reduce cost while maintaining similar levels of thrust

Table 48: Final weighted values result for the 2nd stage engines

Weighted Values			
Items	AJ10	Merlin 1D Vaccum	RL10
Max Thrust (kN)	1	3	2
Isp (s)	4	8	12
Throttle Ability	2	6	4
# of engines needed	3	9	6
Total	10	26	24

Appendix D. – MATLAB Scripts

Ascent Trajectory

```
% AERO-4720
% Author: Jacob Dewey, Group 3
% Calculation of speed, mach number, and altitude:
clc, clear all, close all %#ok<CLALL>
format short g

%% Force Calculations:
% Constants
[T, P, rho] = atmo_model_100km(100); % Atmospheric model (to 100km)
Cd = 0.27; % Drag Coefficient: best guess
s = 72.63; % Planform Surface Area [m^2]
g0 = 9.8067; % Gravitational acceleration [m/s^2]
mu = 398600; %
gam = pi/2; % Initial flight path angle (measured from the horizontal) [deg]
mass_0 = 3076259.09; % kg
mass_1 = 1944415.29; % kg
mass_2 = 325559.02; % kg
burnoutMass1 = 431673.29; % kg
burnoutMass2 = 98530.96; % kg
minThrottle1 = 0.65;
minThrottle2 = 0.39;
fuelmass_0 = 1092000; % kg
fuelmass_1 = 1512472; % kg
fuelmass_2 = 227028; % kg
T0 = 28.32e6; % Zero Stage Thrust [N]
T1 = 9.6e6; % First Stage Thrust [N]
T2 = 480e3; % Second Stage Thrust [N]
mdot_0 = 8000; % Solid Booster Fuel Mass Flow Rate [kg/s]
mdot_1 = 3272.88; % First Stage Fuel Mass Flow Rate [kg/s]
mdot_2 = 157.33; % Second Stage Fuel Mass Flow Rate [kg/s]
re = 6378e3; % Radius of Earth [m]
gamInit = 1; % Initial kickover angle in degrees
deg1 = 0.5;
deg2 = 0.7;
deg3 = 1.6;
dt = 0.01;
gTurnTime = 40/dt;

% Calculations
burnTime0 = fuelmass_0/(mdot_0); % s
burnTime1 = fuelmass_1/(mdot_1); % s
burnTime2 = fuelmass_2/(mdot_2); % s
totalBurn = burnTime1 + burnTime2; % s

%% Ascent Calculations:
%Initial:
burnmass = mdot_0+mdot_1;
fmass(1) = mass_0 - dt*burnmass;
```

```

D(1) = 0;
acc(1) = (T0 + T1)/fmass -D(1)/fmass(1) - g0*sin(gam);
% racc(1) = (T0+T1)/fmass;
v(1) = dt*acc(1);
alt(1) = dt*v(1)*sin(gam);
xdis(1) = dt*v(1)*cos(gam);
gam(1) = gam;

% Loop
orbit = false;
t = dt;
i = 2;
while fmass(i-1) > burnoutMass2
    if t(i-1) < burnTime0 % First Stage burn with boosters
        g(i) = g0/(1+alt(i-1)/re)^2;
        if alt/1000 < 100
            D(i) = dragCalc(v(i-1), rho(fix(alt(i-1)*1e-3)+1), Cd, s);
        else
            D(i) = 0;
        end
        [acc(i), fmass(i), racc(i)] = accFunction(fmass(i-1), (T0+T1),
(mdot_1+mdot_0), D(i), 1, g(i), gam(i-1), dt, (t(i-1)+dt));
        [v(i), alt(i), xdis(i)] = trajectoryFunction(alt(i-1), xdis(i-1),
v(i-1), acc(i), dt, gam(i-1));
        if i < gTurnTime
            gam(i) = gam(i-1);
        elseif i == gTurnTime
            gam(i) = gam(i-1) - gamInit*pi/180;
        else
            gam(i) = gamCalc(gam(i-1), g(i), v(i-1), alt(i), degl, dt);
        end

    elseif abs(t(i-1)+dt - burnTime0) < 0.001 % Staging the boosters
t(i-1) == burnTime0
        g(i) = g0/(1+alt(i-1)/re)^2;
        if alt/1000 < 100
            D(i) = dragCalc(v(i-1), rho(fix(alt(i-1)*1e-3)+1), Cd, s);
        else
            D(i) = 0;
        end
        [acc(i), fmass(i), racc(i)] = accFunction((mass_1 - i*dt*mdot_1),
(T1), (mdot_1), D(i), 1, g(i), gam(i-1), dt, (t(i-1)+dt));
        [v(i), alt(i), xdis(i)] = trajectoryFunction(alt(i-1), xdis(i-1),
v(i-1), acc(i), dt, gam(i-1));
        gam(i) = gamCalc(gam(i-1), g(i), v(i-1), alt(i), degl, dt);

    % fprintf('Booster Separation at t+%3.2fs \n\n', t(i-1)+dt)

    elseif t(i-1) > burnTime0 && fmass(i-1) > (burnoutMass1 + mdot_1) % Rest
of First Stage Burn
        g(i) = g0/(1+alt(i-1)/re)^2;
        if alt/1000 < 100
            D(i) = dragCalc(v(i-1), rho(fix(alt(i-1)*1e-3)+1), Cd, s);
        else
            D(i) = 0;
        end
    end

```

```

[acc(i), fmass(i), racc(i)] = accFunction(fmass(i-1), (T1), (mdot_1),
D(i), minThrottle1, g(i), gam(i-1), dt, (t(i-1)+dt));
[v(i), alt(i), xdis(i)] = trajectoryFunction(alt(i-1), xdis(i-1),
v(i-1), acc(i), dt, gam(i-1));
gam(i) = gamCalc(gam(i-1), g(i), v(i-1), alt(i), deg2, dt);

elseif t(i-1) > burnTime0 && fmass(i-1) > burnoutMass1 && fmass(i-1) <
(burnoutMass1 + mdot_1) % Staging between First and Second Stage
    g(i) = g0/(1+alt(i-1)/re)^2;
    if alt/1000 < 100
        D(i) = dragCalc(v(i-1), rho(fix(alt(i-1)*1e-3)+1), s, dt);
    else
        D(i) = 0;
    end
    [acc(i), fmass(i), racc(i)] = accFunction(mass_2, (T2), (mdot_2),
D(i), minThrottle2, g(i), gam(i-1), dt, (t(i-1)+dt));
    [v(i), alt(i), xdis(i)] = trajectoryFunction(alt(i-1), xdis(i-1),
v(i-1), acc(i), dt, gam(i-1));
    gam(i) = gamCalc(gam(i-1), g(i), v(i-1), alt(i), deg3, dt);

fprintf('First Stage Separation at t+%3.2fs \n\n', t(i-1)+dt)

else % Second Stage Burn
    g(i) = g0/(1+alt(i-1)/re)^2;
    D(i) = 0;
    [acc(i), fmass(i), racc(i)] = accFunction(fmass(i-1), T2, (mdot_2),
D(i), minThrottle2, g(i), gam(i-1), dt, (t(i-1)+dt));
    [v(i), alt(i), xdis(i)] = trajectoryFunction(alt(i-1), xdis(i-1),
v(i-1), acc(i), dt, gam(i-1));
    gam(i) = gamCalc(gam(i-1), g(i), v(i-1), alt(i), deg3, dt);

end

% disp(acc(i))
% disp(v(i))

t(i) = t(i-1) + dt;

dragLoss(i) = D(i)*dt/fmass(i);
gravityLoss(i) = g(i)*sin(gam(i))*dt;

vOrbit = sqrt(mu*1000/(re+alt(i)));
if v(i)/1000 + 0.40859 - vOrbit > 0 && abs(gam(i)) < 0.001
    deltaV = 3050.91*log(fmass(i)/burnoutMass2);
    orbit = true;
    disp('Success! You''re in orbit!')
    fprintf('t+%6.2f seconds\n', t(i))
    fprintf('Fuel Left = %9.2f kg\n', (fmass(i) - burnoutMass2))
    fprintf('Delta-V Left = %4.2f m/s\n\n', deltaV)
    break
end

```

```

if alt(i) < 0
    disp('You crashed :(')
    break
end

i = i+1;
end

if orbit == true
    totalDrag = sum(dragLoss);
    totalGravity = sum(gravityLoss);
    targetR = (re+800000)/1000;
    vTarget = sqrt(mu/targetR);
    maneuverV = abs(v(length(v)))+408.59 - vTarget*1000;

    fprintf('Drag Losses: %4.2f m/s\n', totalDrag)
    fprintf('Gravity Losses: %4.2f m/s\n', totalGravity)
    fprintf('Delta-V to Target: %3.2f m/s \n', maneuverV)
    fprintf('Final Delta-V: %3.2f m/s \n\n', deltaV - maneuverV)

end

%% Plots:
% Alt vs Time:
figure;
plot([1:1:length(alt)]*dt,alt/1000,'Linewidth',2)
title('Altitude vs Time')
xlabel('Time [s]')
ylabel('Altitude [km]')

% Acceleration vs Time
figure;
plot([1:1:length(acc)]*dt,acc,'Linewidth',2) %#ok<NBRAK>
title('Acceleration vs Time')
xlabel('Time [s]')
ylabel('Accelaration [m/s^2]')

% Velocity vs Time
figure;
plot([1:1:length(v)]*dt,v,'Linewidth',2) %#ok<NBRAK>
title('Velocity vs Time')
xlabel('Time [s]')
ylabel('Velocity [m/s]')

% % No-Loss Acceleration vs Time
% figure;
% plot([1:1:length(racc)]*dt,racc,'Linewidth',2) %#ok<NBRAK>
% title('Reference Acceleration vs Time')
% xlabel('Time [s]')
% ylabel('Acceleration [m/s^2]')

```

```
% Drag vs Time
figure;
plot([1:1:length(D)]*dt,D,'Linewidth',2) %#ok<NBRAK>
title('Drag vs Time')
xlabel('Time [s]')
ylabel('Drag [N]')

% Mass vs Time
figure;
plot([1:1:length(fmass)]*dt,fmass,'Linewidth',2) %#ok<NBRAK>
title('Mass vs Time')
xlabel('Time [s]')
ylabel('Mass [kg]')

% for i = 1:length(v)
%     gdr(i) = -(g(i)/v(i) - v(i)/(alt(i)+re));
% end
%
% figure;
% plot([1:length(gdr)]*dt,gdr)

% FPA vs Time
figure;
plot([1:length(gam)]*dt,gam*180/pi)
title('Flight Path Angle vs Time')
xlabel('Time [s]')
ylabel('Flight Path Angle [deg]')

% FPA vs Altitude
figure;
plot(alt/1000,gam*180/pi)
title('Flight Path Angle vs Altitude')
xlabel('Alt [km]')
ylabel('Flight Path Angle [deg]')

%
% figure;
% plot([1:length(g)]*dt,g)

%% Functions:
% Gravity Turn:
function gam = gamCalc(gamIn, g, v, alt, deg, dt)
real = 0;
if real == 1
    Re = 6378*1000; % Radius of the Earth [km]
    r = Re+alt;
    gDot = -(g/v - v/r)*cos(gamIn);
    gam = gamIn + gDot*dt;
elseif real == 0
    gDot = -deg*sin(gamIn)*pi/180;
    gam = gamIn + gDot*dt;
```

```

end
end

% Drag Calculator
function D = dragCalc(v, rho, Cd, s)
D = 0.5*Cd*s*rho*v^2;

end

% Acceleration Function (includes a throttling mechanism):
function [acc, fMass, rAcc] = accFunction(fMassIn, thrust, mDotIn, D,
minThrottle, g, gam, dt, t)
g0 = 9.8067; % m/s^2
refAcc = (thrust - D)/(fMassIn-mDotIn) - g*sin(gam);
rAcc = thrust/(fMassIn-mDotIn);

% Ensures the acceleration is under 2 g's
if refAcc <= 3*g0 % If under 2 g's, no throttling occurs
    acc = refAcc;
    fMass = fMassIn - dt*mDotIn;
elseif refAcc > 3*g0 % If greater than 2 g's, it throttles the engines
    disp(refAcc)
    desThrust = (3*g0 + g*sin(gam))*fMassIn + D;
    throttle = desThrust/thrust;
    if throttle > minThrottle % Ensures the throttle doesn't exceed limits
        mDot = dt*throttle*mDotIn;
        fMass = fMassIn - mDot;
        acc = (throttle*thrust - D)/fMass - g*sin(gam);
        fprintf('Throttled to %1.2f% at t+%1.2fs \n\n', throttle*100, t)
    else % If throttle ability is exceeded, ensures lowest g's possible
        mDot = dt*minThrottle*mDotIn;
        fMass = fMassIn - mDot;
        acc = (minThrottle*thrust - D)/fMass - g*sin(gam);
        fprintf('Throttled to %1.2f% at t+%1.2fs \n\n', minThrottle*100, t)
    end
end
end

% Trajectory Finder:
function [v, alt, xdis] = trajectoryFunction(altIn, xdisIn, vIn, accIn, dt,
gam)
v = vIn + dt*accIn; % Determines the velocity [m/s]
alt = altIn + dt*v*sin(gam); % Determines the altitude [m]
xdis = xdisIn + dt*v*cos(gam); % Determines downrange distance [m]
end

```

Standard Atmosphere Model

```
%Author: Jacob Dewey, Group 3
function [T, P, rho] = atmo_model_100km(maxAlt)

% Defining constants
g0 = 9.81; % m/s^2, gravity at sea level
T0 = 288.16; % K, temp at sea level
P0 = 101325; % Pa, pressure at sea level
rE = 6378.154; % km, radius of Earth
R = 287.05; % J/kg-K, gas constant for air
rho0 = P0/(R*T0); % kg/m^3, density at sea level

% Defining lapse rates for gradient regions
a1 = -6.5e-3; % K/m
a2 = 3e-3; % K/m
a3 = -4.5e-3; % K/m
a4 = 4e-3; % K/m

for alt = 0:1:maxAlt
    % Gradient Region: 0 km to 11 km
    if 0 <= alt && alt <= 11
        T(alt+1) = T0 + (a1*alt*1000); % K
        P(alt+1) = P0*((T(alt+1)/T0)^((-g0/(a1*R)))); % Pa
        rho(alt+1) = rho0*((T(alt+1)/T0)^(-((g0/(a1*R))+1))); % kg/m^3

    % Isothermal Region: 11 km to 25 km
    elseif 12 <= alt && alt <= 25
        T(alt+1) = T(12); % K
        P(alt+1) = P(12)*exp((-g0/(R*T(alt+1)))*(alt-11)*1000); % Pa
        rho(alt+1) = rho(12)*exp((-g0/(R*T(alt+1)))*(alt-11)*1000); % kg/m^3

    % Gradient Region: 25 km to 47 km
    elseif 26 <= alt && alt <= 47
        T(alt+1) = T(26) + (a2*(alt-25)*1000); % K
        P(alt+1) = P(26)*((T(alt+1)/T(26))^(-(g0/(a2*R)))); % Pa
        rho(alt+1) = rho(26)*((T(alt+1)/T(26))^(-((g0/(a2*R))+1))); % kg/m^3

    % Isothermal Region: 47 km to 53 km
    elseif 48 <= alt && alt <= 53
        T(alt+1) = T(48); % K
        P(alt+1) = P(48)*exp((-g0/(R*T(alt+1)))*(alt-47)*1000); % Pa
        rho(alt+1) = rho(48)*exp((-g0/(R*T(alt+1)))*(alt-47)*1000); % kg/m^3

    % Gradient Region: 53 km to 79 km
    elseif 54 <= alt && alt <= 79
        T(alt+1) = T(54) + (a3*(alt-53)*1000); % K
        P(alt+1) = P(54)*((T(alt+1)/T(54))^(-(g0/(a3*R)))); % Pa
        rho(alt+1) = rho(54)*((T(alt+1)/T(54))^(-((g0/(a3*R))+1))); % kg/m^3

    % Isothermal Region: 79 km to 90 km
    elseif 80 <= alt && alt <= 90
        T(alt+1) = T(80); % K
        P(alt+1) = P(80)*exp((-g0/(R*T(alt+1)))*(alt-79)*1000); % Pa
```

```
rho(alt+1) = rho(80)*exp((-g0/(R*T(alt+1)))*(alt-79)*1000); % kg/m^3

% Gradient Region: 90 km to 100 km
elseif 91 <= alt && alt <= 100
T(alt+1) = T(91) + (a4*(alt-90)*1000); % K
P(alt+1) = P(91)*((T(alt+1)/T(91))^(-(g0/(a4*R)))); % Pa
rho(alt+1) = rho(91)*((T(alt+1)/T(91))^(-((g0/(a4*R))+1))); % kg/m^3

end
end
% Dynamic Viscosity
mu(alt+1) = ((1.458e-6)*sqrt(T(alt+1)))/(1+(110.4/T(alt+1))); % Pa-s
end
```

Stage Mass Calculations

```
%G3LATTO Stage Mass Calcs
%Author: Trey Philpott, Seth Hawkins, Group 3

clc
clear all
close all

mult = 1;
%% Get Individual Masses (kg)
mSRB = 273e3;
mStage0Prop = 960000;
mStage0Structure = 3.984384414831337e+04*mult;

mStage1Prop = 1512472.233489;
mStage1Structure = 1.063840425284484e+05*mult;
mwetCore = mStage0Structure + mStage1Structure + mStage0Prop + mStage1Prop;
mdotCore = 3.272887197897170e+03; % kg/s

mStage2Prop = 227028.056439;
mStage2Structure = 2.353091512862024e+04*mult;
mwet2 = mStage2Prop + mStage2Structure;
mPayload = 75e3;

%% Get Total Mass
mLaunch = mStage0Structure + mStage1Structure + mStage2Structure +
mStage1Prop + mStage2Prop + (4*mSRB) + mPayload
disp('kg')
Stage1 = mLaunch - (mStage1Prop - (mdotCore*140)) - (4*mSRB) -
mStage0Structure
disp('kg')
Stage2 = Stage1 - mStage1Structure - mStage1Prop
disp('kg')

%% Get Mass Fractions
mf_inert_core = ((mStage0Structure + mStage1Structure) / (mwetCore +
mPayload))*100
disp('percent')
mf_inert_2 = (mStage2Structure / (mwet2 + mPayload))*100
disp('percent')
mf_pl_core = (mPayload / (mwetCore + mPayload))*100
disp('percent')
mf_pl_2 = (mPayload / (mwet2 + mPayload))*100
disp('percent')
mf_structure =
((mStage0Structure+mStage1Structure+mStage2Structure) / mLaunch)*100
disp('percent')
mf_Prop = ((mStage1Prop+mStage2Prop+(4*mSRB) ) / mLaunch)*100
disp('percent')

%% Get TWR
TBE4 = 2.4e6; %N
TSRB = 7080e3; %N
```

```
WLaunch = mLaunch*9.81  
TWR = ( (4*TBE4) + (4*TSRB) ) /WLaunch
```

Propellant Mass Sizing

```
% Propellant Mass Sizing - G3
% Author: Seth Hawkins, Group 3

clc
clear all
close all

%% INPUTS
% Delta V
dV0 = 7; % Delta V for stage 0, km/s
dV1 = 2; % Delta V for stage 1, km/s
dV2 = 2; % Delta V for stage 2, km/s
dV = [dV0, dV1, dV2];

% Payload Mass
mpl = 75000; % kg

% Isp
Isp_0 = 258; % Stage 0 - SRB & Methalox, s
Isp_BE4 = 299; % Stage 1 - Methalox, s
Isp_Merlin = 311; % Stage 2 - LOX/RP1 (Vacuum), s

% Structural Factor
sigma_0_core = 0.08;
sigma_1 = 0.1;
sigma_2 = 0.1;

%% OUTPUTS
% Propellant Mass Fractions
%[pmf_0, pmf_1, pmf_2] = MassFrac(dV, Isp);

%% Stage 2 Parameters
[stage2_params] = stage2(dV2, Isp_Merlin, mpl, sigma_2);
mp_2 = stage2_params(1);
m0_2 = stage2_params(2);
mf_2 = stage2_params(3);
ms_2 = stage2_params(4);
mpl_1 = stage2_params(5);

%% Stage 1 Parameters
[stage1_params] = stage1(dV1, Isp_BE4, mp_1, sigma_1);
mp_1 = stage1_params(1);
m0_1 = stage1_params(2);
mf_1 = stage1_params(3);
ms_1 = stage1_params(4);

%% Stage 0 Parameters
n_BE4 = 4; % Number of BE4 engines on core stage
mdot_core = n_BE4*(2.4e6/(299*9.81)); % kg/s
t_bo_SRB = 140; % s
[stage0_params] = stage0(sigma_0_core, mdot_core, t_bo_SRB);
mp_0_core = stage0_params(1);
ms_0_core = stage0_params(2);
```

```

ms_core = ms_0_core + ms_1; % Stage 0 + 1 (core)
mp_core = mp_0_core + mp_1; % Stage 0 + 1 (core)
ms_SRB = 33000*4; % Ariane 5 SRB dry mass
mp_SRB = 240000*4; % Ariane 5 SRB prop mass

%% Total Structural Mass
ms_total = ms_core + ms_SRB + ms_2;

%% Total Propellant Mass
mp_total = mp_core + mp_SRB + mp_2;

%% Total Vehicle Mass
m_G3 = ms_total + mp_total + mpl;

%% Core Tank Sizing (Stage 0 + 1)
rho_LOX = 1141; % kg/m^3
rho_CH4 = 424; % kg/m^3
Mix_BE4 = 2.77; % mixture ratio = 2.77:1

[h_oxi_1, h_fuel_1, m_oxi_1, m_fuel_1, V_oxi_1, V_fuel_1] = tanksize(mp_core,
rho_LOX, rho_CH4, Mix_BE4);

%% Merlin Tank Sizing
% rho_LOX = 1141; % kg/m^3
rho_RP1 = 810; % kg/m^3
Mix_Merlin = 2.35; % mixture ratio = 2.35:1

[h_oxi_2, h_fuel_2, m_oxi_2, m_fuel_2, V_oxi_2, V_fuel_2] = tanksize(mp_2,
rho_LOX, rho_RP1, Mix_Merlin);

%% Output Results
fprintf(' -----\n\n');

fprintf(' The height of the stage 0+1 oxidizer tank is %.3f m\n', h_oxi_1);
fprintf(' The height of the stage 0+1 fuel tank is %.3f m\n\n', h_fuel_1);
fprintf(' The oxidizer mass for stage 0+1 is %.3f kg\n', m_oxi_1);
fprintf(' The fuel mass for stage 0+1 is %.3f kg\n\n', m_fuel_1);
fprintf(' The volume of the stage 0+1 oxidizer tank is %.3f m^3\n',
V_oxi_1);
fprintf(' The volume of the stage 0+1 fuel tank is %.3f m^3\n\n', V_fuel_1);

fprintf(' -----\n\n');

fprintf(' The height of the stage 2 oxidizer tank is %.3f m\n', h_oxi_2);
fprintf(' The height of the stage 2 fuel tank is %.3f m\n\n', h_fuel_2);
fprintf(' The oxidizer mass for stage 2 is %.3f kg\n', m_oxi_2);
fprintf(' The fuel mass for stage 2 is %.3f kg\n\n', m_fuel_2);
fprintf(' The volume of the stage 2 oxidizer tank is %.3f m^3\n', V_oxi_2);
fprintf(' The volume of the stage 2 fuel tank is %.3f m^3\n\n', V_fuel_2);

fprintf(' -----\n\n');

fprintf(' The total structural mass is %.3f kg\n', ms_total);

```

```
fprintf(' The total propellant mass is %.3f kg\n', mp_total);
fprintf(' The total vehicle mass is %.3f kg\n\n', m_G3);

fprintf(' -----\n\n');

%% Function for stage 2 calculations
function [stage2_params] = stage2(dV, Isp, mpl, sigma)
g = 9.81e-3; % km/s^2

% Mass Ratio Mu
mu = exp(dV/(g*Isp));

% Propellant Mass
mp = mpl*((mu-1)*(1-sigma))/(1-mu*sigma);

% Initial Mass
m0 = mpl*((mu*(1-sigma))/(1-mu*sigma));

% Final Mass
mf = mpl*((1-sigma)/(1-sigma*mu));

% Structural Mass
ms = mp*(sigma/(1-sigma));

% Payload mass for 1st Stage Calculations
mpl_1 = m0;

stage2_params = [mp; m0; mf; ms; mpl_1];

end

%% Function for stage 1 calculations
function [stage1_params] = stage1(dV, Isp, mpl, sigma)
g = 9.81e-3; % km/s^2

% Mass Ratio Mu
mu = exp(dV/(g*Isp));

% Propellant Mass
mp = mpl*((mu-1)*(1-sigma))/(1-mu*sigma);

% Initial Mass
m0 = mpl*((mu*(1-sigma))/(1-mu*sigma));

% Final Mass
mf = mpl*((1-sigma)/(1-sigma*mu));

% Structural Mass
ms = mp*(sigma/(1-sigma));

stage1_params = [mp; m0; mf; ms];

end
```

```
%% Function for stage 0 calculations
function [stage0_params] = stage0(sigma, mdot, tbo)

    % Core propellant mass
    mp_0_core = mdot*tbo; % kg

    % Core structural mass
    ms_0_core = (sigma*mp_0_core)/(1-sigma);

    stage0_params = [mp_0_core; ms_0_core];

end

%% Function for tank sizing
function [h_oxi, h_fuel, m_oxi, m_fuel, V_oxi, V_fuel] =
tanksize(mprop,rho_oxi,rho_fuel,mix)

% Define tank radius
r = 4.25; % m

% Calculate fuel and oxidizer mass
m_oxi = (mix/(mix+1))*mprop; % kg
m_fuel = (1/(mix+1))*mprop; % kg

% Calculate fuel and oxidizer tank volumes
V_oxi = (1/0.95)*(m_oxi/rho_oxi); % m^3, adjust for 95% prop volume
V_fuel = (1/0.95)*(m_fuel/rho_fuel); % m^3, adjust for 95% prop volume

% Calculate tank height
h_oxi = V_oxi/(pi*r^2);
h_fuel = V_fuel/(pi*r^2);

end
```

Engine Gimbal Radius Calculations

```
%Engine Gimbal Radius Calculator
%Author: Trey Philpott, Group 3

clc
clear all
close all
format long g

%% Get Constants

BE4_Height = 5; %m
BE4_R = 3.5/2; %m
BE4_Gimble = 7; %deg

SRB_Height = 3.8; %m
SRB_R = 3/2; %m
SRB_Gimble = 7.3; %deg

%% Get Gimbal Radius
%BE4
xBE4 = BE4_Height*tan(BE4_Gimble*pi/180);
BE4_GimbleD = (BE4_R + %BE4)*2
disp('meters')

%SRB
xSRB = SRB_Height*tan(SRB_Gimble*pi/180);
SRB_GimbleD = (SRB_R + xSRB)*2
disp('meters')
```

Estimated Burn Times

```
% Stage Burn Time Script
% Author: Trey Philpott, Group 3

clc
clear all
close all
format long g

%% Get Mass Flow Rates
throttleBE4 = 1;
mdotBE4 = 4*((2.4e6*throttleBE4)/(299*9.81)); % kg/s (from tank sizing
script)

throttleMerlin = 1;
mdotMerlin = ((981e3*throttleMerlin)/(311*9.81)); %kg/s

%% Get Propellant Masses
%Stage 1 Core
VFuel1 = 945.750288; %m^3
rhoFuel1 = 424; % kg/m^3
VLOX1 = 974.122797; %m^3
rhoLOX = 1141; % kg/m^3

mFuel1 = VFuel1*rhoFuel1; %kg
mLOX1 = VLOX1*rhoLOX; %kg
mProp1 = mFuel1 + mLOX1; %kg

%Stage 2
VFuel2 = 87.113746; %m^3
rhoFuel2 = 810; % kg/m^3
VLOX2 = 137.130519; %m^3

mFuel2 = VFuel2*rhoFuel2; %kg
mLOX2 = VLOX2*rhoLOX; %kg
mProp2 = mFuel2 + mLOX2; %kg

%% Get Burn Times
Stage1_BurnTime = mProp1/mdotBE4; %sec
Stage2_BurnTime = mProp2/mdotMerlin; %sec

%% Get Burnout Times (T+ time (sec))
Stage1_BurnOut = Stage1_BurnTime; %sec
Stage2_BurnOut = Stage1_BurnOut + Stage2_BurnTime; %sec

%% Get Outputs
fprintf(' 1st stage LCH4 mass is %.6f kg \n', mFuel1);
fprintf(' 1st stage LOX mass is %.6f kg \n', mLOX1);
fprintf(' 1st stage total propellant mass is %.6f kg \n', mProp1);
fprintf('\n');

fprintf(' 2nd stage RP1 mass is %.6f kg \n', mFuel2);
fprintf(' 2nd stage LOX mass is %.6f kg \n', mLOX2);
```

```
fprintf(' 2nd stage total propellant mass is %.6f kg \n', mProp2);
fprintf('\n');

fprintf(' 1st stage burn time is %.6f sec \n', Stage1_BurnTime);
fprintf(' 2nd stage burn time is %.6f sec \n', Stage2_BurnTime);
fprintf('\n');

fprintf(' 1st stage burnout will occur at T+ %.6f sec \n', Stage1_BurnOut);
fprintf(' 2nd stage burnout will occur at T+ %.6f sec (assuming constant
burn)\n', Stage2_BurnOut);
```

Structural Calculations

```
% Structural Calculations - G3
% Author: Joseph Ammons & Wesley Upchurch, Group 3

clc
clear all
close all

fprintf(' \n ----- Structural Calculations - G3 ----- \n \n');
%%
% Constants
g = 9.81*3; % m/s^2
payload = 75000; % kg
FS1 = 1.5;
FS2 = 1.5;
AL6061_sigma = 310e6; % Pa
AL6061_E = 68.9e9; % Pa
rho_AL6061 = 2700; % kg/m^3
AL6061T6_sigma = 310e6; % Pa
rho_AL6061T6 = 2700; % kg/m^3

%%
% STAGE 2
%% Inputs
% Variables from TankSizingR4.m
V_RP12 = 30.03; % m^3
V_LOX2 = 50.111; % m^3
rho_LOX = 1141; % kg/m^3
rho_RP1 = 810; % kg/m^3

%% Geometry Definitions
d_RP12 = 4;
d_LOX2 = 4;

h_RP1 = V_RP12 ./ (pi*(d_RP12/2)^2);
h_LOX = V_LOX2 ./ (pi*(d_LOX2/2)^2);

%% Max Pressure (hydrostatic) calculation
```

```

LOX_ullage = 448159; %pascals (50 psia) from
https://ntrs.nasa.gov/api/citations/19990009082/downloads/19990009082.pdf
RP1_ullage = 344738; %pascals (65 psia) from
https://ntrs.nasa.gov/api/citations/19990009082/downloads/19990009082.pdf

% Absolute Pressure
LOX_P = LOX_ullage + (rho_LOX * g * h_LOX) - 101325;
RP1_P = RP1_ullage + (rho_RP1 * g * h_RP1) - 101325;

fprintf('RP1 Hydrostatic Pressure: %.3f MPa \n',RP1_P/1e6)
fprintf('LOX Hydrostatic Pressure: %.3f MPa \n',LOX_P/1e6)

fprintf(' ----- \n');

%% Skin Thickness from Hoop Stress
LOX_t = LOX_P * (0.5*d_LOX2) / AL6061T6_sigma;
RP1_t = RP1_P * (0.5*d_RP12) / AL6061T6_sigma;
LOX_t_mm = LOX_t * 1000 * FS2;
RP1_t_mm = RP1_t * 1000 * FS2;

fprintf('RP1 Tank Minimum Thickness: %.3f mm \n',RP1_t_mm)
fprintf('LOX Tank Minimum Thickness: %.3f mm\n',LOX_t_mm)

fprintf(' ----- \n');

sigmaH_LOX = (LOX_P * (0.5*d_LOX2))/(LOX_t+0.001);
sigmaH_RP1 = (RP1_P * (0.5*d_RP12))/(RP1_t+0.001);
sigmaL_LOX = 0.5 * sigmaH_LOX;
sigmaL_RP1 = 0.5 * sigmaH_RP1;

fprintf('RP1 Hoop Stress: %.3f MPa \n',sigmaH_RP1/1e6)
fprintf('LOX Hoop Stress: %.3f MPa\n',sigmaH_LOX/1e6)
fprintf('RP1 Longitudinal Stress: %.3f MPa \n',sigmaL_RP1/1e6)
fprintf('LOX Longitudinal Stress: %.3f MPa\n',sigmaL_LOX/1e6)

fprintf(' ----- \n');

%%
% Stage 2 Tank Masses
vol_LOX_stage2 = pi * ((d_LOX2/2)^2 - (d_LOX2/2 - LOX_t)^2) * h_LOX; % volume
of LOX tank
vol_RP1_stage2 = pi * ((d_RP12/2)^2 - (d_RP12/2 - RP1_t)^2) * h_RP1; % volume
of RP1 tank

m_LOX_stage2 = vol_LOX_stage2 * rho_AL6061T6; % mass of LOX tank
m_RP1_stage2 = vol_RP1_stage2 * rho_AL6061T6; % mass of RP1 tank

fprintf('Stage 2: LOX tank mass: %.3f kg \n',m_LOX_stage2)
fprintf('Stage 2: RP1 tank mass: %.3f kg \n',m_RP1_stage2)
fprintf(' ----- \n');

```

```

%%

%% AUX PROPULSION

rho_MMH = 880; % kg/m^3
vol_AUX = 53.97; % m^3
rho_helium = 1.114; % kg/m^3
vol_hel = 53.97; % m^3

%% Geometry Definitions
d = 5;

h = 2.5;

%% Max Pressure (hydrostatic) calculation
He_ullage = 3000000; %pascals (30 bar)
MMH_ullage = 180000; %pascals (1.8 MPa)

% Absolute Pressure
He_P = He_ullage + (rho_helium * g * h) - 101325;
MMH_P = MMH_ullage + (rho_MMH * g * h) - 101325;

fprintf('Helium Hydrostatic Pressure: %.3f MPa \n',He_P/1e6)
fprintf('MMH Hydrostatic Pressure: %.3f MPa \n',MMH_P/1e6)

fprintf(' ----- \n');

%% Skin Thickness from Hoop Stress
He_t = He_P * (0.5*d) / AL6061T6_sigma;
MMH_t = MMH_P * (0.5*d) / AL6061T6_sigma;
He_t_mm = He_t * 1000 * FS2;
MMH_t_mm = MMH_t * 1000 * FS2;

fprintf('Helium Tank Minimum Thickness: %.3f mm \n',He_t_mm)
fprintf('MMH Tank Minimum Thickness: %.3f mm\n',MMH_t_mm)

fprintf(' ----- \n');

sigmaH_He = (He_P * (0.5*d)) / (He_t+0.001);
sigmaH_MMH = (MMH_P * (0.5*d)) / (MMH_t+0.001);
sigmaL_He = 0.5 * sigmaH_He;
sigmaL_MMH = 0.5 * sigmaH_MMH;

fprintf('He Hoop Stress: %.3f MPa \n',sigmaH_He/1e6)

```



```

fprintf('MMH Hoop Stress: %.3f MPa\n',sigmaH_MMH/1e6)
fprintf('He Longitudinal Stress: %.3f MPa \n',sigmaL_He/1e6)
fprintf('MMH Longitudinal Stress: %.3f MPa\n',sigmaL_MMH/1e6)

fprintf(' ----- \n');

% Stage 2 Tank Masses
vol_He_stage2 = pi * ((d/2)^2 - (d/2 - He_t)^2) * h; % volume of LOX tank
vol_MMH_stage2 = pi * ((d/2)^2 - (d/2 - MMH_t)^2) * h; % volume of RP1 tank

m_He_stage2 = vol_He_stage2 * rho_AL6061T6; % mass of LOX tank
m_MMH_stage2 = vol_MMH_stage2 * rho_AL6061T6; % mass of RP1 tank

fprintf('Stage 2: Helium tank mass: %.3f kg \n',m_He_stage2)
fprintf('Stage 2: MMH tank mass: %.3f kg \n',m_MMH_stage2)

%%

fprintf('\n\n ----- \n');
fprintf(' ----- STAGE 1 ----- \n');
fprintf(' ----- \n');

%% Inputs
% Variables from TankSizingR4.m
V_CH41 = 418.03; % m^3
V_LOX1 = 430.298; % m^3
rho_LOX = 1141; % kg/m^3
rho_CH4 = 424; % kg/m^3

%% Geometry Definitions
d_CH4 = 7;
d_LOX1 = 7;

h_CH4 = (V_CH41 ./ (pi*(d_CH4/2)^2));
h_LOX = (V_LOX1 ./ (pi*(d_LOX1/2)^2));

%% Max Pressure (hydrostatic) calculation
LOX ullage = 344738; %pascals (50 psia) from
https://ntrs.nasa.gov/api/citations/20100026018/downloads/20100026018.pdf
CH4 ullage = 341290.5; %pascals (49.5 psia) from
https://ntrs.nasa.gov/api/citations/20100026018/downloads/20100026018.pdf

% Absolute Pressure
LOX P = LOX ullage + (rho LOX * g * h LOX) - 101325;

```



```

%% Inputs for Stage 2
% Stringer Geometry
t_2 = 0.25; % m
w_2 = 0.157; % m
L_2 = 1.33; % m
struct_area_2 = 6.28; % m^2

% Moment of inertia
MOI_x2 = (1/12)*t_2*w_2^3; % Moment of inertia of stage 1 stringer - about x
MOI_z2 = (1/12)*w_2*t_2^3; % Moment of inertia of stage 1 stringer - about z

% Stage 1 mass
total_ms_2 = m_LOX_stage2 + m_RP1_stage2; % total stage 1 tank mass
total_mp_2 = (V_RP12 * rho_RP1) + (V_LOX2 * rho_LOX); % Total propellant mass
total_m_2 = total_ms_2 + total_mp_2 + payload; % Stage 1 total mass

% Critical Buckling
crit_buckling_x2 = (pi^2 * AL6061_E * MOI_x2) / L_2^2; % Critical buckling load
crit_buckling_z2 = (pi^2 * AL6061_E * MOI_z2) / L_2^2; % Critical buckling load

% Accel Load
accel_load_2 = (total_m_2 * g)/(struct_area_2);

fprintf(' -----\n');
fprintf('Stage 2: Stringer X-Buckling: %.3f MPa \n',crit_buckling_x2/1e6)
fprintf('Stage 2: Stringer Z-Buckling: %.3f MPa \n',crit_buckling_z2/1e6)
fprintf('Stage 2: Launch Load: %.3f MPa \n',accel_load_2/1e6)

%% Inputs for Stage 1
% Stringer Geometry
t_1 = 0.25; % m
w_1 = 0.2; % m
L_1 = 6.52; % m
struct_area_1 = 15.9; % m^2

% Moment of inertia
MOI_x1 = (1/12)*t_1*w_1^3; % Moment of inertia of stage 1 stringer - about x
MOI_z1 = (1/12)*w_1*t_1^3; % Moment of inertia of stage 1 stringer - about z

% Stage 1 mass
total_ms = m_LOX_stage1 + m_CH4_stage1; % total stage 1 tank mass
total_mp = (V_CH41 * rho_CH4) + (V_LOX1 * rho_LOX); % Total propellant mass
total_m = total_ms + total_mp + total_m_2; % Stage 1 total mass

% Critical Buckling
crit_buckling_x1 = (pi^2 * AL6061_E * MOI_x1) / L_1^2; % Critical buckling load
crit_buckling_z1 = (pi^2 * AL6061_E * MOI_z1) / L_1^2; % Critical buckling load

% Accel Load
accel_load_1 = ((total_m+payload) * g)/(struct_area_1);

```

```
fprintf(' -----\n');
fprintf('Stage 1: Stringer X-Buckling: %.3f MPa \n',crit_buckling_x1/1e6)
fprintf('Stage 1: Stringer Z-Buckling: %.3f MPa \n',crit_buckling_z1/1e6)
fprintf('Stage 1: Launch Load: %.3f MPa \n',accel_load_1/1e6)
```